DIGITAL MICROSCOPIC METHODS FOR SHARP FORCE TRAUMA IN BURNED HUMAN AND NONHUMAN REMAINS

by

Hailey G. Collord-Stalder, B.A.

A thesis submitted to the Graduate Council of
Texas State University in partial fulfilment
of the requirements for the degree of
Master of Arts
with a Major in Anthropology
May 2020

Committee Members:

Nicholas P. Herrmann, Chair

Michelle D. Hamilton

Daniel J. Wescott

FAIR USE AND AUTHOR'S PERMISSION STATEMENT

Fair Use

Duplication Permission

ACKNOWLEGDMENTS

I would like to take this opportunity to express my gratitude to several people who helped this thesis come to fruition. I would like to first thank my committee chair, Dr. Nicholas Herrmann, who helped me mold my thesis, held me back from attempting several wildly implausible ideas, and patiently read and responded to my confused emails about statistics. I would also like to thank my other committee members, Dr. Michelle Hamilton and Dr. Daniel Wescott, for their support when I needed to shift my thesis research topic and for providing valuable feedback and guidance as committee members. I also appreciate the assistance Dr. Tim Gocha provided regarding some very technical aspects of disarticulation and for the training Sophia Mavroudas provided with the Leica stereomicroscope.

I would further like to heartily thank Dr. Grady Early as this material is based upon work supported by the Grady Early Research Endowment in Forensic Anthropology. Additionally, I would like to thank Mr. George Strait for his financial (and musical!) support through the Freeman Fellows Graduate Research Fellowship, and Mr. Chris Thomas at Freeman Ranch for his interest and assistance with helping prepare for safe burning conditions.

My husband, Nicholas Stalder, was an unwavering beacon of encouragement throughout this entire process, and I could not have completed this project or degree without him and his disconcertingly deep knowledge of concrete. Great thanks also to my sister and parents for supporting my goals and listening to my tales of woe during this process.

I would also like to thank Nathan Blair and McKensey Miller for always making me laugh and Hannah Trevino for being a lab goblin with me for many, many long days and nights. Thanks to Crystal Crabb for her generous help with reformatting my data, Megan Veltri for continually being my champion, and to Tamara Tyner for always being a cheerleader and trying to keep me out of trouble as best she could.

Finally, I would like to thank the willed body donor without whose generous and selfless contribution to science this research would not have been possible.

TABLE OF CONTENTS

Page

LIST OF TABLES

Table **Page**

LIST OF FIGURES

Figure **Page**

I. INTRODUCTION

Attempting to destroy traumatic evidence on human remains with fire has been a technique of many past criminal offenders, but few studies have attempted to rigorously research the effects of burned trauma (Waltenberger & Schutkowski, 2017). Research examining trauma from different tool types in burned remains is important because both trauma and fire can cause fracturing and splitting in bone; in a forensic context, it is important to determine the differences between trauma occurring around the time of death (perimortem) and damage occurring after death (postmortem). Of further forensic concern is understanding whether tool class differentiations can be made following thermal alteration.

As technology in the field of forensics has increased, the use of DNA for identification purposes has become an excellent technique for making identifications (Gin et al., 2018), adding an element of redundancy to the traditional role of forensic anthropologists in producing biological profiles for identification purposes. Because of this advancement in forensic science, the role of the forensic anthropologist has turned more heavily toward interpretations of trauma (DiGangi & Moore, 2012). This shift toward trauma analysis, and more specifically, sharp force trauma analysis, becomes of special importance when the growing rate of fatal stabbings in countries such as Great Britain is considered (Nolan, Hainsworth, & Rutty, 2018; Waltenberger & Schutkowski, 2017). Furthermore, according to statistics on the United States from 2012 to 2016 issued by the Federal Bureau of Investigations, sharp force instruments are the second most common weapons used in homicides after firearms (*Murder Victims by Weapon, 2012-2016*, 2016).

Though forensic investigators deal with human remains in their casework, experimental research – especially in the realm of trauma analysis – has primarily used nonhuman remains. Because there are substantial differences between human and nonhuman bone morphology and composition, it is important for forensic investigators to understand that there may be different research outcomes utilizing nonhuman proxies than what may be seen in actual forensic casework. With the comparative research of human and nonhuman remains in the current study, critical analysis of past studies using nonhuman proxies to draw forensic conclusions is necessary, as they may not present results directly applicable to human casework.

The purpose of this research is to improve forensic methodology in collecting and analyzing perimortem sharp force trauma (SFT) on postmortem burned remains. This project attempts to address whether SFT in burned human remains can be examined effectively with different digital microscopic methods, to what degree tool class and individualization may be assessed in burned remains with the use of digital microscopy, and whether pigs are good proxies for humans in forensic research. The goal of this research is to evaluate the differences in SFT signatures based on tool type, and the results of this comparative research may help to implement recommendations for future research with nonhuman analogues

A secondary component of this study will be to understand how digital microscopes with varying sophistication can help mitigate difficulties in determining thermally altered SFT in various human elements to make a recommendation for future investigators. Moreover, this study will examine the forensic significance of past research

utilizing nonhuman remains. This research will also work toward refining practices for preparing, analyzing, and assessing burned remains with trauma.

The current study will progress the field of forensic and biological anthropology by examining the ways in which fire can alter toolmarks on remains. This has implications not only for enhancing our understanding of modern forensic circumstances, but for archaeological contexts as well within the realm of violence and mortuary practices. This research can benefit bioarchaeology in producing methodology for assessing types of tools used for dismemberment (e.g. trophy taking practices) as well as questions about funerary behaviors and nonhuman animal consumption in which burned bone may retain toolmark characteristics. Moreover, this research can help establish better forensic methods for law enforcement, fire department personnel, and death investigators in the absence of forensic anthropologists.

The research questions for this study are differentiated below.

Research Questions

1.)	Can tool class still be assessed from sharp force trauma in burned skeletal remains using digital microscopy?
2.)	Can SFT in burned human skeletal remains be examined effectively by both expensive and inexpensive digital microscopes?
3.)	Are pigs an acceptable nonhuman proxy in forensic toolmark research?
4.)	Can casting materials help distinguish kerf and saw mark characteristics for tool class identification?

Literature Review

Though this research examines the combined effects of sharp force trauma and thermal alteration in human and nonhuman bones, it is important to review the literature regarding these individual areas of research and their contributions to forensic anthropology.

Many studies have observed the effects of thermal alterations, or fire, on remains (Carroll & Smith, 2018; Castillo, Ubelaker, Acosta, & de la Fuente, 2013; Collini et al., 2015; Gonçalves, Cunha, & Thompson, 2015; Gourrier et al., 2017; Kasbleek & Richter, 2006; Schmidt & Symes, 2015; Shipman, Schoeninger, & Foster, 1984; Siegert, 2016; Thompson, 2005; Vassalo, Cunha, Batista de Carvalho, & Goncalves, 2016). Heat exposure results in chemical and structural alterations in bone with the denaturing of collagen, changes to the inorganic matrix, and evaporation (Schmidt & Symes, 2015). Thompson (2005) noted that the transformations of bone in fire are complicated due to their complex composition. This sentiment is reiterated throughout the literature, and Collini et al. (2015) acknowledged that extreme heat can lead to misleading effects resembling traumatic defects. Mistakes in differentiating heat related fractures from traumatic fractures are possible, so it is important that the investigator is knowledgeable about what characteristics to look for.

Shipman, Foster, and Schoeninger (1984) developed a series of stages for the coloration and textural differences of bone at varying degrees of heat exposure. The authors described several different bone characteristics such as microscopic structure and color, creating five stages or phases for the burned remains. Each phase is categorized by a range of temperatures. However, coloration and texture are affected by more factors

than just heat such as skeletal composition of the element, duration of thermal alteration, fluctuation of temperature, and presence or absence of soft tissue. Due to all of these contributing factors, color changes in bone are more related to the pyrolysis of water and organic materials such as collagen (Pope & Smith, 2004). The following tables are simplified versions of the phases produced by Shipman et al. (1984), which can be useful in providing a baseline of how the skeletal materials move through stages of thermal alteration, but their findings should not be viewed as an accurate guide for determining simply how much heat a skeletal element was exposed to.

Table 1. Modified Chart of Burned Bone Characteristics. *Chart reproduced by the findings of Shipman et al. (1984).*

Phase	Temperature Range	Defining Microscopic Characteristics of Burned Bone at Different Phases
I	20°C – 184°C	Bone texture is normal, the surface may be slightly undulating though intact
II	185°C – 284°C	Bone texture becomes more porous and granular, the surface remains intact
III	285°C – 439°C	Bone texture loses porosity and becomes smooth or glassy, polygonal cracking patterns occur, especially around bone defects (e.g. trauma or taphonomic damage)
IV	440°C – 799°C	The surface moves into a highly particulate, grainy texture
V	800°C – 940°C	The previous particles coalesce to form larger, smooth polygonal structures

Table 2. Modified Chart of Burned Bone Color. *Chart reproduced by the findings of Shipman et al. (1984).*

Phase	Temperature Range	Color of Burned Bone at Different Phases
I	20°C – 284°C	Neutral white, pale yellow, yellow
II	285°C – 524°C	Reddish brown, dark grey-brown, neutral dark-grey, reddish yellow
III	525°C – 644°C	Neutral black, some medium blue and reddish yellow present
IV	645°C – 939°C	Mostly neutral white, some light blue-grey and light grey may be present
V	940°C+	Neutral white, medium grey, and reddish yellow present

In addition to these studies, Buikstra and Swegel (1989) researched how varying temperatures and the varying state of bone – fleshed, green, and dry – affect the ways in which fracturing, shrinkage, and warping propagate. They also redefined the term "clinker," first coined by Wells (1960). Initially, "clinker" was used to denote the incomplete incineration of hair (Wells, 1960). Buikstra and Swegel (1989) revisited this definition and instead used the word "clinker" to describe the buildup up debris on and around the bone as a result of incompletely incinerated bone marrow and other soft tissue residues that form from oxygen deficient contexts.

While there are several studies examining bone following thermal alterations, there is a lack of literature on how to appropriately clean burned bone with remaining soft tissue for analysis. Though it may be the case that many of the burned remains recovered from a scene no longer retain soft tissue, that is not always true. The case study examined by Baier et al. (2017) involved a charred lump of flesh that contained the proximal section of a humerus. While the researchers were able to take radiological scans of the charred lump before dissecting it, Baier et al. (2017) note that further fragmentation occurred during the soft tissue removal process. No methodology on how the soft tissue was being removed was given.

This type of vague avoidance of technique for cleaning burned bone is not uncommon throughout the literature. *The Analysis of Burned Human Remains*, edited by Symes and Schmidt (2015), provides valuable collection techniques and case studies, but it does not contain information on cleaning burned bone. The book does, however, provide steps for cleaning burned teeth which is certainly useful (Schmidt, 2015). In another study on burned remains, Jackson (2005) simply reported that he carefully

cleaned any remaining soft tissue from his burned samples with a scalpel. This gap in the literature on proper methodology for cleaning burned bone, especially burned bone with trauma, must be addressed in future research to prevent further bone fragmentation and loss of toolmark data.

Thermal alteration studies are useful to help identify bone and make determinations about the pre-burning conditions of remains. This corpus of experimental research has been instrumental in addressing both forensic and archaeological questions. The combined findings from these studies, such as the probability of bone warping, the effects of different temperatures on bone, the effects of burning on fleshed versus defleshed remains, and the probable positionality of the remains during thermal alteration, provide a solid body of literature regarding burned human and nonhuman remains. Furthermore, this research on burned remains has helped standardize proper collection and preservation techniques which are invaluable in forensic and research contexts, though research on cleaning soft tissue from burned bone still needs to be fortified.

There have also been many studies which examined the effects of trauma on remains (Baier et al., 2017; Bailey et al., 2011; Coelho & Cardoso, 2013; J. H. B. A. Humphrey & Hutchinson, 2001; Marinho & Cardoso, 2016; Mason, 2000; Norman et al., 2018; Pelletti, Cecchetto, et al., 2017; Pelletti, Viel, et al., 2017; Symes et al., 2010; Walsh-Haney, 1999; Wieberg & Wescott, 2008). One area of focus in sharp force trauma research has centered around saw mark analysis since these tools are often used in dismemberment and other forensic contexts (Bailey et al., 2011; Herrmann & Bennett, 1999; Marciniak, 2009; Nogueira, Alunni, Bernardi, & Quatrehomme, 2018; Symes et

al., 2010; Symes, Dirkmaat, Ousley, Chapman, & Cabo, 2012), but there has also been significant literature on blunt, ballistic, and sharp force trauma including puncture and cut injuries.

Many studies found that sharp force trauma left discernible tool class identifiers in the bone including distinguishing factors for chopping blades, flat edge blades, serrated edge blades, and various saw marks (Alunni-Perret et al., 2010; Bailey et al., 2011; Humphrey, Kumaratilake, & Henneberg, 2017; J. H. B. A. Humphrey & Hutchinson, 2001; Nogueira et al., 2018; Nogueira, Quatrehomme, Rallon, Adalian, & Alunni, 2016; Symes et al., 2010; Tegtmeyer, 2012). Symes et al. (2010) note that saw marks can't often be matched to an individual tool during saw mark analysis, but features such as kerf wall and floor characteristics can be indicative of saw directionality, size, set, and power. The conglomeration of these characteristics can help identify a particular tool class. The researchers explain that many design features of saws involve the set, number, and shape of the teeth on the blade. Additionally, saw mark analysis involves examinations of the kerf and false start overall shape as well as floor and wall contours. Symes et al. (2010) point out that when examining a saw mark, the kerf floor and walls will include the most diagnostic information, as they can reveal defining saw teeth characteristics such as teeth per inch (TPI), power, directionality, and the relationship of the teeth to each other.

Bailey et al. (2011) also highlight the fact that kerf width is integral for approximating the thickness of the saw blade and the width between the saw teeth that was used. After examining 100 saw kerfs made by 10 different saws on bovine (cow) bone with a digital stereomicroscope, the researchers determined that the kerf width was

an informative measurement to take. They discovered that just by examining the width of the kerf mark, around 70-90% of saws could be eliminated as the tool that was used.

Additionally, Norman et al. (2018) examined eight different saw and knife marks in eight cadaveric full human legs. The researchers used two knife classes (serrated and flat-edge) and six various saw types, including reciprocating saws and handsaws, to examine kerf marks using micro-CT. Regarding mechanically powered saws, Norman et al. (2018) observed tooth-hopping, which appeared as several smaller and shallower kerfs adjacent to the main kerf, and they observed exit chipping wherein the floor of the kerf perforated into the trabeculae. The authors also noted that serrated-edge knife blades tended to produce Y shaped kerfs while flat-edge knife blades produced V shaped kerfs. Overall, Norman et al. (2018) found that each toolmark presented unique characteristics, which made identifying tool class much simpler.

Furthermore, research on the accuracy rate of forensic investigators correctly identifying knife class has also been conducted (Crowder, Rainwater, & Fridie, 2013). The researchers analyzed serrated, partially serrated, and flat-edge knife cuts on pig cartilage and deer long bones with a digital microscope. They found that classification rates were excellent when separating serrated from non-serrated blades due to the distinct striated pattern that serrated-edge blades leave, but accuracy fell when they attempted to discern partially serrated from fully serrated blades. Crowder, Rainwater, and Fridie (2013) found the ability of the digital microscope to make digital recreations and kerf profiles was extremely helpful in their research when trying to determine serrated-edge blades from flat-edge blades. They also noted, however, that with serrated-edge blades, the distance and morphology between the blade teeth as well as the amount of tissue the

knife must pass through affects the ability to perform an accurate analysis (Humphrey et al., 2017).

Humphrey et al. (2017) used a standardizing trauma device to create stab marks of different force on pig forelimbs. Using five different knives, including flat-edge and serrated edge knives, the researchers created 80 stab marks to analyze using sliding calipers. The observed the length, width, and depth of each of the cuts. They found that the greater the force behind the stabbing motion, the longer and deeper the cut mark was. These results were statistically significant and can tell the forensic investigator what kind of forces and weapons may have been behind an attack. The researchers also note that using a standardizing device for trauma research is pivotal for producing replicable results and helping forensic investigators understand weapon class differences

This research represents a select few of the studies done with sharp force trauma experimentation, which have laid the foundation for answering questions about discernibility of tool class and characteristics. Questions such as proper measurements and techniques as well as specific toolmark qualities are thoroughly addressed. Moreover, it has provided a range of methodology for forensic investigators who are examining trauma on remains.

Research examining the combined effects of trauma and thermal alteration on remains has been limited, and Symes et al. (2015) point out that the absence of standards in examining trauma in burned remains has hindered research and investigations. While some past research (de Gruchy & Rogers, 2002; Herrmann & Bennett, 1999; Jackson, 2005; Macoveciuc, Márquez-Grant, Horsfall, & Zioupos, 2017; Marciniak, 2009; Pope & Smith, 2004; Poppa et al., 2011; Waltenberger & Schutkowski, 2017) examining both

trauma and burning has increased knowledge in the field regarding the ability to determine heat defects from sharp force traumatic defects, or kerfs, it has been restricted in applicability. This restriction stems from the popular use of nonhuman remains in various stages of skeletonization in addition to unknown or unclear methodology for inflicting the trauma and processing the burned remains for analyses.

Because stabbing and slashing movements produced by both perpetrators and experimental trauma researchers on samples are difficult to quantify and measure, many studies have avoided addressing their methodology for inflicting trauma during experiments (de Gruchy & Rogers, 2002; Herrmann & Bennett, 1999; Kooi & Fairgrieve, 2013; Pope & Smith, 2004; Poppa et al., 2011; Symes et al., 2012). There have been, however, a number of studies that examined the force behind stabbing attacks (Chadwick, Nicol, Lane, & Gray, 1999; Miller & Jones, 1996; Ní Annaidh, Cassidy, Curtis, Destrade, & Gilchrist, 2013; Nolan et al., 2018; O'Callaghan et al., 1999).

With the availability of this data on sharp force trauma events, a few studies have developed standardized trauma infliction methods, especially to examine the effects of different temperatures on identical cut marks (Macoveciuc et al., 2017; Waltenberger & Schutkowski, 2017). Waltenberger and Schutkowski (2017) inflicted the trauma in their study with a force-measuring system to standardize the lesions. This standardized and measurable manner of trauma infliction allowed for identical cut marks across the various samples they utilized. They were then able to analyze the differences in bone composition and response to the identical trauma as well as to analyze the different outcomes that varying degrees of thermal alteration had on the sharp force trauma.

In addition, the issue of using an appropriate research proxy is not a new concern in the field of trauma research with researchers such as Aerssens, Lowet, and Dequeker (1998), Wang, Mabrey, and Agarwal (1998), and Zephro and Galloway (2014) voicing concern over using nonhuman analogues. However, many studies fail to address their own use of nonhuman proxies. The plurality of studies examining burned bone, bone trauma, or both have used nonhuman proxies due to multiple factors, not the least of which are ethical concerns regarding the use of human remains for such destructive analysis. However, the importance of understanding how sharp force trauma and heat affects human bone is necessary in a forensic context.

Nonhuman animal bone is typically arranged in a plexiform pattern, which has implications for fracture patterns and fracture propagation, and it is often much denser than the homologous human elements. Because nonhuman mammals usually become mobile much earlier than humans do following birth, they have different bone structure with a higher organic and lower mineral makeup meaning they have greater stiffness (Zephro & Galloway, 2014). Additionally, larger animals such as sheep, bovine, and pigs have a greater tendency toward microcracks in their bone structure, which makes it weaker overall and results in more localized damage in the presence of trauma (Zephro & Galloway, 2014).

Furthermore, with the number of trauma studies conducted over the years on nonhuman models, few studies have actually addressed whether or not those models were appropriate (Zephro, Galloway, & Wedel, 2014). Wang, Mabrey, and Agrawal (1998) studied fracture differences in human, baboon, canine, bovine, and rabbit bone. They argued that in order to appropriately use nonhuman bone, the nonhuman animal proxy

needs to have a similar life history in terms of age and collagen content. The researchers found that there were significant differences in the density and fracture toughness among the species studied (Wang, Mabrey, & Agrawal, 1998). This is significant because the common practice of using juvenile nonhuman remains in trauma and burn research does not seem to account for the higher levels of collagen present which may affect bone fracturing, warping, and shrinkage. Issues with the ways in which sharp force trauma may appear in burned nonhuman proxies may result in misleading conclusions for forensic investigators during their casework (Liebschner, 2004).

There have been further conflicting views on whether nonhuman proxies are good models for humans. Aerssens, Lowet, and Dequeker (1998) also conducted research on the use of human versus nonhuman proxies. They were especially interested in comparing interspecies differences in bone density, collagen content, ash weight, and metabolic weight to determine the best specimen to use as a human proxy. Ultimately, Aerssens, Lowet, and Dequeker (1998) discovered that "significant interspecies differences are present for each of the examined bone composition parameters, both in cortical and trabecular bone" (p. 667). The authors concluded by reiterating that their research showed considerable interspecies variation regarding the composition, density, and mechanical abilities of the bones, and they cautioned against swapping any species out for another as a proxy (Aerssens, Boonen, Lowet, & Dequeker, 1998).

Similar results were discovered by Prat et al. (2012) who examined ballistic trauma in human and pig remains. Prat et al. (2012) found that overall motion of the pigs' thoracic cavity during the ballistic event was much greater than that of the post-mortem human cadavers experiencing the same force, and that the "bone quality of the ribs plays

an important role in the biomechanical behavior of the chest wall" (p. 184). The authors acknowledged that the pigs were useful analogues for studying pathophysiology in humans but were not useful for studying biomechanics (Prat et al., 2012).

Symes et al. (2012) conducted a trauma and thermal experiment with multiple different saws on pig and human long bones. They found extremely similar results between the two species. Symes et al. (2012) include data and results that make density and collagen differences between humans and porcine proxies essentially null. This research, however, may be contingent on the age of the pig and human samples used. Additionally, Croft and Ferllini (2007) conducted research on sharp force trauma on pig ribs with screwdrivers and found that pigs can be viewed as acceptable proxies. The researchers noted that porcine ribs are similar in their structure, shape and weight (Croft & Ferllini, 2007). However, the findings of these two studies were not supported by Nogueira et al. (2018).

Nogueira et al. (2018) conducted saw mark research on both pig and human femora. The researchers found several significant differences in results between the pig and human femora, and they concluded their study by warning that pig femora may not be a good model for human femora as was previously claimed by Symes et al. (2012). Nogueira et al. (2018) also acknowledged that without sufficient caution, it is "difficult to extrapolate the results from pig bones to human samples…and it is not recommended to perform these experiments only on pig bones" (p. 161). These inconsistent findings and recommendations make examining human and nonhuman skeletal response an important factor in moving forward with forensic research.

Of further concern for some past literature is the use of defleshed samples. Soft tissues can often serve as insulators and protectors for the underlying bone tissue (Haglund & Sorg, 1997). In intact bodies, soft tissues that shrink and contract in heat have been shown to pull the limbs into certain positions which differentially exposes elements to the heat (Castillo et al., 2013). Additionally, Collini et al. (2015) found that in burned, pre-skeletonized bovine ribs, heat-related fractures were found around the margins of the trauma lesion while in burned fleshed ribs, heat-related fractures appeared more longitudinal and transverse, far from the site of the trauma lesion.

Of further significance, Buikstra and Swegel (1989) studied thermal alteration variation in cattle, dog, and human long bone samples that were fleshed, green defleshed, and dry. They found that dry bone did not fragment nearly as much or in the same locations as the fleshed and green bone did. Additionally, there were some slight differences between the ways in which the fleshed and the defleshed green bone reacted to heat. There was a higher fracture rate in the fleshed samples than in the still green but defleshed samples (Buikstra & Swegel, 1989).

Collini et al. (2015) reaffirmed the findings of Buikstra and Swegel (1989). They discovered that the remains that were fleshed when burned experienced significantly higher degrees of fragility and susceptibility to fragmentation than their skeletonized counterparts. Many studies (Bailey et al., 2011; Bandini et al., 2013; Castillo et al., 2013; Collini et al., 2015; Fujisaki, Hasegawa, Yokoyama, & Sasagawa, 2017; Gonçalves, Thompson, & Cunha, 2011; J. H. B. A. Humphrey & Hutchinson, 2001; Macoveciuc et al., 2017; Nogueira et al., 2018; Nogueira et al., 2016) have worked with defleshed, though often still green, bone. The lack of soft tissue presence may have impacted their

results. Haglund and Sorg (1997, p.3) caution researchers against ignoring the impact that soft tissue has on taphonomy, calling this bias the "myth of flesh." The current study addresses this issue by working with fleshed remains.

Access to resources and technology for some previous studies has also been a limiting factor. Among others, some of the most common past methodology for examining trauma has included standard microscopy, scanning electron microscopy, and histology, which can be highly destructive forms of analyses that require samples to be taken for examination. Further, because tissue must be removed in order to use these forms of analysis, data from the traumatic defects on fragile burned bone may be lost due to the high susceptibility of fragmentation, a concern addressed by Baier et al. (2017).

With the current progression of technology and its availability, more intensive and less invasive examination of trauma in burned bone is possible. A recent study done by Waltenberger and Schutkowski (2017) shows that both micro computed tomography (micro-CT) and digital microscopic methods are excellent resources for analyzing thermally altered trauma in bone, though they used only pig ribs. The researchers found that the digital microscopic measurements and imagery they took from the kerfs of their experimentally burned bone were more detailed than those produced by the micro-CT.

While the radiological micro-CT method used by Waltenberger and Schutkowski (2017) is appealing for its high resolution and noninvasive scanning technique, it is stymied in accessibility by its extremely high cost. Digital microscopes, however, can be cost effective for forensic labs hindered by budget constraints. Additionally, digital microscopes are easier and more comfortable to work with than traditional microscopes, and the images are comparable in quality and field of view (Derose, 2018).

With the success of digital microscopy in examining trauma on burned and unburned remains, it is useful to assess the appropriate strength, and thus cost, of the microscope needed to make determinations on tool class and the potential for individualization. Additionally, the ability to use photogrammetry and produce 3-D models and sample profiles with certain digital microscopes makes them even more appealing for investigators. Various methods of digital microscopy — expensive versus inexpensive digital microscopes — have not been used to conduct a comparative study between their relative effectiveness in examining kerf alterations at different stages of burning. A reevaluation of the applications of digital microscopy technology must be assessed. These new digital techniques open a range of possibilities for further research in understanding the effects of thermal alterations on traumatically injured human remains.

Silicone casting has additionally proven a useful method for modern forensic investigators in looking at tool type. Making casts is a nondestructive method of preserving trauma in bone in the form of direct negatives of the toolmarks. Products such as AccuTrans, Mikrosil, and Alec Tiranti RTV putty silicone casting material are simultaneously cost effective, time efficient, and easy to use, making them ideal for forensic investigators. Success with using these products for trauma analysis of skeletal material is documented in the literature (Dittmar, Errickson, & Caffell, 2015; Prieto, 2007; Tegtmeyer, 2012).

Dittmar and colleagues (2015) used three different silicone casting materials in sheep femora and in well-preserved archaeological skeletal samples with indications of trauma to make a recommendation for the most appropriate casting material. The researchers used Xantropen L Blue, Mikrosil, and Alec Tiranti RTV putty silicone. They

found that the paste ratios were difficult to approximate with the Xantropen and Mikrosil amounting to either non-setting casting material or material that set too quickly. Of further concern is the staining left behind on the bone samples by both Mikrosil and Xantropen. The researchers also warned about the issues of air gapping with improperly mixed or insufficient casting materials which can lead to loss of data.

Dittmar et al. (2015) also discovered that bone morphology was unaltered, and no damage occurred to the bone cortex with the use of any of the materials. Their final recommendation is for the use of Alec Tiranti RTV putty silicone. However, this casting material is available only in the United Kingdom, limiting its applicability to the forensic science community. Tegtmeyer (2012) used AccuTrans red silicone casting material and did not report any of the issues noted by Dittmar et al. (2015).

Conclusion

Several issues have been addressed throughout this literature review including the use of nonhuman remains as research proxies, whether different technological levels of digital microscopy can tell us forensically significant information about tool class, and the ways in which the bones and kerfs may alter in the presence of heat. Because trauma analysis is so heavily scrutinized due to its legal ramifications, these issues must be addressed (Schmidt & Symes, 2015). The current research reexamines these issues while addressing the lack of literature on cleaning and preparing burned remains for analysis.

II. MATERIALS AND METHODS

Sample Materials

This study used two different species: *Sus scrofa* (pig) remains and a single individual's donated human remains. Neither IACUC approval nor IRB approval was required for this project as no live subjects were used, and the pig remains were purchased from a butcher shop and the human remains were provided through the Texas State Willed Body Donation Program. Several pilot studies with individual pig elements were conducted to ensure the reliability and repeatability of the methodology and analyses.

Following the 10 total pilot studies conducted with pig ribs, femora, trotters, and ham hocks, a whole, deceased pig weighing 54.43 kg. (102 lbs.) dressed (~ 66 kg. or ~145 lbs. live) was purchased from Granzin's Meat Market in New Braunfels, Texas. The exact age of the pig was unknown; however, many of the long bone epiphyses were not fully fused suggesting that the pig was of a young age (Zeder, Lemoine, & Payne, 2015). This assessment was corroborated by the meat producer who estimated a pig that size to be about 16 weeks old. The pig was gutted, so the ventral side of the ribs were already cut upon receiving the pig.

An individual donated to the Texas State Willed Body Donation Program under the Universal Anatomical Gift Act for trauma research was also used in this study following full ethical approval by the Forensic Anthropology Center at Texas State board of directors. The individual (donor 2020.006) was an unautopsied 80-year-old White male weighing 59.87 kg. (132 lbs.) with a stature of 168 cm. (5'6"). Only half of this human donor was traumatically and thermally altered to minimize the destructive

analysis done on human remains. Multiple elements were selected from both the human and nonhuman samples to increase the efficiency and sample size. From each set of human and nonhuman remains, the femora, humeri, radii, ulnae, tibiae, fibulae, and ribs were used.

Preparing the Sample Materials

For the pig, extraction of the sample materials was achieved by carefully measuring and planning of the incisions sites (see *Fig. 1*). The limbs were carefully removed from the carcass at the joints with the use of a scalpel (see *Fig. 2*).

Figure 1. Pig Preparation. *Pig marked with sections for removal of necessary elements. The ventral portion of the pig was cut before purchase for removal of the internal organs.*

The rib cage was separated from the vertebral column with the use of a Lem™ 16-inch heavy duty handheld meat saw with a ½" wide blade. Fourteen ribs were removed on the right side of the pig, and 15 ribs were removed from the left side of the pig.

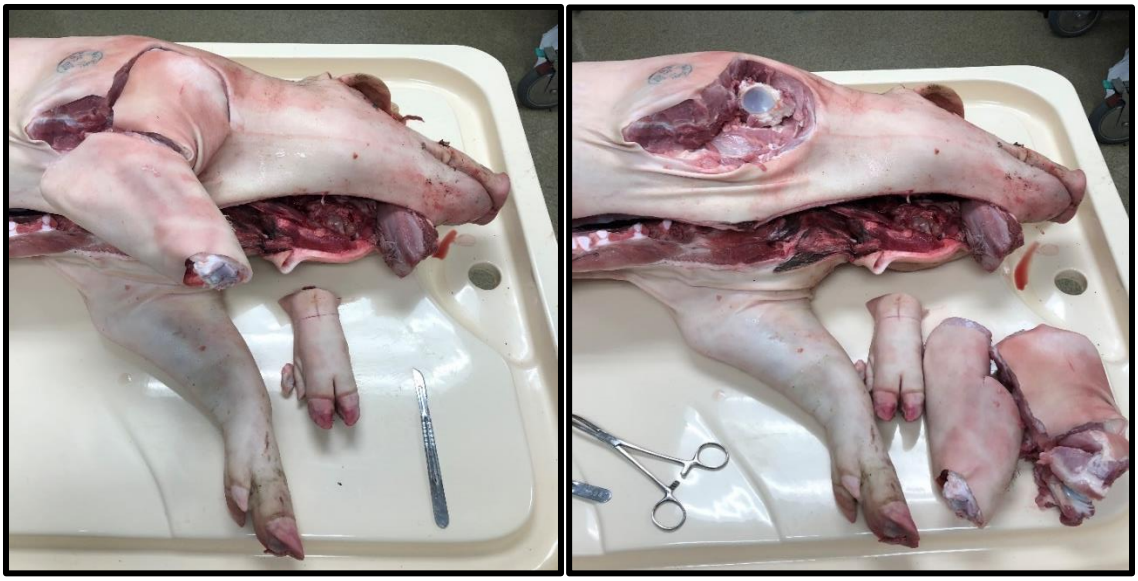

Figure 2. Pig Dismemberment. *Beginning to remove elements at their joint margins. In the image on the left, the trotter containing the carpals, metacarpals, and phalanges have been removed, exposing the distal radius and ulna. In the image on the right, the radius, ulna, and humerus have also been removed, exposing the glenoid fossa of the scapula.*

One half of a human donor was permitted for use in this study, so research was conducted on only the right side of the individual's body. Each long bone element was carefully removed from the donor at the joint with the use of scalpels in order to preserve the integrity of the soft tissue, full bone, and the adjacent bones. The right humerus, radius, ulna, femur, tibia, and fibula were removed. The right ribs were removed by cutting through the anterior costal cartilage at the fourth rib and moving laterally and posteriorly. Extreme care was taken to avoid accidentally cutting the rib shafts as they were removed from the vertebral column. A Stryker autopsy saw was used to remove ribs four through ten from the vertebral column as well as from the sternum, as much of the cartilage had ossified. Because just a half of a human donor was being used, each of the long bone elements was cut in half proximally and distally with the Lem™ handsaw to maximize the number of samples being studied (n=19).

Tissue depth was also measured for each pig and human element by cutting a small slit in the tissue and inserting a measuring rod at the midpoint of each element.

These measurements were important to determine before inflicting the trauma so that the pig and human samples received identical skeletal trauma. Soft tissue from the human or pig remains were carefully removed with scalpels so that the same tissue depth was present in each matching element. The skin for each element was preserved, so it could be rewrapped around the sample before burning.

Sharp Force Trauma

The weapons used to inflict the stab and cut wounds were four different IKEA Vorda Chef's flat-edge (FE) knives and four different IKEA Vorda serrated-edge (SE) bread knives, which are both standard household blade types. Additionally, these were the blades used in Waltenberger and Schutkowski (2017), so the data from this study could be compared with their results using sheep ribs. The Chef's knife with the non-serrated or flat-edge (FE) blade had a total length of 337 mm, a blade length of 203 mm, and a maximum blade width of 50 mm. The bread knife with the serrated edge (SE) had a total length of 368 millimeters. The maximum blade length was 230 millimeters, the width was 40 millimeters, and there were 6 millimeters between each tooth on the blade.

A Chicago Electric Power Tools heavy duty 6-amp reciprocating saw (RS) and Warrior General Purpose Bi-metal saw blades with six teeth per inch (TPI) were used to help create kerf marks. This saw was selected because it is the type of mechanical saw used most commonly in modern dismemberment cases (Symes et al., 2010). The reciprocating saw was used with a serrated blade in this study. The blade had a length of six inches with 4.23 millimeters between each tooth (6 TPI).

Additionally, the Lem™ 16-inch heavy duty handheld meat saw (HS) with a ½" wide blade, selected because it is a highly popular model of handsaw, was used to create kerf marks on each sample. An incomplete saw mark was made on the most distal portion of each long bone diaphysis and on the posterior portions of each rib. The total blade length was 16 inches with four and a half teeth per centimeter (see *Fig. 3*).

Figure 3. Tools Used in the Study. *From left to right, Ikea Vorda Chef's knife (flat-edge); Ikea Vorda bread knife (serrated-edge); Lem ™ handsaw; and Chicago Electric® reciprocating saw.*

For each of these tools, dial calipers were used to measure the thickness of each blade. Before measuring each blade, the calipers were always fully closed and set to "0." Each of the blade thicknesses can be seen in Table 3.

Table 3. Weapon Measurements. *Blade measurements of all the weapons used in the study.*

WEAPON	BLADE LENGTH	MAX WIDTH	TEETH PER CM	BLADE THICKNESS
FE KNIFE	203mm	50mm	----------	0.05 mm – 2.00 mm
SE KNIFE	230mm	40mm	~ 2 teeth	0.07 mm – 2.00 mm
RSAW	125mm	18mm	~ 3 teeth	.95 mm
HANDSAW	406mm	12.7mm	~4.5 teeth	.70 mm

A device was constructed in order to standardize the trauma motion and impact (see *Figs. 4-5*). The trauma device is closely related to the design from the study done by Waltenberger and Schutkowski (2017). Two trauma carriages were created – one for the flat-edge knife and one for the serrated-edge knife. The basic design of the trauma carriage is a PVC pipe inlaid in a concrete block with two perpendicular bolts through the PVC pipe in the concrete to keep it from rotating. A PVC coupler was added to either end of the inlaid PVC pipe. The trauma stand consisted of two metal rods that were erected and attached to two, threaded floor flanges, which were bolted to a wooden base. The trauma carriage could then slide easily down the erected rods without friction. Each knife was positioned and attached to the trauma carriages with adhesive.

Figure 4. Trauma Carriage Forms. *Two bolts were inserted perpendicularly into the inner pipe to stabilize and prevent rotation since internal pipe rotation was discovered in the pilot studies.*

Furthermore, because the trauma carriage was dropped with a known weight, force was able to be calculated. Each knife weighed approximately 150 grams, and the carriage itself weighed 2,988 grams. This weight gave a respective force of about 31 Newtons (N) while the carriage in the study done by Waltenberger and Schutkowski had a force of about 24 N.

$$Force = mass \times acceleration \qquad F = (3.138kg)(9.81m/s^2) \qquad F = 30.78\ N$$

However, it is more appropriate for this experiment to be measured using potential energy rather than force. This change is necessary since the force calculated above is simply the measure of the weight of an object, which neglects the effects of the increase in velocity during freefall. The trauma carriage, of predetermined mass, was raised to a set height and allowed to freefall, ultimately impacting the samples and

creating standardized kerfs. In order to normalize the destructive capability of the testing implement, the quantity which must be controlled is work – a change in the state of energy. For calibration purposes, the work done by this study's knives in freefall was equivalent to the work done in Waltenberger and Schutkowski (2017).

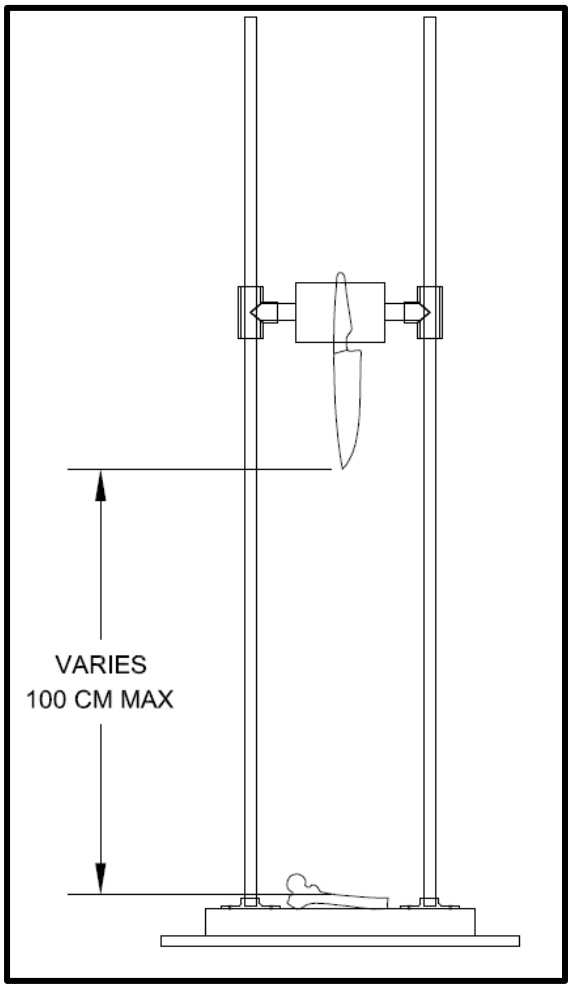

Figure 5. Standardized Trauma Device Rendering.
Rendering of sharp force trauma device constructed for this research. Note that the femur vector is rotated 90° from its regular trauma position for ease of viewability.

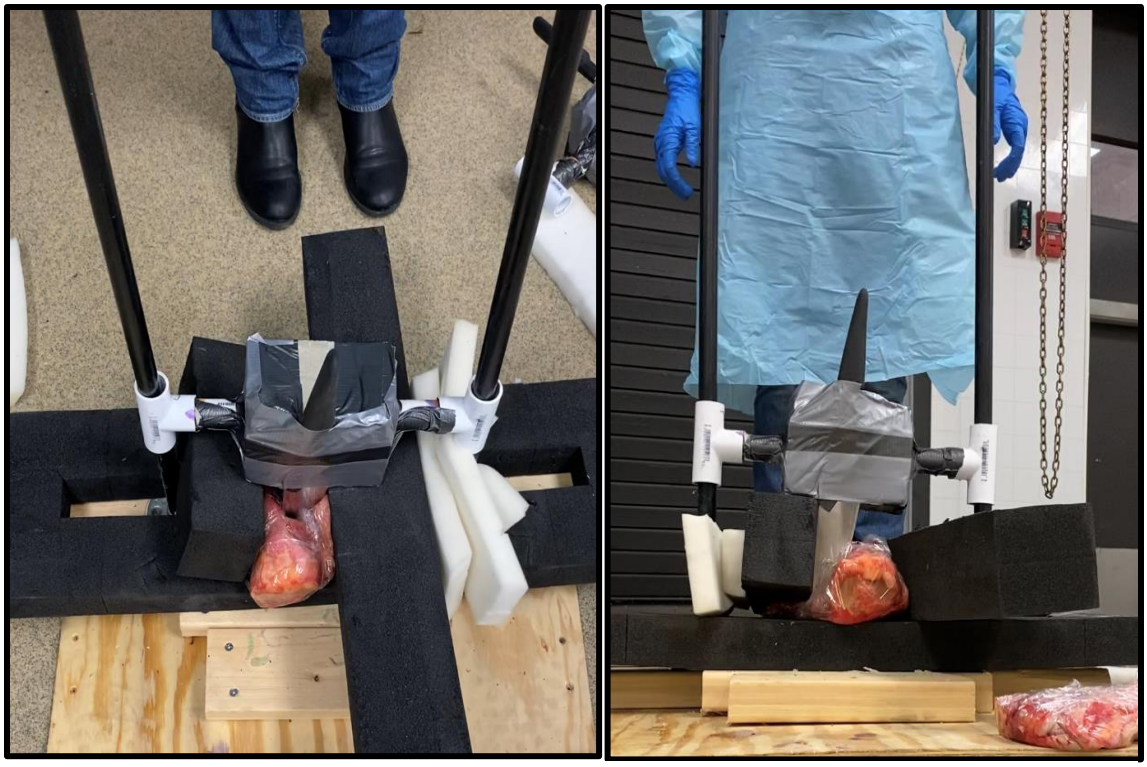

Figure 6. Standardized Trauma Device with Sample. *In the image on the left, the trauma device is impacting between the tibia and the fibula, with the sharp edge of the blade creating a kerf mark on the fibula. In the image on the right, the trauma device is impacting the medial tibia. Notice the tilt of the knife; the space around the PVC couplers created room for slight tilt of the carriage.*

This calibration was achieved by calculating the knives' potential energy and adjusting the height of the current study's trauma carriage to produce the same number of joules. The work done may be calculated as the change in potential energy from the knife and carriage in the raised position to the neutral or ground-level position.

$$E_{potential} = mass \times acceleration \times distance = mass \times gravitational\ constant \times height$$

After estimating the height at which Waltenberger and Schutkowski's (2017) carriage was dropped into freefall (~0.65 meters), their device's potential energy was calculated to be equivalent to about 15 joules.

$$E_{potential} = (2.404kg)(9.81m/s^2)(0.65m) = 15.30\ joules$$

The current study thus used a drop height – from the tip of the blade to the top of each sample – for the knife and carriage of 0.5 meters to produce equivalent energy.

$$E_{potential} = (3.138kg)(9.81m/s^2)(0.50m) = 15.30\ joules$$

However, doing this caused the ribs to be fully severed, which was likely due to the relative differences in both the age of this study's pig samples compared with the age of Waltenberger and Schutkowski's (2017) samples as well as species-level differences in the ratio of compact to cortical bone depth in the ribs. The height was thus adjusted to 0.20 meters, which can be understood to produce just 6.16 joules.

$$E_{potential} = (3.138kg)(9.81m/s^2)(0.20m) = 6.16\ joules$$

Waltenberger and Schutkowski (2017) only studied ribs. Because the current study is examining multiple elements, the relative energy used was doubled on long bone elements to create measurable data on the bone since the cortical bone on these elements is thicker, and pilot samples demonstrated that greater potential energy was needed to produce cut marks. The same calculated energy and implements on matching elements of both the nonhuman and human sample (e.g. pig femur and human femur) were used.

Long bones: $E_{potential} = (3.138kg)(9.81m/s^2)(1.15m) = 35.40\ joules$

The sharp force trauma with the trauma device was inflicted bilaterally and symmetrically on the whole pig remains. Each element was measured, and the knives were dropped on the same approximated points for each side. Each proximal and distal half of the human long bone elements were treated like separate elements and received identical stab and saw marks. Two stab marks were inflicted on each human and nonhuman element on the proximal and mid-portion of the diaphysis. The ribs received each of the stab marks on the anterior and mid-lateral portions (human) and the ventral and mid-lateral portions (pig) of the elements for a total of 41 flat-edge kerfs and 41 serrated-edge kerfs represented on the elements.

Each element was held in place by foam on a foam block base inside a wooden box (see *Fig. 7*) or packed tightly with foam on top of the foam block base without the wooden box depending on the length of the element. A series of stabs (vertical knife position) was conducted to create different kerfs and toolmarks. Each of the stab marks were carefully created so that the knife tip did not directly enter the bone, as the tips either broke off in the bone or the knives came off the carriage during the pilot studies. Instead, the knife tip remained clear, and the sharp edge of each knife was brought down perpendicularly against the bone margin of each sample. There was some space between the couplers and the vertical rods, so slight lateral movement of the carriage did occur. This affected the precision with which the elements were impacted.

Figure 7. Stabilizing Method for SFT. *Pig femur packed with foam in a wooden box to prevent movement during the trauma event.*

For the pig ribs, stab marks were made at approximately the same positions on each left and right rack of ribs. For the human ribs, four grouped ribs (rib four through rib seven) were stabbed and set aside to be used as the control sample once macerated. The remaining three ribs (rib eight through rib ten) were also stabbed and then set aside for use in the burn study. Because both the human and pig ribs were removed from the pig nearly whole, the curved nature of the ribs caused some difficulty in correctly approximating where the knife would hit as the ribs were difficult to align. Additionally, the weight of the falling knife and carriage often created fractures in the ribs ranging from incomplete to complete transverse and oblique fractures though foam was arranged to prevent the carriage from hitting the ribs.

The incomplete dismemberment cuts made with the two types of saws – reciprocating and handsaw – were additionally made to be as identical as possible on each element. This was difficult as the reciprocating saw tended to rebound, and the samples, though strapped tightly to a board (see *Fig. 8*), sometimes rotated with the force of the vibration from the saw. Each element from the pig and human remains received one reciprocating saw mark on the distal end (n= 41 reciprocating saw marks). Though the saw marks were not meant to be complete or continuous, due to the thinness of the samples, several of the pig ribs fully separated into anterior and posterior (human) or ventral and dorsal (pig) portions.

Furthermore, the Lem™ heavy-duty handsaw was used to create an incomplete saw mark distal to the reciprocating saw marks on the distal end of the diaphysis for the long bones and on the posterior portion of the ribs (n=41 handsaw marks). This type of saw was much easier to control both in terms of kerf placement as well as kerf depth.

Figure 8. Stabilizing Method for Saw Marks. *Defleshed pilot pig femur Velcro-strapped to a 2 x 4 board to hold in place during use of the reciprocating and handsaws. Two reciprocating saw marks are visible on the diaphysis.*

Tables 4 and 5 provide a description of the trauma location and the purpose of each sample from both the pig and human remains that were used. The samples marked "Control" were unburned.

Table 4. Pig Pilot Sample Descriptions and Purposes

Sample#	Element	Sharp Force Trauma	Location	Purpose
Pilot 1	Pig ribs (4)	Flat and Serrated Edge(F/SE)	Mid	Burn
Pilot 2	Pig ribs (4)	Flat Edge (FE)	Mid	Burn
Pilot 3	Pig ribs (6)	F/SE, Recip. Saw (RS)	Mid, Prox	Burn
Pilot 4	Trotters (4)	FE	Prox, Dist	Burn
Pilot 5	Trotters (4)	F/SE	Prox, Dist	Burn
Pilot 6	Pig ribs (6)	F/SE	Mid	Control
Pilot 7	Pig femur (1)	F/SE, RS	Prox, Mid, Dist	Control
Pilot 8	Pig femur (1)	F/SE, RS	Prox, Mid, Dist	Control
Pilot 9	Pig femur (1)	F/SE, RS	Prox, Mid, Dist	Burn
Pilot 10	Pig femur (1)	F/SE, RS	Prox, Mid, Dist	Burn

Table 5. Human and Pig Study Sample Descriptions and Purposes

Sample#	Element	Sharp Force Trauma	Location	Purpose
1	Pig femur (R)	F/SE, RS, HS	Prox/Mid, Dist	Burn
2	Pig femur (L)	F/SE, RS, HS	Prox/Mid, Dist	Control
3	Pig humerus (R)	F/SE, RS, HS	Prox/Mid, Dist	Burn
4	Pig humerus (L)	F/SE, RS, HS	Prox/Mid, Dist	Control
5	Pig tibia (R)	F/SE, RS, HS	Prox/Mid, Dist	Burn
6	Pig tibia (L)	F/SE, RS, HS	Prox/Mid, Dist	Control
7	Pig fibula (R)	F/SE, RS, HS	Prox/Mid, Dist	Burn
8	Pig fibula (L)	F/SE, RS, HS	Prox/Mid, Dist	Control
9	Pig ulna (R)	F/SE, RS, HS	Prox/Mid, Dist	Burn
10	Pig ulna (L)	F/SE, RS, HS	Prox/Mid, Dist	Control
11	Pig radius (R)	F/SE, RS, HS	Prox/Mid, Dist	Burn
12	Pig radius (L)	F/SE, RS, HS	Prox/Mid, Dist	Control
13	Pig ribs (R)	F/SE, RS, HS	Ant, Post	Burn
14	Pig ribs (L)	F/SE, RS, HS	Ant, Post	Control
15	Human femur (Dist)	F/SE, RS, HS	Prox/Mid, Dist	Burn
16	Human femur (Prox)	F/SE, RS, HS	Prox/Mid, Dist	Control
17	Human humerus (Dist)	F/SE, RS, HS	Prox/Mid, Dist	Burn
18	Human humerus (Prox)	F/SE, RS, HS	Prox/Mid, Dist	Control
19	Human tibia (Dist)	F/SE, RS, HS	Prox/Mid, Dist	Burn
20	Human tibia (Prox)	F/SE, RS, HS	Prox/Mid, Dist	Control
21	Human fibula (Dist)	F/SE, RS, HS	Prox/Mid, Dist	Burn
22	Human fibula (Prox)	F/SE, RS, HS	Prox/Mid, Dist	Control
23	Human ulna (Dist)	F/SE, RS, HS	Prox/Mid, Dist	Burn
24	Human ulna (Prox)	F/SE, RS, HS	Prox/Mid, Dist	Control
25	Human radius (Dist)	F/SE, RS, HS	Prox/Mid, Dist	Burn
26	Human radius (Prox)	F/SE, RS, HS	Prox/Mid, Dist	Control
27	Human ribs (4-7)	F/SE, RS, HS	Ant, Post	Control
28	Human ribs (8-10)	F/SE, RS, HS	Ant, Post	Burn

Post-Trauma Radiographs

Following trauma infliction with the stabbing instrument and the saws, radiographs were taken using a MinXRay HF120/60HPPWV PowerPlus™ portable X-ray machine (see *Fig. 9*). X-rays were taken to ensure that each element exhibited a kerf or toolmark in the appropriate place and to confirm that no structural deformations were present in the bone. Such deformations may affect fracture propagation or how the trauma appeared in the bone. Each element was placed on the image receptor grid directly below the X-ray beam. The individual sample placements and settings can be found in Table 6. See Appendix A for radiographs.

Table 6. MinXRay Settings for Select Elements.

Sample	Element	Sharp Force Trauma	Ht. of beam	kV	mAs/sec
Pilot 6	Pig ribs (6)	F/SE	40cm	40	0.15
Pilot 6	Pig ribs (6)	F/SE	33.5cm	40	0.15
Pilot 7	Pig femur (R)	F/SE, RS	40cm	40	0.10
Pilot 8	Pig femur (L)	F/SE, RS	40cm	40	0.10
Pilot 9	Pig femur (R)	F/SE, RS	40cm	40	0.10
Pilot 10	Pig femur (L)	F/SE, RS	40cm	40	0.10
15	Human femur (Prox)	F/SE, RS, HS	22cm	40	0.20
16	Human femur (Dist)	F/SE, RS, HS	22cm	40	0.40
17	Human humerus (Prox)	F/SE, RS, HS	22cm	40	0.10
18	Human humerus (Dist)	F/SE, RS, HS	22cm	40	0.10
19	Human tibia (Prox)	F/SE, RS, HS	22cm	40	0.40
20	Human tibia (Dist)	F/SE, RS, HS	22cm	40	0.40
21	Human fibula (Prox)	F/SE, RS, HS	22cm	40	0.40
22	Human fibula (Dist)	F/SE, RS, HS	22cm	40	0.40
23	Human ulna (Prox)	F/SE, RS, HS	22cm	40	0.10
24	Human ulna (Dist)	F/SE, RS, HS	22cm	40	0.10
25	Human radius (Prox)	F/SE, RS, HS	22cm	40	0.10
26	Human radius (Dist)	F/SE, RS, HS	22cm	40	0.10
27	Human ribs (4-7)	F/SE, RS, HS	32cm	50	0.01
28	Human ribs (8-10)	F/SE, RS, HS	32cm	50	0.01

Figure 9. Portable X-ray Machine. *X-ray used to take radiographs of samples pre- and post-trauma. A pig femur is being imaged here.*

Preparing the Unburned Samples

One half of the pig with the inflicted trauma was set aside to be macerated in an incubator. This half was used as a control to study the ways in which the kerfs and cut marks were modified by thermal alteration. One half of each of the human long bone elements (e.g. the proximal half of the humerus) was additionally incubator processed and used as a control to study the kerf and cut mark differences on the burned counterparts (e.g. the distal half of the humerus). While the elements being compared for the human sample were not bilateral or symmetrical, they were deemed acceptable to use

as the same structure and density is largely present throughout the proximal and distal diaphyseal portions of these elements. The matching stab and saw mark traumas were inflicted solely on the midshaft of each respective proximal and distal section.

The control samples were processed by removing most of the soft tissue carefully by scalpel following trauma infliction. Often, the soft tissue could be removed by hand by gently pulling it back from the bone with some help of the scalpel. Many elements retained a significant amount of cartilage around the proximal and distal portions. A scalpel pressed parallel to the bone was used to carefully scrape some of it away. The scalpel was never used in the vicinity of the kerfs to avoid introducing SFT artifacts.

The samples typically retained a significant amount of grease, cartilage, and some muscle tissue, so they were placed in a Thermo Scientific 2051 incubator. Because incubators are suitable for delicate remains such as fractured fetal bone (Feeser, 2018), they are appropriate to use for the traumatized bone as well to avoid further damage or loss of data. The samples were submerged in a closed plastic container with water and an industrial degreaser called Foremost 1553-ES Super Kleen® (Delta Foremost Chemical Corporation) at a 1:8 ratio. The incubator was set to about 65°C (150°F). Samples varied in how long they needed to remain in the incubator based on the amount of remaining tissue, with most samples remaining for about 48-72 hours. Remaining soft tissue was easily and carefully removed with tweezers, rinsing, and gently brushing with a soft-bristle toothbrush for a final cleaning. The samples were allowed to dry on a labeled tray in the Osteological Research and Processing Laboratory before transport to the Grady Early Forensic Anthropology Research Laboratory for analysis.

Thermal Alteration

Following the infliction of the sharp force trauma with the trauma device, half of the pig remains (n=20 elements) underwent thermal alterations using a 55-gallon grill at the Grady Early Building (see *Fig. 11*) as grills are common and easily accessible to perpetrators (Associated Press, 2007; Zavala, 2018). The human remains were burned in the same grill at the Forensic Anthropology Research Facility as these elements are considered biohazardous. Thermal alterations occurred with the use of an open flame and direct heat instead of indirect heat from an electric furnace as has been commonly used in past studies (Castillo et al., 2013; Collini et al., 2015; Macoveciuc et al., 2017; Thompson, 2005; Waltenberger & Schutkowski, 2017). This open-flame, direct heat technique was achieved through the use charcoal briquettes. Charcoal briquettes are suitable because they are both inexpensive and easily attainable, making them an ideal fuel for perpetrators. Further, charcoal briquettes burn steadily, at consistent temperatures, and aren't hindered by seasonality as can be the case with firewood.

Before burning, each element was placed within an individual, small, wire basket (see *Fig. 10*). These fine mesh wire baskets allowed for easy turning and removal of the samples as well as a method for easy collection of the burned remains. It also mitigated issues with bone fragment collection, a common problem when dealing with carbonized and calcined bone.

Figure 10. Mesh Baskets for Burned Samples. *The left image shows a superior view of a pig femur inside a wire basket, prepared to be burned. The right image shows the same element in the wire basket from a lateral view.*

Figure 11. Grill with Data Loggers. *The left image shows the open grill with inner mesh removed. The NeuLog® data loggers are seen inside the grill on the two wire baskets containing pilot samples. The right image shows the same grill from a lateral view.*

The temperatures to which the samples were exposed were tracked and recorded with the use of two NeuLog® Wide Range Temperature sensors that can record data between -200°C and 1200°C. Additionally, a ThermoWorks® Type-K Hi-Temp ceramic-insulated thermocouple probe rated for -58°C to 1200°C (-50°F to 2200°F) with an EasyLog USB data collection logger (see *Fig. 12*) was used to supplement the NeuLog ® Wide Range Temperature sensors as the ThermoWorks® thermocouple probe proved to

Figure 12. ThermoWorks USB Data Logger. *Logger was used to track temperature of charcoal to which samples were directly exposed.*

be more heat resilient.

Temperature is an important measurement to discover how varying thermal ranges affect kerfs and fracture propagation. Each sensor was placed in strategic positions to collect as much temperature data as possible. One sensor was placed into the charcoal in direct contact with the samples, one sensor was placed at the proximal end of the superior surface of the samples not in contact with the charcoal, and the last sensor was placed at the distal end of the superior surface of the samples; the temperatures were tracked and averaged for each sample throughout the duration of each burn period (see *Table 7*). The graphs for the corresponding table data are shown in Appendix B. Each sample was flipped once during burning to ensure even coverage of heat and to partially represent the act of "stoking" that perpetrators often use while burning evidence. Depending on the observed temperatures, the samples were burned for approximately one to two hours until fully or almost fully carbonized and often with some calcination present.

Unfortunately, the NeuLog® Wide Range Temperature sensors stopped working part of the way through burning the last set of pig samples, so the data on temperature for the pig rib and human samples is limited to the ThermoWorks® thermocouple probe, which was placed in the charcoal under the samples. The NeuLog® sensors likely became damaged during the multiple pilot studies in which they were used. The elements were burned for approximately the same length of time with temperatures reaching similar maximum temperatures. The data for the first set of nonpilot pig remains shows a lot of variation in the temperatures when compared with the ThermoWorks temperature data taken from the pig ribs and the human burn samples. This discrepancy indicates that it's possible the NeuLog sensors were not recording accurately, as they did stop collecting temperatures above 50.0°C during the following burn.

Table 7. Temperature Data from Various Burns. *Data has been presented with the maximum temperature reached, minimum temperature reached, and average temperature reached.*

Species and Elements	Logger	Duration of Burn	Maximum Temp.	Minimum Temp.	Avg. Temp
Pig Burn: femur (R), humerus (R), tibia (R), fibula (R), ulna (R), radius (R)	NeuLog®	2:57:53	871.3°C (charcoal) 443.6°C (superior sample surface)	24.1°C (charcoal) 25.7°C (superior sample surface)	151.78°C (charcoal) 163.63°C (superior sample surface)
Pig Burn: ribs 1-14 (R)	ThermoWorks®	1:45:58	589.5°C (charcoal)	151.0°C (charcoal)	----
Human Burn: femur (R), humerus (R), tibia (R), fibula (R), radius (R), ulna (R), ribs 8-10 (R)	ThermoWorks®	2:34:21	678.0°C (charcoal)	109.0°C (charcoal)	----

Collection and preservation of the burned remains followed standard forensic techniques (Dirkmaat, Olson, Klales, & Getz, 2012; Symes et al., 2012). Both Dirkmaat et al. (2012) and Symes et al. (2012) suggest that because the burned remains are so fragile and friable, they should be packaged carefully in heavy-duty plastic wrap for transport to a lab. Any elements still associated with soft tissue were loosely wrapped in plastic and immediately transported to the Osteological Research and Processing Laboratory. Each sample was given a label with human or nonhuman, bone section, and length of burn.

Preparing the Burned Samples

During the course of the multiple pilot studies, the most efficient and the gentlest method for cleaning remaining tissue or clinker from the burned bone was pursued. However, there is a serious lack of literature on how to properly clean burned remains (see *Discussion*), so the cleaning techniques utilized were experimental. Several attempts at various cleaning methods were made including using metal and wooden scraping tools and tweezers, pulling charred tissue away by hand, steaming using an incubator and a microwave, and warm water baths with degreaser. Each of these methods had various drawbacks and advantages.

The metal and wooden scraping tools often required some pressure to be placed on the bone, which could be highly fragile in places. Though fairly efficient, the use of these tools caused higher rates of fragmentation than did other methods. Removing tissue by hand was additionally cumbersome and dependent upon the level of clinker and tissue char. In order to remove tissue as gently as possible, the time constraints as well as the

inability to fully clean the tissue away with this method were outweighed by the relatively good preservation of the bone.

Steaming using the Thermo Scientific 2051 incubator was additionally attempted wherein samples were set on a fine-mesh sieve to avoid loss of bone fragments and enclosed in a plastic container. A few millimeters of water were placed in the bottom of the plastic container below the samples, and the incubator was set to about 65°C. The samples were checked every 24 hours to examine how the steaming process was going. After five days, the adhering tissue was warm and slightly easier to pull away from the bone. However, the method was largely unsuccessful in tissue removal, so it was not used with the study samples.

Another method with the incubator was attempted as well. Full submersion of pilot samples that were carbonized (not calcined) and still largely covered in adhering, charred tissue in water and Super Kleen® degreaser in a 1:8 ratio was conducted. These samples were enclosed in a plastic container and placed in the incubator at about 65°C for 24 to 36 hours. Because the water merely warmed and there was no movement of the samples in their container over the 24 to 36-hour period, there was extremely limited fragmentation observed. This method was highly successful in removing the charred tissue. A total of three traumatized and burned pilot samples (two trotters and one femur) were cleaned using this method, and one fragment was observed. This single fragmentation occurred as the sample was being macroscopically observed for remaining tissue.

To ensure that placing the carbonized samples in the incubator with the Super Kleen® degreaser was safe for burned remains with trauma, microscopic assessment of

some samples pre- and post-cleaning was conducted using a Leica M205 C digital stereomicroscope with the accompanying software, Leica Application Suite X (LAS X) purchased with National Science Foundation Major Research Instrumentation grant (Award #1920218). The kerfs and toolmarks on the samples were carefully cleaned for microscopic viewing using fine tipped brushes and a gentle air pump bulb to remove debris and clinker. The stereomicroscope and LAS X application were used to examine and measure length, depth, width, and unique tool class characteristics in the burned bone. Toolmarks were examined and measured at 20-fold and 67-fold magnification. Once the images were analyzed and recorded, the samples were brought to the Osteological Research and Processing Laboratory for cleaning in the incubator.

Following cleaning in the incubator, the same samples were imaged and measured to examine whether surface changes or significant alterations within the toolmarks occurred. There was mild obscuring of striae but adjusting the lighting settings on the stereomicroscope made almost all striae from the pre-cleaned samples visible. There was no significant loss of data observed. In fact, without the cleaning of the bone, the flat-edge kerf mark was not visible microscopically. Following the incubator cleaning, the flat-edge kerf mark could be viewed microscopically, and measurements could be taken. The warm water bath with degreaser method was therefore deemed acceptable for cleaning remaining tissue and clinker from carbonized remains.

Once the study's pig and human remains were brought to the Osteological Research and Processing Lab, they were examined for remaining soft tissue, and they were cleaned mechanically as necessary, or in the incubator if the tissue was too hardened to remove without causing damage to the elements. Every precaution was taken

to prevent further fracturing and damaging the remains. Each sample was then placed into sturdy, foam-packed cardboard boxes to prevent any sort of movement and further damage during transport and storage.

Analytical Techniques

The Leica M205 C digital stereomicroscope and Dino-Lite Edge digital microscope were used to examine both the burned and the unburned, cleaned kerfs and saw marks and were instrumental in determining whether blade type indicators remained present and discernible following thermal alteration. Both microscopes were also used to determine how differences in fracture propagation affect the ability to estimate tool class, and how the use of human or nonhuman remains alters the appearance of the trauma defects. See Appendix C for images produced with the Leica stereomicroscope.

The Leica digital stereomicroscope was used with LAS X software and Leica Map 7.4 software, and the Dino-Lite Edge digital microscope was used with DinoCapture 2.0 software. Each toolmark examined with the Leica stereomicroscope was analyzed under 20, 67, and 110-fold magnification. Using the Leica digital stereomicroscope, a total of 175 out of the original 216 toolmarks were examined. However, for each toolmark, multiple cross-sections of the kerfs were analyzed in Leica Map to gather as much data as possible regarding the characteristics being assessed, such as depth, width, and striae.

Using the Leica Map software, profiles of each multidimensional, complete kerf mark that were imaged on the stereomicroscope were extracted and analyzed for depth measurements. Additionally, these images were then transformed into manipulatable, three-dimensional models of which some examples may be viewed in Appendix D. These

models are being compiled into a reference library complete with information on species (human or pig), status (unburned or burned), tool type (flat-edge knife, serrated-edge knife, reciprocating saw, and handsaw), and duration of burn, if applicable. This digitized reference library of over one hundred models requires the use of MeshLab, an open source 3-D mesh processing program, and will be accessible and proprietary to the Forensic Anthropology Center at Texas State and the author.

Each toolmark (n = 61) examined with the Dino-Lite Edge digital microscope was examined at about 25 and 85-fold magnification, though this magnification was entirely dependent on the sample height and limitations of the microscope stand. The data collected from the Dino-Lite Edge digital microscope (n = 227 measurements) was used solely to compare with the Leica digital stereomicroscope. Both digital microscopes were used to gather data on cutmark length, width, and striae patterns as seen in Table 8.

Difficulties imaging high, curved surfaces were encountered with both microscopes, though the Leica stereomicroscope was better at dealing with the issue. Because there was more space to move the stage and to stitch together tile scans of varying depths, the Leica stereomicroscope and LAS X software were much more proficient in producing fully focused images. See Figure 13.

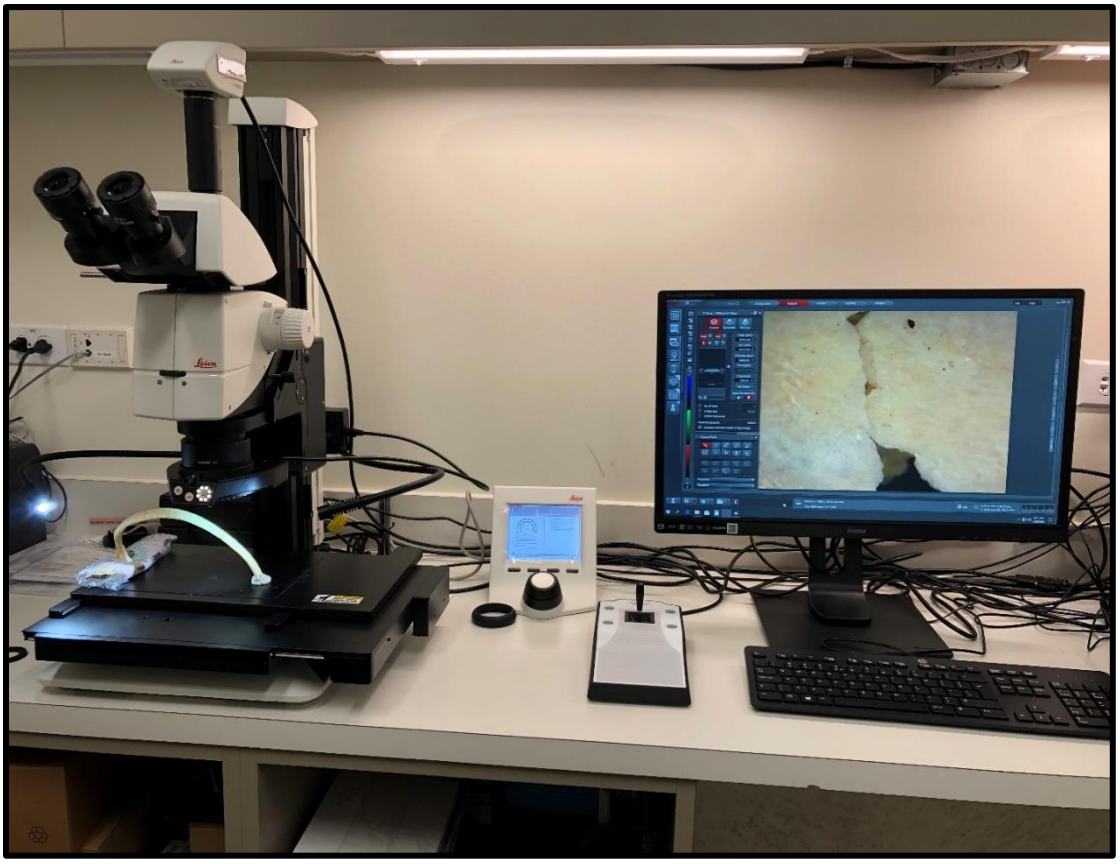

Figure 13. Leica Digital Stereomicroscope. *Imaging a flat-edge kerf mark on a human rib. The curved, high surfaces of the ribs proved challenging to image.*

Following these initial analyses with the digital microscopes, casts of the unburned and burned saw-mark kerfs were taken using Coltene President microSystem light body casting material (see *Fig. 14*). This material was selected as it was readily accessible in the Grady Early Forensic Anthropology Research Laboratory, its flexible, durable composition made it a good candidate for intact removal from the kerfs, and it was not likely to be plagued by the difficulties with other casting materials examined by Dittmar et al. (2015) such as staining since it is often used on living patient's teeth to make dental casts. These casts were taken by inserting the casting material cylinder into a Coltene Whaledent casting gun with a mixing tip. Each saw mark kerf was filled

continuously with the casting material and then left to dry for about five minutes. The casts were then gently peeled away for analysis.

Figure 14. Silicone Casting of Control Pig Samples. *Casting various saw marks in pig bones with Colten President microsystem light casting body material.*

Table 8. Tool Type and Associated Measurements. *Measurements for each tool type collected with the Leica and/or DinoLite digital microscopes.*

Tool Type	Measurements
Flat-edge blade	Length, width (max), width (mean), width (min), depth (max), depth (mean), opening angle
Serrated-edge blade	Length, width (max), width (mean), width (min), depth (max), depth (mean), opening angle, striae
Reciprocating saw	Length, width (max), width (mean), width (min), depth (max), depth (mean), striae
Handsaw	Length, width (max), width (mean), width (min), depth (max), depth (mean), striae

While casts from shallow kerfs were easily removed on burned and unburned bone, some of the deeper kerfs were more resistant to releasing the cast. This necessitated a few of the kerfs needing to be recast or removed from the dataset as they were simply too deep to cast. One of the burned reciprocating saw kerfs exhibited breakage in the form of cortical bone sloughing as the cast was attempted to be removed. This resulted in an entire section of cortical bone breaking away from the trabeculae around the toolmark.

As previously noted, taking casts of paired kerfs is helpful in determining kerf features that may have been overlooked or were too difficult to see on the inner walls. These casts were then viewed under the Leica digital stereomicroscope to illuminate any data which may have gone unnoticed in the initial analyses.

Statistical Analysis

Following the experimentation and data collection phase, statistical analyses were conducted in the Statistical Package for the Social Sciences (SPSS) software to address the current study's research questions. Data analysis on measurements including kerf length, kerf width, kerf depth, opening angle and the presence of striations for both the burned and unburned samples was done using descriptive statistics (range, mean, standard deviation, standard error of the mean, variance, skewness, and kurtosis). A Shapiro-Wilks test was conducted to test normality in the data, and it exhibited data that was not normally distributed necessitating the use of nonparametric tests.

A nonparametric Kruskal-Wallis one-way analysis of variance test was used to compare all the ratio-level measurement data to burned and unburned human and pig elements. The Kruskal-Wallis test is a broader test than the Mann-Whitney U-test and can determine stochastic dominance in a set of samples. Following the Kruskal-Wallis tests,

Mann-Whitney U-tests were used to compare the independent pairs of data including measurements from the control to burned human elements, control to burned pig elements, control human to control pig elements, and burned human to burned pig elements. These tests were done to consider where the source of variation was with significant Kruskal-Wallis results.

To study the presence of striae in the bone samples, chi-square tests of independence and goodness of fit tests were conducted. Silicone casts were reviewed qualitatively. Finally, the nonparametric equivalent of a Students T-test, the Wilcoxon Signed-Rank test, was used to evaluate the quality of measurements from the less expensive DinoLite microscope with the measurements taken with the more expensive Leica microscope.

Statistical tests

DATA COLLECTION	STATISTICAL TEST
1.) Kerf widths, lengths, and depths (min and max) pre- and post-burn (human vs. pig)	Descriptive statistics, Kruskal-Wallis, Mann-Whitney U-tests
2.) Presence of striae microscopically and with the silicone casted kerfs	Chi-Square Test of Independence, Goodness of Fit, qualitative assessment
3.) Comparable measurements between the expensive (Leica) and inexpensive (DinoLite) microscopes	Wilcoxon Signed-Rank Test

III. RESULTS

Eighteen long bones and 36 ribs in total had trauma administered to them and were macerated or burned for examination. Two-hundred and sixteen toolmarks were inflicted on the bones, but a total of just 175 toolmarks (81%) produced usable measurements (see *Fig. 15*). From these 175 toolmarks, seven measurements for flat-edge blades, eight measurements for serrated-edge blades, seven measurements for reciprocating saws, and seven measurements for handsaws were attempted to be pulled from each respective toolmark. These measurements can be seen listed in Table 8. Not all the toolmarks yielded the full set of data for a number of reasons ranging from the destruction of the kerf floor to complete separation of the kerf into divided bone halves to destruction of the kerf altogether.

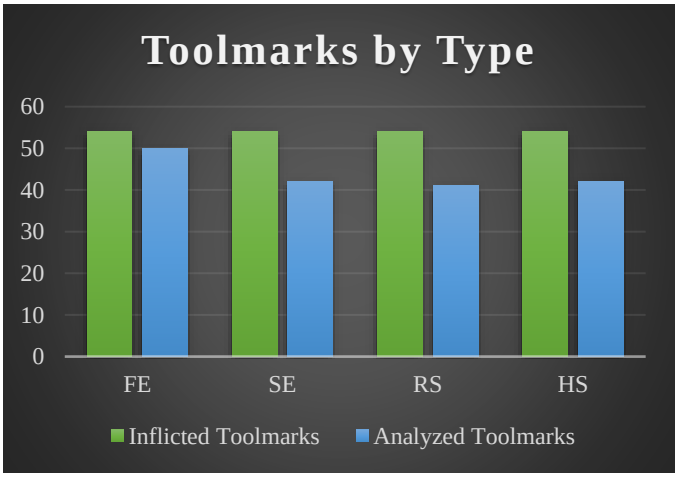

Figure 15. Inflicted vs. Analyzed Toolmarks.

Bone coloration in the burned samples varied from unburned areas to blackened areas, some white areas, and some white-blue areas with almost every sample showing some degree of calcination. Fragmentation and or fracturing occurred in every sample that underwent burning, with the pig remains and both human and nonhuman ribs being especially fragmentary. A much higher degree of fragmentation and bone loss occurred within the pig bone sample than within the human bone sample. Fracture patterns

included longitudinal and oblique cracking in the long bones and ribs, with some complete transverse fracturing appearing around cutmarks. Patina cracking and irregular, web-like cracking also appeared in the burned samples.

The unburned samples also exhibited some fracturing. Transverse and oblique fracturing were especially evident in the ribs of both the human and nonhuman samples, likely occurring due to the weight of the trauma carriage and the unsupported curvature of the ribs. The complete fractures occurred most often at the site of the flat-edge blade trauma.

Different types of trauma could be macro- and microscopically differentiated through several indicators. The flat-edge and serrated-edge knives could be distinguished by examining whether there was evidence for any crushing around the kerf and whether there was lifting of one of the kerf shoulders. Evidence of crushing, or sharp-blunt damage, around the kerf was indicative of trauma caused by the serrated-edge knife. The sharp-blunt damage caused by the serrated-edge blade was likely because the tip was blunter, so any contact with the bone surface produced more of a crushing than a slicing effect (Alunni-Perret et al., 2005). Though found in only two of the serrated-edge samples, the blade also left a scalloped edge in the kerf, which followed the blade pattern.

The flat-edge blade exhibited lifting of one of the kerf shoulders above the original surface of the bone. The kerf shouldering occurred on the side of the kerf that was in contact with the back side of the blade. All shouldering that occurred was

indicative of trauma caused by the flat-edge knife and should not be confused with the cortical peeling that sometimes occurred with the serrated-edge blade (*Figs. 16 & 17*).

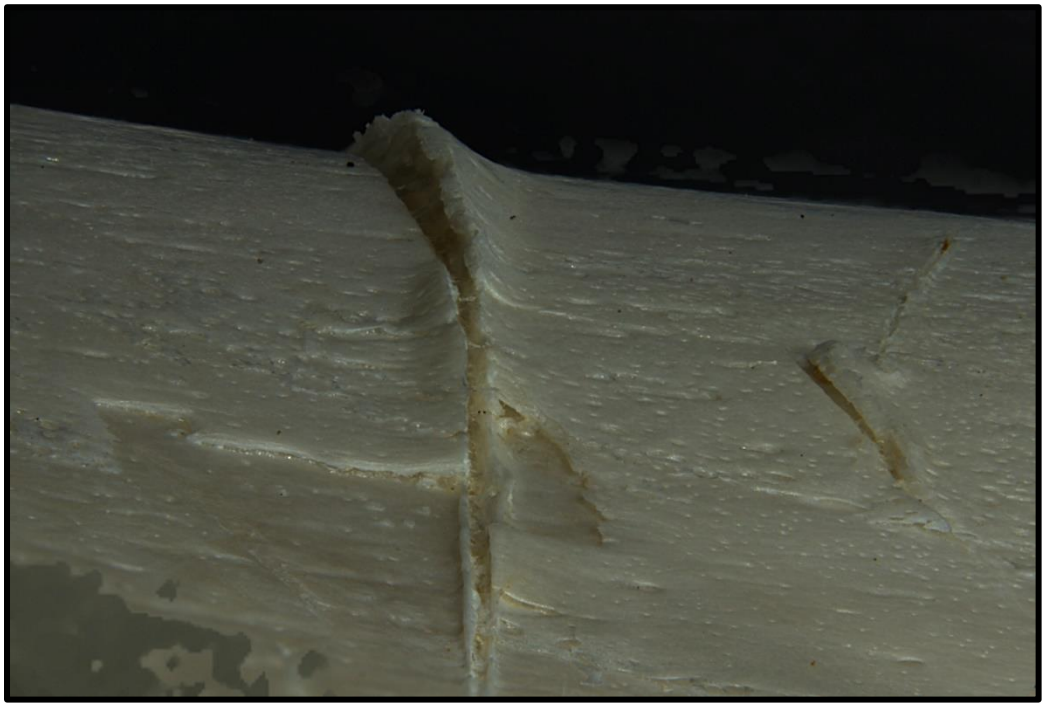

Figure 16. Shouldering from Flat-edge Knife. *Shouldered flat-edge kerf on an unburned pig humerus. The right wall of the kerf is pulled up, which was indicative of flat-edge blades.*

Figure 17. Sharp-blunt Damage from a Serrated-edge Knife. *Sharp-blunt damage around kerf on an unburned pig femur. The kerf is widened, and there is cortical crushing and peelback indicative of the serrated tool class.*

Further, while the opening angle of the kerf created from the flat-edge blades typically fell within a range of about 40° - 60°, kerfs created when the knife passed directly through a ridge of bone, such as the fibular interosseous border, tended to be much wider (e.g. 120° or more). This disparity in opening angle measurements was due to divots of bone being removed by the impact of the knife across the ridge or crest of bone.

The saw marks were also relatively easily distinguished from one another. From a superior view, the reciprocating saw marks created much more even and parallel walls than the handsaw did. Additionally, the reciprocating saw exhibited many more false starts, tooth hopping, exit chipping, and floor dipping than the handsaw did. This means that there was more saw jumping and breakaway spurs at the top of some of the kerfs. The handsaw produced a much more bowed or neck-shaped kerf with wider ends and a narrow center (see *Fig. 18*).

Both saw types produced floor striae that were visible macro and microscopically. The DinoLite digital microscope was able to image the striae, but they were typically unclear and unable to be measured. The Leica stereomicroscope, however, was able to clearly produce the striae at various zoom factors and they were able to be measured and reproduced in the 3-D models.

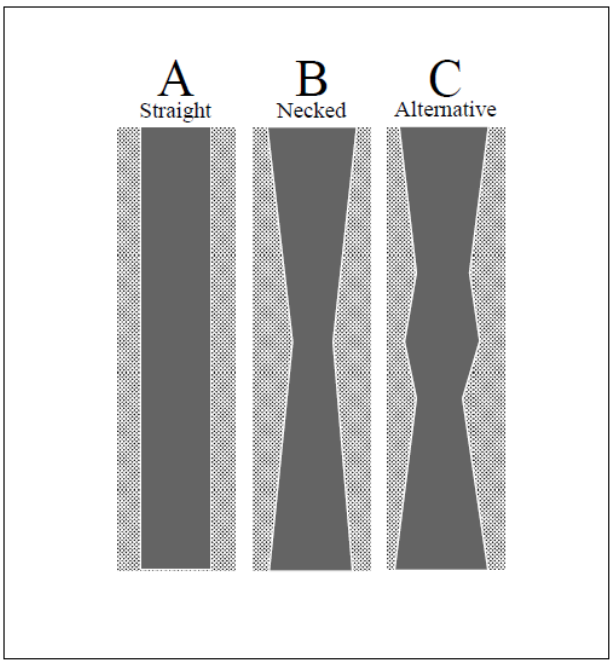

Figure 18. Reciprocating Saw Mark Profiles. *Reproduced figure from Norman et al. (2018). The reciprocating saw tended to produce type A toolmarks while the handsaw tended to produce type B toolmarks.*

Kerf Length

Descriptive statistics conducted on the length of cutmarks exhibit incredibly different results (see Tables 9 and 10). The Kruskal-Wallis one-way analysis of variance test also shows a significant difference among the length measurements for the serrated-edge samples – control human, control pig, burned human, and burned pig ($H = 11.294$, $df = 3$, $p = .010$). Further, there are significant differences in the length of the serrated edge blade cut marks with two of the Mann-Whitney U-tests – the control human sample versus the burned human sample and the control human sample versus the control pig sample ($U = 4$, $p = .002$ and $U = 26$, $p = .019$, respectively). The Mann-Whitney U-test for the burned human versus the burned pig sample is trending toward significant ($U = 20$, $p = .063$). Finally, the Mann-Whitney U-test shows a significant difference among the length measurements from the control human versus control pig sample group for the

handsaw ($U = 32$, $p = .026$), but the Kruskal-Wallis test did not find any significance ($H = 4.624$, $df = 3$, $p = .201$). These results may be viewed in Appendix E.

However, the length of the cutmarks in this study is not useful in indicating tool class for a variety of reasons. Because of the different surface areas of each bone, the knives and saw marks produced vastly different lengths of cutmarks. The greater the width of the impacted bone, the longer the cutmark and vice versa. This difference also affected the length of cutmarks on the homologous pig and human elements, as they are morphologically different and are much different in size due, in part, to age. Moreover, slight lateral movement in the trauma carriage created various cut lengths due to imprecise impact of the knives on the samples. These various issues contributed to a lack of significance and importance with the cutmark length measurements.

Table 9. Descriptive Statistics for Control Human and Pig. *Statistical analysis of measurements from all elements.*

Descriptive Statistics – Control Measurements for Human and Pig												
	N	Range	Min.	Max.	Mean		Std. Dev.	Variance	Skewness		Kurtosis	
	Stat.	Stat.	Stat.	Stat.	Stat.	Std. Err.	Stat.	Stat.	Stat.	Std. Err.	Stat.	Std. Err.
FE length (mm)	25	13.66	3.92	17.58	9.3864	0.77881	3.89406	15.164	0.460	0.464	-0.810	0.902
FE width max (mm)	23	0.79	0.15	0.94	0.4022	0.04854	0.23277	0.054	1.357	0.481	1.186	0.935
FE width mean (mm)	22	0.710	0.120	0.830	0.25955	0.039105	0.183419	0.034	2.331	0.491	5.106	0.953
FE width min	22	0.58	0.06	0.64	0.1182	0.02549	0.11955	0.014	4.326	0.491	19.552	0.953
FE depth max (mm)	21	0.818	0.048	0.866	0.37662	0.047384	0.217142	0.047	0.805	0.501	0.153	0.972
FE depth mean (mm)	21	2.712	0.048	2.760	0.44110	0.124129	0.568832	0.324	3.676	0.501	15.209	0.972
FE FA°	15	63.47	34.91	98.38	58.9980	4.13245	16.00490	256.157	0.720	0.580	1.358	1.121
SE length	23	12.14	4.35	16.49	9.2678	0.74753	3.58501	12.852	0.528	0.481	-0.635	0.935
SE width max (mm)	18	1.170	0.210	1.380	0.61839	0.086106	0.365316	0.133	1.086	0.536	-0.039	1.038
SE width mean (mm)	17	0.79	0.16	0.95	0.4229	0.06012	0.24789	0.061	0.932	0.550	-0.280	1.063
SE width min	16	0.53	0.06	0.59	0.1963	0.03148	0.12590	0.016	2.105	0.564	6.175	1.091
SE depth max (mm	18	1.074	0.196	1.270	0.53161	0.069003	0.292757	0.086	1.209	0.536	0.958	1.038
SE depth mean (mm)	17	1.017	0.173	1.190	0.48247	0.071451	0.294599	0.087	1.175	0.550	0.598	1.063
SE FA°	13	89.23	34.25	123.48	60.9015	6.85430	24.71352	610.758	1.794	0.616	2.940	1.191
RS Length (mm)	22	20.52	3.44	23.96	11.1305	1.15047	5.39619	29.119	0.577	0.491	0.136	0.953
RS width max (mm)	23	3.83	1.56	5.39	2.3017	0.16880	0.80953	0.655	2.780	0.481	9.535	0.935
RS width mean (mm)	22	3.59	1.06	4.65	1.8595	0.15799	0.74106	0.549	2.722	0.491	9.584	0.953
RS width min	22	1.54	0.84	2.38	1.4223	0.08460	0.39682	0.157	0.920	0.491	0.534	0.953
RS depth max (mm)	22	8.634	0.506	9.140	2.72941	0.476086	2.233043	4.986	1.523	0.491	2.310	0.953
RS depth mean (mm)	22	8.401	0.219	8.620	2.49305	0.474998	2.227938	4.964	1.402	0.491	1.772	0.953
HS length (mm)	24	16.29	2.45	18.74	9.8429	0.87024	4.26330	18.176	0.443	0.472	-0.840	0.918
HS width max (mm)	24	2.50	0.59	3.09	1.5346	0.11835	0.57978	0.336	1.308	0.472	2.108	0.918
HS width mean (mm)	24	1.56	0.55	2.11	1.1929	0.07739	0.37915	0.144	0.795	0.472	0.397	0.918
HS width min	22	1.09	0.36	1.45	0.9491	0.06029	0.28277	0.080	-0.119	0.491	-0.564	0.953
HS depth max (mm)	23	3.780	0.580	4.360	1.54387	0.229305	1.099710	1.209	1.497	0.481	1.289	0.935
HS depth mean (mm)	22	3.822	0.158	3.980	1.33927	0.228562	1.072051	1.149	1.542	0.491	1.747	0.953

Table 10. Descriptive Statistics for Burned Human and Pig. *Statistical analysis of measurements from all elements.*

Descriptive Statistics – Burned Measurements for Human and Pig												
	N	Range	Min.	Max.	Mean		Std. Dev.	Variance	Skewness		Kurtosis	
	Stat	Stat.	Stat.	Stat.	Stat.	Std. Err.	Stat.	Stat.	Stat.	Std. Err.	Stat.	Std. Err.
FE length (mm)	25	12.20	2.35	14.55	7.1084	0.67304	3.36521	11.325	0.479	0.464	-0.249	0.902
FE width max (mm)	20	0.78	0.06	0.84	0.3295	0.04233	0.18931	0.036	0.831	0.512	1.535	0.992
FE width mean (mm)	20	0.540	0.050	0.590	0.22115	0.030471	0.136270	0.019	1.277	0.512	2.016	0.992
FE width min	19	0.34	0.04	0.38	0.1321	0.02117	0.09229	0.009	1.580	0.524	2.422	1.014
FE depth max (mm)	23	1.700	0.030	1.730	0.36591	0.076073	0.364835	0.133	2.564	0.481	8.574	0.935
FE depth mean (mm)	23	1.690	0.030	1.720	0.32383	0.074337	0.356508	0.127	2.943	0.481	10.806	0.935
FE FA°	10	30.08	37.62	67.70	55.0290	3.58283	11.32990	128.367	-0.467	0.687	-1.671	1.334
SE length	19	12.33	1.87	14.20	7.5095	0.78108	3.40463	11.591	0.116	0.524	-0.733	1.014
SE width max (mm)	17	3.060	0.240	3.300	0.85647	0.175633	0.724154	0.524	2.601	0.550	8.337	1.063
SE width mean (mm)	17	2.37	0.20	2.57	0.6288	0.13659	0.56318	0.317	2.860	0.550	9.382	1.063
SE width min	17	1.55	0.10	1.65	0.3406	0.09413	0.38810	0.151	2.825	0.550	8.548	1.063
SE depth max (mm	16	1.324	0.126	1.450	0.70213	0.102842	0.411370	0.169	0.340	0.564	-0.807	1.091
SE depth mean (mm)	16	1.317	0.113	1.430	0.63363	0.100168	0.400671	0.161	0.581	0.564	-0.330	1.091
SE FA°	9	65.82	37.60	103.42	64.1522	6.22917	18.68751	349.223	0.974	0.717	1.981	1.400
RS Length (mm)	17	21.81	3.91	25.72	13.6753	1.44550	5.95995	35.521	0.673	0.550	0.241	1.063
RS width max (mm)	18	2.34	1.02	3.36	2.4494	0.15420	0.65420	0.428	-0.258	0.536	-0.343	1.038
RS width mean (mm)	18	2.10	0.94	3.04	1.9456	0.14917	0.63286	0.401	0.422	0.536	-0.882	1.038
RS width min	15	1.99	1.00	2.99	1.6873	0.15179	0.58790	0.346	1.091	0.580	0.301	1.121
RS depth max (mm)	16	6.320	0.440	6.760	2.82038	0.449138	1.796551	3.228	0.887	0.564	0.334	1.091
RS depth mean (mm)	16	6.692	0.058	6.750	2.56175	0.446348	1.785392	3.188	0.773	0.564	0.775	1.091
HS length (mm)	18	20.95	2.83	23.78	10.2467	1.26362	5.36108	28.741	0.897	0.536	1.085	1.038
HS width max (mm)	15	2.09	0.58	2.67	1.6713	0.14116	0.54670	0.299	0.350	0.580	0.556	1.121
HS width mean (mm)	15	2.24	0.56	2.80	1.3273	0.13067	0.50607	0.256	1.888	0.580	5.069	1.121
HS width min	13	2.00	0.64	2.64	1.1115	0.13823	0.49838	0.248	2.699	0.616	8.455	1.191
HS depth max (mm)	16	3.750	0.220	3.970	1.36069	0.261054	1.044216	1.090	0.998	0.564	0.954	1.091
HS depth mean (mm)	14	3.217	0.213	3.430	1.21686	0.253305	0.947782	0.898	1.072	0.597	0.775	1.154

Kerf Width

The kerf widths of the toolmarks has varying results. The initial Kruskal-Wallis test indicates that there are significant differences with the flat-edge maximum width measurements among the four groups ($H = 8.737$, $df = 3$, $p = .033$) and there are significant differences with the reciprocating saw maximum width measurements among the four groups ($H = 10.868$, $df = 3$, $p = .012$). No significant differences are detected for serrated-edge knives or handsaws, nor are there significant differences for minimum width measurements.

The Mann-Whitney U-tests were run between pairs to determine the source of the variation. There are two sources of variation indicated for the flat-edge maximum width measurements. Significant differences arose between the flat-edge width measurements for the control human sample versus the burned human sample ($U = 6$, $p = .032$, two-tailed) and with the burned human sample versus the burned pig sample ($U = 10$, $p = .008$, two-tailed).

The significance of the reciprocating saw maximum width was also investigated with Mann-Whitney U-tests. These tests indicate significant differences in three of the four groups. The control pig sample versus the burned pig sample ($U = 16$, $p = .007$, two-tailed), the control human versus the control pig ($U = 26$, $p = .016$, two-tailed), and the burned human versus the burned pig ($U = 18.5$, $p = .050$, one-tailed) exhibit significant differences.

There are an additional two groups trending toward significance, including the controlled pig versus the burned pig measurement for reciprocating saw minimum width ($U = 28$, $p = .065$, two-tailed) and the control human versus control pig measurements for

flat-edge minimum width (U = 22.5, p = .056, two-tailed). See Appendix E for individual tables.

Maximum, mean, and minimum kerf widths were also tested against one another based on tool class using Mann-Whitney U-tests. The burned and control flat-edge knife measurements were tested against the serrated-edge knife measurements to determine whether the different blade types left different distinguishing marks. The results of the test show significant differences for maximum kerf width (U = 354, p = .000), mean kerf width (U = 262.5, p = .000), and minimum kerf width (U = 268.5, p = .000) between the two blade types.

The same test was conducted for the kerf widths of the burned and control reciprocating saw and handsaw. The results show significant differences for maximum kerf width (U = 251, p = .000), mean kerf width (U = 252.5, p = .000), and minimum kerf width (U = 195.5, p = .000).

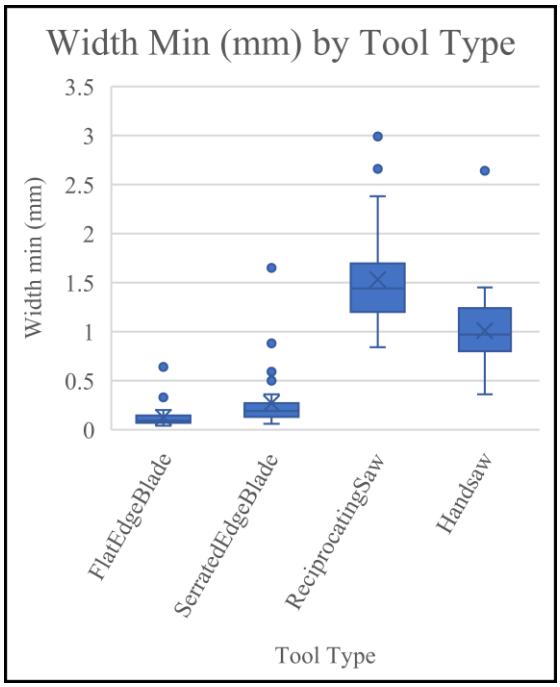

Figure 19. Width Min. by Tool Type. *Simple boxplot showing the minimum widths of the various tool types.*

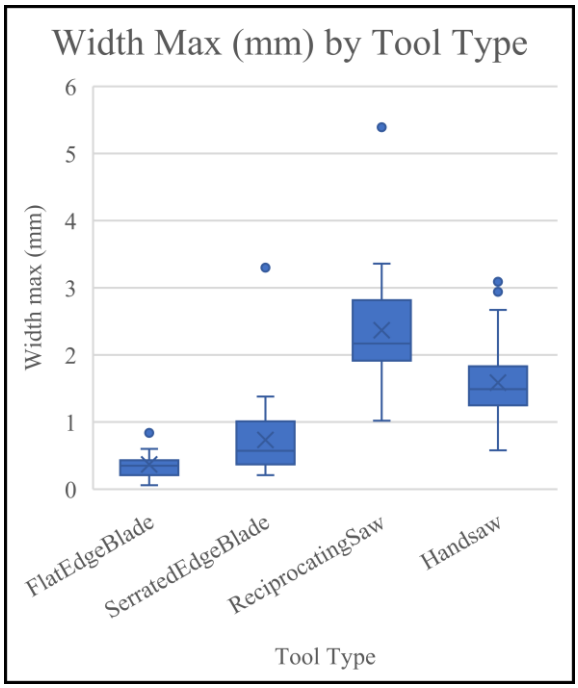

Figure 20. Width Max. by Tool Type. *Simple boxplot showing the maximum widths of the various tool types.*

Kerf Depth

The Kruskal-Wallis for burned and control kerf depth of each of the toolmarks do not indicate any significance among the four groups compared. Additionally, after running various pairs of Mann-Whitney U-tests, no significance is found between homologous measurement pairs for any of the tools used. See Appendix E.

However, when a Mann-Whitney U-test was conducted to test maximum and mean kerf depth between flat-edge knives and serrated-edge knives, there are significant differences (U = 420, p = .001 for maximum depth and U = 421.5, p = .002 for mean depth). The reciprocating saw and handsaw kerf maximum and mean depths were also tested, and results indicate significant differences as well (U = 425.5, p = .001 for maximum depth and U = 432, p = .006 for mean depth).

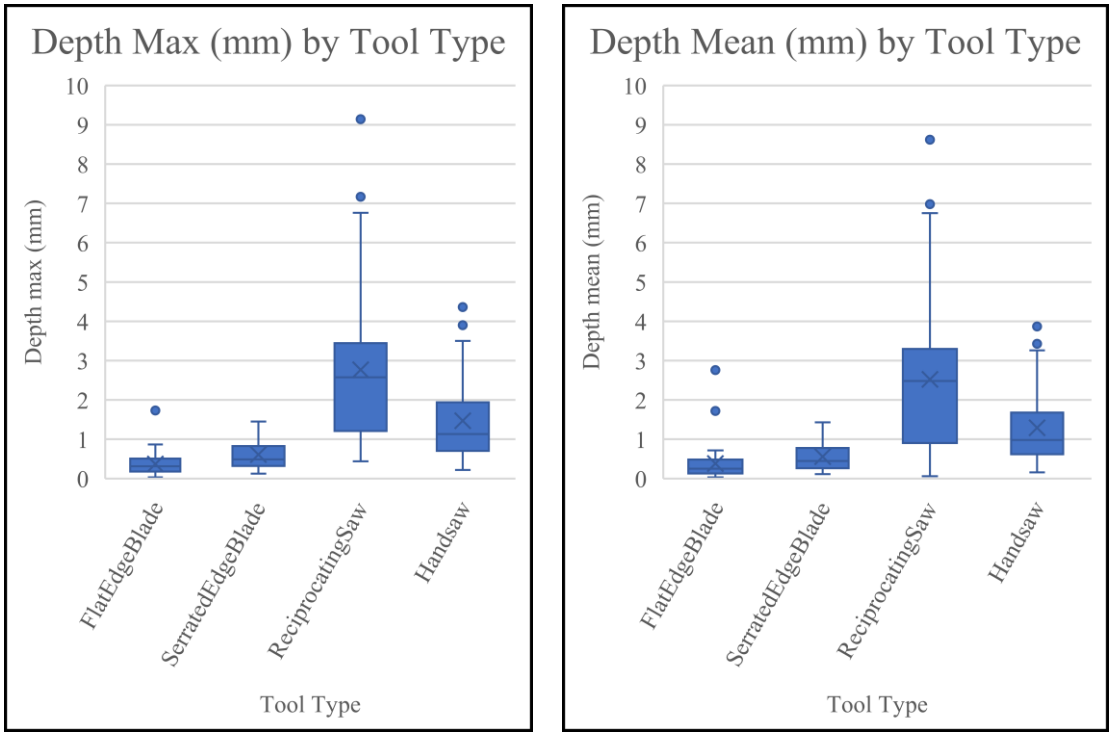

Figure 21. Depth Max. and Mean by Tool Type. *Simple boxplots showing maximum depth (left) and mean depth (right) for the various tool types. Notice the various ranges inhabited by the tools and the variation, especially with the reciprocating saw.*

Kerf Opening Angle

The opening angles of the flat-edge and serrated-edge kerfs were attempted to be measured. Relatively few measurements could be taken (n = 47, combined). The initial Kruskal-Wallis test indicates no significance among the four groups compared. However, one of the Mann-Whitney U-test pairs, control pig versus burned pig, produced significance for the serrated-edge knife opening angle measurements (U = 3, p = .027, two-tailed). No other significance for opening angle is detected. See Appendix E.

Tool Class Identifiers

In order to examine the presence or absence of striae following burning, a Chi-Square Test of Independence with a post-hoc Cramer's V test was conducted in SPSS for both reciprocating saws and handsaws. The results exhibit that there is no statistical significance between the control and burned samples in presence of striae for the reciprocating saw and that there is a weak correlation among the variables (χ^2 = 0.865, p = 0.352, Cramer's V = 0.136). The results for the handsaw additionally exhibit that there is no statistical significance between the control and burned samples regarding presence of striae and that there is a weak correlation among the variables (χ^2 = 0.481, p = 0.488, Cramer's V = 0.107). See Figures 22 and 23.

The Goodness of Fit tests for the reciprocating saw presence of striae and the handsaw presence of striae were then conducted. The results for the striae with the reciprocating saw depict statistical significance (χ^2 = 26.064, p = 0.000). The results for the striae with the handsaw also depict statistical significance (χ^2 = 18.667, p = 0.000). See Appendix E for the full results.

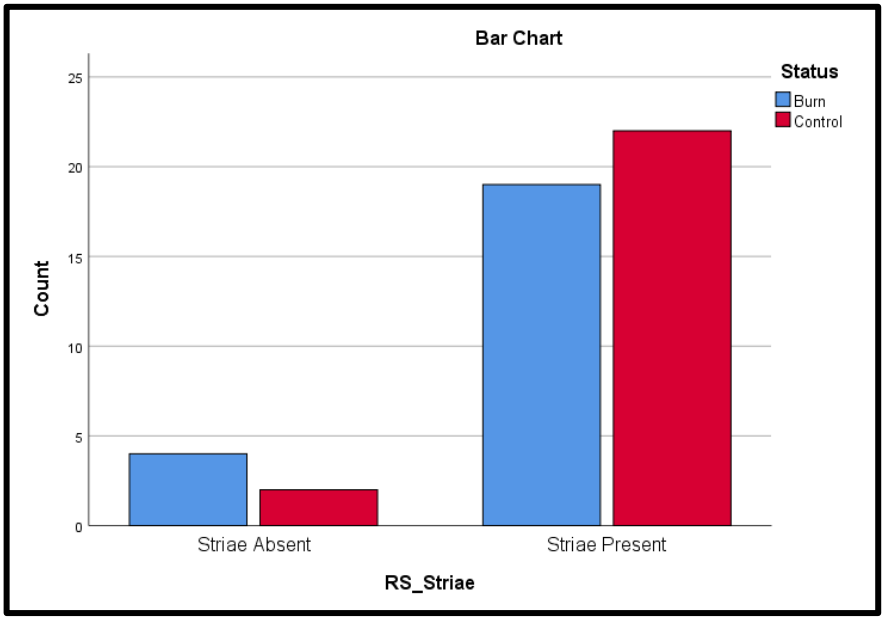

Figure 22. Burned vs. Control Reciprocating Striae. *Chi-Square Test of Independence results for the observed presence of reciprocating saw striae in burned and unburned samples.*

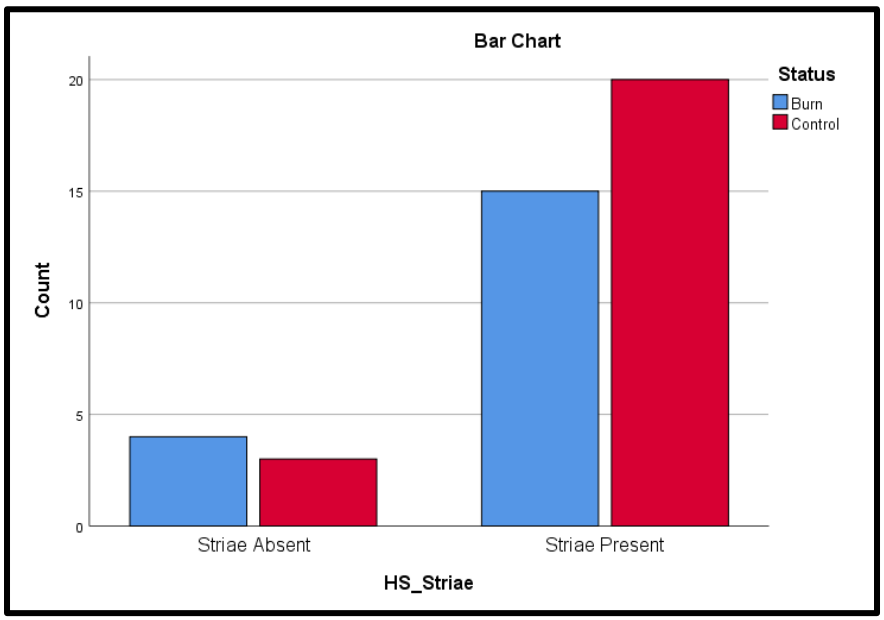

Figure 23. Burned vs. Control Handsaw Striae. *Chi-Square Test of Independence results for the observed presence of handsaw striae in burned and unburned samples.*

The intact silicone casts taken from the burned and unburned saw kerfs exhibited clear indications of saw directionality, teeth per inch, and power. Though not all casts were successfully removed from the kerfs, those that were recovered intact unanimously exhibited the important characteristics for identifying saw class.

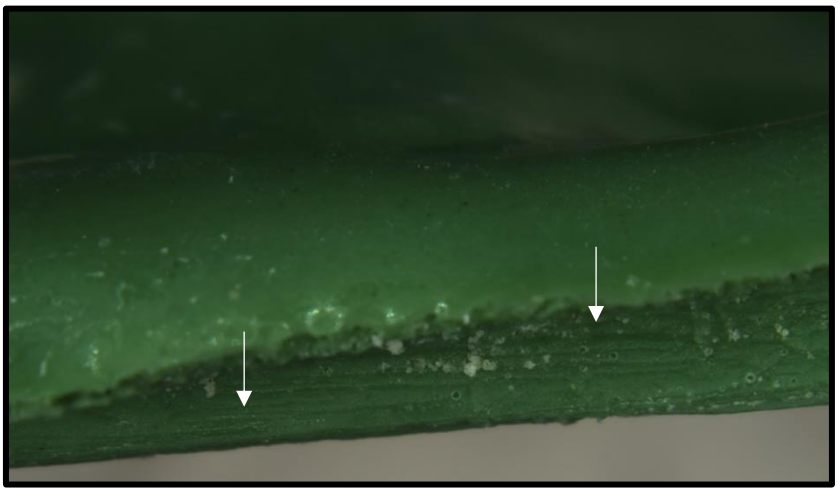

Figure 24. Silicone Cast of a Handsaw Striae. *Saw kerf cast in a pig element. Notice the narrow and even striae that came from the kerf walls.*

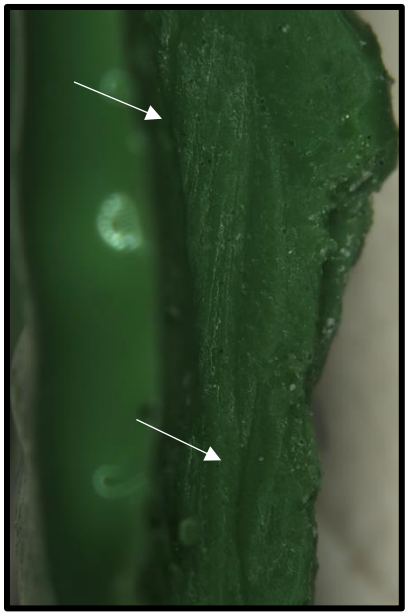

Figure 25. Silicone Cast of a Reciprocating Saw Striae. *Striae are visible, but they are not very parallel as there was movement of the saw.*

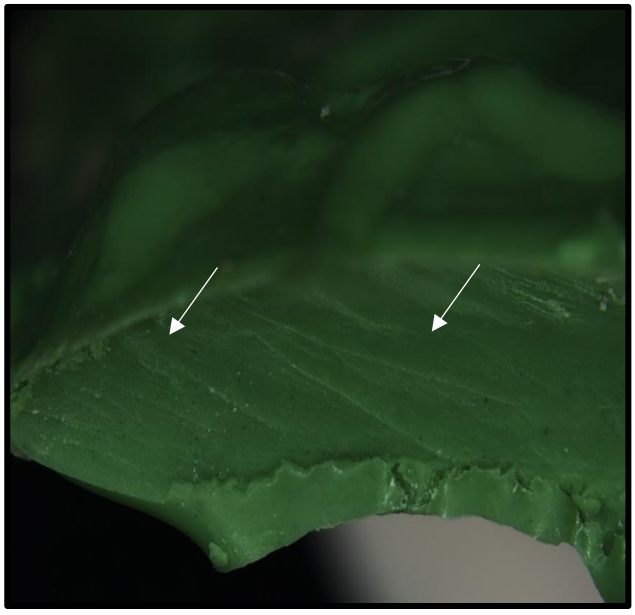

Figure 26. Silicone Cast of a Reciprocating Saw Striae. *Kerf with visible striae. Like the image before, the striae are not as evenly spaced as with the handsaw kerf.*

Leica vs. DinoLite Edge Digital Microscope Data

The Wilcoxon Signed-Rank test was implemented to examine whether any significant differences between the expensive Leica stereomicroscope and the more affordable DinoLite Edge digital microscope. The statistical results suggest that there are significant statistical differences between the homologous measurement pairs taken from each microscope ($Z = -7.387$, $p = .000$). Of the 227 measurements taken with the DinoLite digital microscope, 153 were smaller than their Leica measurement counterparts. The DinoLite digital microscope also produced 69 measurements that were greater than the same measurements taken with the Leica digital stereomicroscope, and only five measurements that matched the measurements taken with the Leica digital stereomicroscope. See Appendix E for full results.

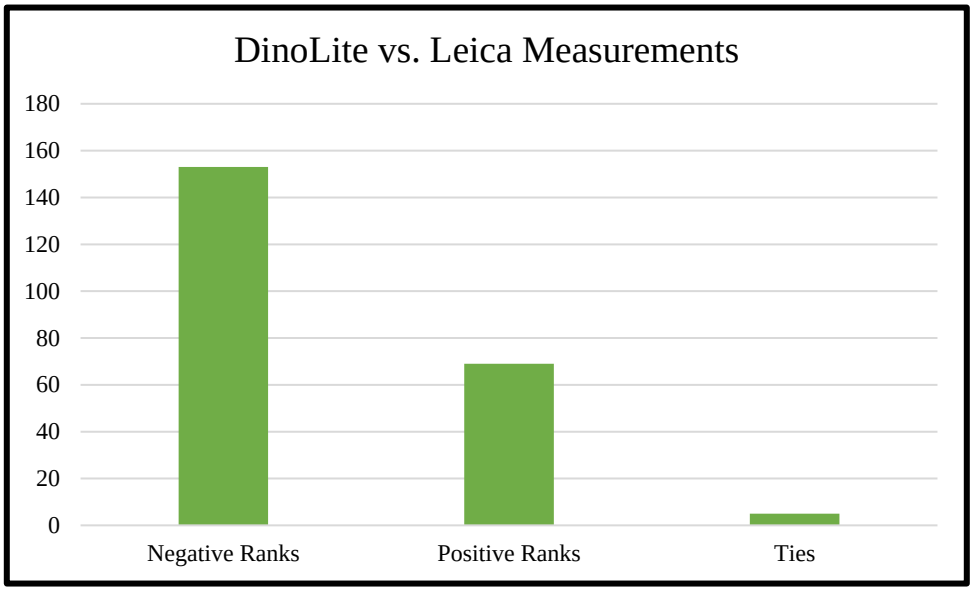

Figure 27. Leica vs. DinoLite Accuracy. *Simple bar chart of Wilcoxon Signed-Rank test results indicating the number of measurements from the DinoLite Edge digital microscope that fell below, above, or equal to the measurements taken with the Leica digital stereomicroscope.*

IV. DISCUSSION

Implications

Because the current study used recently deceased human remains, the results produced are more appropriate for casework than using skeletonized, dry remains for trauma and burning. These results may be better applied to future forensic cases than past research on dry, skeletal remains. Additionally, by also analyzing pig remains, the differences between human and nonhuman results were examined, which will help inform past and future studies.

The digital microscopes were used to determine toolmark length, maximum width, mean width, minimum width, maximum depth, mean depth, and opening angle. Furthermore, the floor of the saw marks could be closely examined for striae. This corpus of data was useful in quantifying the alterations to the kerf walls and floor following burning. Fracture propagation and cracking were also important to identify as they can sometimes be mistaken for perimortem trauma. Presence or absence of striations was also examined as this is an important factor in determining tool class.

Though exhibiting some statistical significance, kerf length made by the handsaw and flat-edge and serrated-edge blades is not an important measurement to examine in this study for a number of reasons. The differences in the shape of the surfaces the knife was hitting, the positioning of the sample below the knife carriage, and the possible slight rotation or tilt of the knife as it struck the sample led to a vast array of kerf lengths through the samples, even going so far as to completely sever most of the pig and human ribs.

The statistical results of the Kruskal-Wallis and Mann-Whitney U-tests indicate that maximum kerf width is statistically different for some of the flat-edge blade and reciprocating saw samples between species and burn status. These results likely indicate that though shrinkage has been shown in the literature to occur in burned bone, the two kerf walls may begin to split farther apart rather than shrink together. Spalling of the surrounding cortical bone and fractures originating from the kerf may increase the width significantly. However, the cutmark origin and termination in the bone tended to remain intact with little to no increase in width or morphology when compared with control samples.

The significant differences in reciprocating saw kerf width in the samples are likely not meaningful. Because the reciprocating saw marks were made without a standardizing device and were done freehand, it is possible that the differences in the kerf widths are attributable simply to experimentation bias. If the sample was not strapped tightly enough to the board, it was more likely to move and could have altered the saw mark produced.

The results of the Mann-Whitney U-tests comparing the maximum, mean, and minimum kerf width measurements of flat-edge blades to serrated-edge blades and reciprocating saws to handsaws indicated strong statistical significance. These findings align with past research (Symes et al., 2010; Symes et al., 2012; Tegtmeyer, 2012; Waltenberger & Schutkowski, 2017) and indicate that flat-edge blades leave significantly narrower kerfs than do serrated-edge blades. Reciprocating saws tend to produce wider kerfs than handsaws.

Depth measurements were likely statistically insignificant because kerf depth was only measured with intact floors. The burned kerf floors were often destroyed, falsely

increasing the depth of the kerfs into the trabeculae. Though measurements from destroyed kerf floors were avoided in this study, Waltenberger and Schutkowski (2017) found significant differences in this measurement as they measured depth in kerfs with destroyed floors.

The results of the Mann-Whitney U-tests comparing maximum and mean depth kerf measurements of the flat-edge knife blade to serrated-edge knife blade and reciprocating saw to handsaw showed significance. This means that when stabbed with the same force, a serrated knife blade may cut deeper than a flat-edge knife blade. The significance exhibited between the reciprocating saw and handsaw kerf depth was subject to more limiting factors as the cuts were not standardized. The significant depth results produced in this study are not meaningful and are not useful as tool class indicators.

The results of the Chi-Square Test of Independence for the presence of reciprocating saw and handsaw striae in burned versus unburned samples showed no statistical significance. This means that the presence of striae is not significantly affected by the burning of the element. Additionally, the Goodness of Fit test for both reciprocating saw and handsaw striae was extremely significant and reveals that almost every sample with saw marks also included striae. These results mean that striae are an excellent indicator of tool class and should be examined in detail for evidence of unique patterns for directionality, teeth per inch, power, and possible tool individualization.

The silicone casts that were made to examine any overlooked data on a sample of saw mark kerf walls exhibited clear striations when removed that indicated saw directionality, tooth per inch, and power. Unfortunately, nearly half of the casts were damaged during removal from the kerf as they swelled into any exposed trabeculae during their drying

phase. This may have been a function of the type of silicone used, but it may also be indicative of what can occur when casting kerfs that have damaged kerf walls or floors with exposed trabeculae.

Additionally, Waltenberger and Schutkowski (2017) found that their cutmarks did not significantly change in contrast to previous research suggesting bone shrinkage during thermal alterations. The cutmarks on the pig sample for the current study matched these conclusions relatively well in that the cutmarks did not shrink in size, and some even increased in size based on the descriptive statistics produced though the level of burning varied between the two studies. However, the cutmarks in the human sample had the opposite effect as they tended to decrease in all measurement categories. This observed shrinkage is statistically insignificant, however. These findings suggest that there is a slight difference between the ways in which pig bone alters in thermal conditions as opposed to the ways in which human bone alters. This divergence in results likely has to do with the age of the samples used, the collagen content, bone structure, and the cortical bone density.

This research made several other findings about toolmarks in burned remains. Toolmarks remain relatively stable across the various elements used, with just a few statistical differences occurring likely due to a small sample size or measurement errors. Further, different tool types can be differentiated based on identifying characteristics such as width, depth, shouldering, striae, and shape of the kerf. Additionally, dismemberment saw mark cuts are easily distinguishable based on their width, depth, and overall shape. Flat-edge and serrated-edge knives are still reasonably distinguishable from one another after thermal alterations based on their kerf characteristics and measurements. The

patterned crushing of the cortical bone around the serrated-edge kerfs and the narrow, long surfaces of the flat-edge kerfs were unique and relatively uniform in morphology. Furthermore, the serrated-edge blade kerfs tended to be slightly deeper than the flat-edge kerfs, although this finding would not be helpful forensically without reference to other shallower or deeper cutmarks.

The shape characteristics of the saw marks were retained in the burned bone. The handsaw marks frequently exhibited a necked or bowed appearance while the reciprocating saw marks were parallel and often had tooth jump surrounding the main kerf (see *Fig. 28*). Additionally, the ability to distinguish striae from the burned bone is important as it indicates that a serrated blade or saw was being used, and it also indicates relative vibration of mechanically powered saws. In kerfs created with a more slowly moving reciprocating saw action, there was more observed tooth jump, likely because reciprocating saws are harder to control at slower speeds.

Figure 28. Tooth Jump near Burned Reciprocating Saw Mark. *Kerf in burned human femur. Notice the striae that remain visible even after thermal alterations on the right and left sides of the kerf. These striae indicate a powered saw.*

The trauma device meant to standardize the stab marks worked insofar as it produced visible cutmarks on nearly all the impacted samples and was easy to use. However, though the knives were hitting the samples with the same potential energy, they often produced different cut lengths due to the varying areas of bone the knives impacted on each sample. In some instances, the carriage would rebound and strike the sample multiple times (see *Fig. 29*). This shows that the region of the body being impacted by a knife can alter the way in which the toolmark appears and should be taken into consideration in future investigations. The overall class characteristics of the tool were retained regardless of bone or species, however.

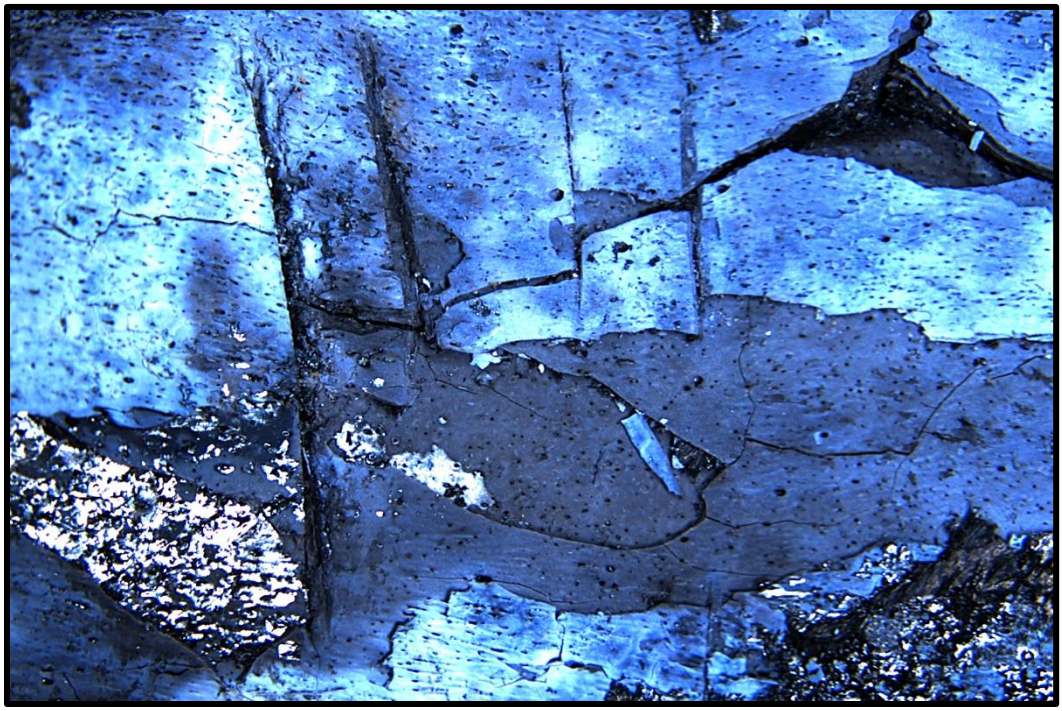

Figure 29. Burned Serrated-edge Knife Rebound. *Multiple kerfs on burned pig femur that occurred with the trauma carriage. The longest kerf on the left is the initial point of impact with three subsequent bounces following on the right.*

Forensics

From a forensic perspective, the results of this study showing little to no significant difference between the burned toolmarks and their unburned counterparts means that knife and saw class may be distinguished in burned remains. This finding echoes the results of several other published experiments on the topic and adds support to closely examining all burned remains for indicators of toolmarks.

Though outside the scope of this research, knife individualization may be possible as well. With use, tools develop unique patterns on their surfaces, and these surfaces can act like temporary fingerprints. For example, pseudo-striations produced by a flat-edge blade due to small defects along the blade edge may make it possible to match the individual knife to the kerf mark. Further research should be undertaken toward the possibility of correctly matching individual blades with toolmarks in burned bone based on individualizing characteristics such as blade chips, nicks, blade curvature or bend, and more. Using casting materials to conduct this research may prove especially useful, as casts can pick up extremely small or concealed unique identifiers within a kerf that may be difficult to visualize with a microscope.

Bioarchaeology

The ability to match tool class to toolmarks and distinguish perimortem trauma from postmortem damage is not exclusively useful for forensic work. Bioarchaeologically, this research has several implications. Digital microscopy has opened up a range of tools for researchers including the ability to take measurements that may have been time-consuming or unavailable in the past. Options such as producing interactive 3-D models and detailed, annotated images may drum up public interest in

bioarchaeological research. Furthermore, the ease of ability to take precise and informative measurements from toolmarks cannot be understated.

These measurements, such as depth, opening angle of the kerf, and the ability to view and measure striae are integral for making tool class matches. Past peoples made an array of tool types, so being able to match a tool class to trauma may be able to provide information on tool purpose, the possible intent behind the toolmark, and cultural relationships among various groups. Moreover, since tools in the past were handmade instead of machine formed, they have significant individual characteristics. In the right preservation conditions, bioarchaeologists may be able to match particular tools in an area with marks on bone.

This research is not limited to distinguishing tool class and individualization for trauma in human remains but also zooarchaeological materials. Faunal remains in the archaeological record, when not used for tools, were often cooked and consumed, leaving behind smoked or charred bone. Examining butchery marks on these bones with a digital microscope could provide insight into the lives of ancient peoples and produce publicly accessible 3-D models for researchers and interested citizens who are invested in the topic worldwide.

Pigs as Analogues for Humans

The results of the Kruskal-Wallis test between the unburned and burned human and pig remains produced largely nonsignificant results. The Mann-Whitney U-tests further supported the Kruskal-Wallis findings with significance occurring in just three samples of toolmark maximum width and two samples of toolmark length, which have already been removed as useful measurements for tool class. The measurement differences in

width were additionally found between burned and control samples of both humans and pigs, indicating that thermal alterations are the more likely culprit behind the significant differences.

Therefore, these results largely indicate that pigs are an acceptable proxy for humans in forensic toolmark research. These results should not be extended to encompass the appropriateness of using pig remains for all areas of experimental research, as this study looked only at toolmarks in burned remains. Further, though these results indicate adequacy in using pigs as a proxy for this type of research, morphological differences should not be overlooked during the analysis phase, and researchers still needs to use caution when assigning significance to results using pigs as human analogues in forensic toolmark research.

Interestingly, the pig remains were much more fragmentary than the human remains when burned. There are several reasons, however, which may account for the deviation of expected fragmentation of the immature pig bones versus the mature human bones. First and foremost, the composition of the pig and human elements were simply not analogous. This is due in part to the fact that the purchased pig was young (~ 4 months old). The relative youth of the pig means that the bones likely had a higher collagen content than the human remains, which would have had lower collagen but greater cortical hardness. Collagen denatures rapidly under thermal conditions, so it's possible that this rapid carbonization of the collagen caused instability in the bone and higher susceptibility to fracture. The sturdier cortical bone in the human sample may have created greater resistivity.

However, this is counter to research conducted on the preservation of youthful versus senescent bone. Research by Waterhouse (2013) indicates that age of the individual greatly impacts the fragmentation and thermal alterations seen in burned remains. The remains of younger individuals are more likely to preserve their original shape and appearance without much fragmentation. It is possible that the higher collagen content and overall greater flexibility in terms of Young's Modulus may help protect the younger remains from fracturing and fragmentation (Waterhouse, 2013).

To account for this discrepancy in the findings of this study, it is possible that the higher degree of fragmentation in the pig remains was related to the overall higher fat content, which may have created a greater fuel source for the fire as it burned through the elements. The pig elements were surrounded by more fat than was observed in the human sample, and the increased fat content may have led to increased temperature and more flare-ups and higher temperatures during the burning process. Furthermore, the pig bones were exposed to slightly longer burning durations than the human bones since complete carbonization and partial calcination appeared to take longer in the pig bones. This increased exposure to heat may have also led to higher fragmentation conditions for the pig elements than the human elements.

Expensive versus Inexpensive Microscope

There are several benefits and drawbacks for each microscope. Both digital microscopes allowed for relatively high-resolution microscopic images to be produced for comparison with each other, and measurements of the length, maximum width, and minimum width were able to be taken with each respective microscope software.

The Dino-Lite Edge digital microscope has several advantages. There is no expensive software associated with the hardware, it is highly transportable, it is easily manipulated, and it has an immovable stage, which means delicate samples like burned bone do not need to be secured to the stage to minimize movement during imaging. This immobility renders the clay used to anchor samples down for the Leica microscope unnecessary, so further fragmentation is made less likely. Moreover, the microscope is extremely easy to learn to use and doesn't require large amounts of disk space.

The drawbacks for the DinoLite digital microscope are extensive, however. Though the immobility of the stage allows for samples to remain unanchored to the stage, samples do need to be moved by hand into view of the microscope, which can increase fragmentation. Further, like the Leica digital stereomicroscope, the DinoLite did offer an extended depth of field feature, though it was extremely limited. This feature was only marginally useful for curved surfaces such as toolmarks spanning across the curved surfaces of bone diaphyses. Unfortunately, the user cannot control the upper and lower limits of the focus. This automation of the process more often than not resulted in partially blurry images with only minimal refocusing of surfaces at different depths (see *Fig. 30*).

Additionally, unlike with the Leica stereomicroscope, the DinoLite requires the user to manually reset the zoom factor in the software each time it is adjusted on the microscope. This could be an issue if the user forgets to make the zoom adjustment update in the software as it affects the measurements that are taken as well. The coarser focus increases the need to continually adjust the zoom factor, accentuating the issue. The

decreased focus may also inhibit the researcher from viewing important kerf characteristics fully.

Figure 30. DinoLite Edge Digital Microscope Kerf. *Reciprocating saw kerf in burned human humerus imaged with the DinoLite Edge digital microscope using the extended depth of field (EDOF) feature. Note the blurriness of both the upper and lower limits in the image.*

Furthermore, the Wilcoxon test indicated there were significant differences in the measurements, and often, the DinoLite digital microscope couldn't visualize the entire kerf mark except at relatively low zoom. This lack of being able to zoom in for a clearer depiction of the cutmarks often led to an inability to see the very narrow ends of the kerfs. This visual inability, in turn, led to ~68% (n = 153) of the kerfs to be measured as shorter or narrower than they actually were. Only ~30% (n = 69) of the kerfs were measured as longer or wider, and just ~2% (n = 5) of the measurements between the microscopes agreed.

The Leica digital stereomicroscope also has several advantages and disadvantages. In addition to basic length and width measurements, this stereomicroscope was able to take angles and depths of cutmarks, tilescans, and produce 3-D, manipulatable, renderings of each kerf and cut mark. These features proved extremely useful in being able to draw conclusions about the tool class, and the 3-D models would certainly be valuable in a court of law as a visual aid. Further, the fine movements and large range of motion for the stage is imperative for maintaining the stability of the often delicate samples, and it reduces the need to manually adjust them.

The tilescan feature offered by the Leica LAS X software allowed cutmarks not fully visualized in a single image to be stitched together through the use of multiple, focused images and rendered into a single file. This tool was especially useful for measuring the lengths of toolmarks as well as producing full toolmark profiles with both high-resolution and high zoom factors. The zoom factor was also always digitally burned into an image, so the image can be viewed at a later time and measurements can be accurately taken from that image.

The disadvantages for the Leica stereomicroscope include the cost of the machinery and software, which is a substantial limiting factor. Further, the stereomicroscope can only move up or down, while other digital microscopes can be rotated side to side as well. The inability of the Leica stereomicroscope to move laterally means that samples must be rotated by hand to view different surfaces. Any repositioning of fragile samples like burned bone puts them at risk for fragmentation and loss of data regarding tool class. Additionally, this stereomicroscope requires a large amount of disk

space, as the layered and high-resolution images and their associated data often produce massive files.

The main takeaway from the relative advantages and disadvantages of each piece of technology is that the microscopes should have different functions. The DinoLite digital microscope is ideal as a cost-efficient piece of equipment than can be learned easily and taken almost anywhere, as its source of power is through a USB cord. It can determine if there are cutmarks present, and it is even sometimes fine enough to pick out striations on a saw mark kerf floor. The Leica stereomicroscope is ideal for labs specializing in looking for extremely minute detail and producing digital replicas of a given feature. Its exorbitant cost likely outweighs its benefits for most law enforcement purposes without a grant with which to purchase it. More affordable, high-quality microscopes will likely prove successful at imaging toolmarks and identifying tool class.

Limitations

This study was limited in the ability to collect data due to the nature of the destructive analyses conducted. Pilot studies were necessary to try and mitigate some of the inherent limitations faced by this research, but many of the limitations were unavoidable. Because burning is such a destructive method, much of the data regarding kerf depth and width measurements could not be feasibly collected due to destruction of the kerf floors and walls. Often, the bone broke at a kerf once it burned, especially at kerfs made by the reciprocating saw, and diminished the amount of information that could be gathered. Furthermore, the samples were exposed to different temperatures and temperature fluctuations during the various burning processes, which may have introduced differentiation in fragmentation susceptibility.

Limitations also include the loss of real biomechanical differences as the bones were held in place during the trauma infliction, disallowing any natural movement, and much of the soft tissue had been removed. This certainly altered the ways in which the tools impacted and left marks on the bone. The ribs are a prime example of the lack of forensic realism with this research. Because they were removed from the body and placed on the floor to be impacted by the trauma carriage, they ended up fracturing in several places.

Though there was a large sample size of toolmarks to examine, the overall diversity of the sample materials was low. A single, juvenile pig and only half of a single donated individual were used. This limitation means that while the results presented here are accurate, they are only accurate insofar that they represent the narrow assortment of sample materials utilized.

There are certainly some limitations to this research in terms of the life history of the individual included in this research. While the higher rate of fragmentation in older burned remains was already discussed, the sex of the individual may have played a role as well. The individual used in this study was a male. Women undergo menopause around their fifties, and these hormonal changes can lead to loss of bone density to the point of osteoporosis. Much more frequently seen in women than in men, it is likely that loss of bone density would also affect the manner and rapidity in which the bone burns and retains toolmark characteristics.

Some of the most significant limitations of this research arose due to lack of literature on how to clean burned bone, and there was some loss of data due to further fragmentation of samples during the cleaning process. Almost every burned pig and

human rib was accidentally broken as mechanical tissue removal was attempted. Unfortunately, the incubator was not deemed a good option for these samples as they were partially calcined and may have been further structurally compromised if exposed to a warm water bath.

Finally, there were limitations to the realism of this research in a forensic context due to the use of wire baskets to contain samples in this study. Remains will likely not be in individual containers in forensic contexts, so collection of remains will produce another factor in which bones may be further fragmented, commingled, or overlooked completely.

Recommendations

Based on the results of this research, several new protocols for future research with trauma and burned remains are being proposed, as well as protocols for handling burned remains in forensic contexts. This research has shown that tissue, even small amounts of remaining charred tissue, can easily obscure important factors, such as trauma. Without a protocol for cleaning burned bone to observe the entirety of the bone surface, some of this trauma may go unnoticed.

One of the fundamental limitations of the research arose from a lack of published methodology in cleaning and preparing burned bone for analysis. The protocol proposed in the following chart is restricted to long bones and ribs only, and more research with the cranium, vertebral column, hands, and feet is needed to shore up some of the limitations of this proposed methodology. This research is especially well suited for the use of nonhuman analogues as it does not deal with bone morphology as greatly and requires new and possibly occasionally destructive experimentation.

Additionally, not all burned bone may be handled in the same way, so sufficient caution should be taken with applying the following approach. Until preliminary findings are published and standards are created, human bone should be cleaned and prepared by the investigator as carefully as possible to both preserve the integrity of the bone and restrict loss of features such as toolmarks.

Table 11. Preliminary Proposed Methods for Cleaning Burned Bone. *Potential methods for cleaning burned bone in various stages of thermal alteration.*

Carbonized (charred) bone with charred tissue remaining on >75% of the bone surface and no calcined bone present	This status indicates fairly low temperature and/or a short duration of burning. While some of the bone may retain a highly charred or calcined appearance, the bone beneath the remaining tissue will be largely unchanged. This bone is likely to be structurally sound, and tissue removal may be undertaken first by attempting to remove tissue mechanically with fingers, scalpels, and scraping tools. Following mechanical removal, bones may be placed in a processing kettle with mild degreaser for a few hours or an incubator with mild degreaser for a few days. Once removed from the kettle or incubator, allow elements to cool briefly, then proceed with processing as normal with wooden tools, toothbrushes, and mild detergent.
Carbonized bone with charred tissue	At this stage, first attempt to remove tissue mechanically with fingers, scalpels, and scraping tools. Blunt dental tools work well for prying up remaining tissue. Be careful not to damage the bone when pulling tissue. If the tissue is too hardened onto the bone, and breakage of the bone is a concern, submersion in water no warmer than 150°F (65°C) with a mild degreaser, (preferably in an incubator with a controlled, consistent temperature) is acceptable. The elements may need to remain submerged for up to three

Table 11. continued.

remaining on 25% – 75% of the bone surface	days in order to fully expose the bone surface. The elements should be checked each day, and the water should be changed out as necessary. After removal of the elements from the incubator, they should be drained and rinsed with warm water or allowed to cool for approximately ten minutes before being rinsed with cool water to avoid further stressing the bone. They should then be allowed to dry for at least 24 hours. The bones may still retain a significant amount of grease, but as long as the bone surface is visible, this is acceptable for analysis. Further cleaning to aid in grease removal may be necessary following analysis.
Carbonized and calcined bone with some tissue remaining	Often, at this stage, any remaining tissue is highly desiccated and/or charred. It is typically easy to rub the charred tissue and clinker away gently with your fingers or a toothbrush. For any tissue that remains adhered, a scalpel may be used to lightly flick charred tissue away as needed. Be extremely careful not to nick the bone or apply too much pressure. This bone is highly fragile and easily breakable, handling the elements as little as possible before analysis is crucial in maintaining their structural integrity. No submersion in water is recommended at this stage.
Calcine bone	At this stage, there should be no tissue remaining, and all the bone surfaces have been exposed. Handle the bones as gently and infrequently as possible. It is recommended to look into using consolidants such as resins and emulsions to preserve bone integrity upon recovery and subsequent transport and analysis. Preliminary research conducted by Siegert (2016) on burned bone consolidants found that Acryloid™ B-72 consolidant is especially efficient and cost-effective in maintaining the integrity of the burned bones.

Future Research

Future research regarding this subject is imperative in order to shore up some of the limitations facing this study. Not only can future research look at validating the conclusions found in this study, but it can also expand into examining other types of trauma such as ballistic, blunt, or blast and the impact thermal alteration has on their traumatic signatures. Furthermore, finding a more financially accessible microscope than the Leica M205 C digital stereomicroscope for investigative agencies that can still yield high quality measurements and images is important. With the appropriate equipment, data regarding tool class and perhaps tool individualization from toolmarks on bone may be attained.

Previous research has also indicated that microcomputed tomography (micro-CT) is a useful method and may be used in tandem with microscopic methods to supplement findings. The ability to image remains without defleshing or cleaning the bone mitigates issues with data loss through increased fragmentation. Future research could attempt to refine methodology combining digital microscopy and micro-CT to attain the most information possible.

In addition to examining different toolmarks with different equipment, further research on pigs as nonhuman research analogues is encouraged. The discrepancies in findings throughout the literature regarding the appropriateness of using pigs remains an unresolved issue. While the findings of this study suggest there is little to no difference in the ways that cutmarks may be retained and examined in human and pig elements, these results may have occurred due to experiment setup or the myriad limitations that arose.

Finally, developing standards of procedure for cleaning burned bone, including elements not examined in this research such as cranial and vertebral, is an area of both research and practice that needs to be strengthened. Developing appropriate ways of removing tissue and clinker to preserve the underlying bone structure is all the more topical with the increased risk and exposure of communities to wildfire dangers. While investigators in this case may not be necessarily looking for evidence of toolmarks or trauma, maintaining skeletal integrity of already compromised elements is necessary for assisting with positive identifications and for returning as delicately handled and cared for remains to the respective loved ones as possible.

V. CONCLUSION

Exposure of human remains to thermal settings is an ideal method for perpetrators attempting to conceal trauma or identifying tool class characteristics. However, identifiable toolmarks remain visible even on fragmentary, highly friable, calcined bone. As such, thermal alterations to bone must be considered carefully and handled delicately. This research examined sharp force trauma in burned and unburned human and pig remains to address questions related to forensic investigators' technological needs, techniques for toolmark analysis, and the use of nonhuman analogues on forensic research.

There were several goals of this research including determining whether kerfs from knife cut marks and two different types of saw marks changed significantly with thermal alterations, whether pigs are an acceptable research proxy for humans, and whether a less expensive microscope is accurate enough for investigators in forensic contexts. This study found that tool marks in burned bone remained relatively stable when compared with their unburned counterparts. This finding means that investigators should be able to accurately determine tool class from well-preserved cutmarks in burned remains. Flat-edge blades, serrated-edge blades, reciprocating saws, and handsaws appear to produce unique toolmark characteristics that are retained in bone even after thermal alterations to a calcinated level, and kerf width measurements appear to be especially useful in determining a tool class.

Taking silicone casts of cut marks, especially saw marks, is also recommended in order to examine kerf wall data obscured from microscopic visualization. These casts may be taken delicately from burned kerfs as well, but it is recommended as the final step

in analysis in case of accidental fragmentation while filling or removing the casts. Striae left on the kerf walls can be highly important for determining directionality of the saw, teeth per inch, and power, which are all essential questions to address when investigators are looking for potential tools used in committing a crime.

Additionally, while research on nonhuman analogues needs to be further explored, the findings of this research were that humans and pigs produced similar results in terms of cutmark patterns and retention of detail such as striae in burned remains. However, the pig remains were much more fragmentary, and differences in overall bone morphology and life history between humans and pigs should still be regarded cautiously in future research and while digesting the results of past related research.

While the less expensive DinoLite Edge digital microscope did an inadequate job in comparison with the Leica digital stereomicroscope, the latter is exorbitantly priced and likely unnecessary for investigators in answering questions regarding tool class and individualization. A higher quality microscope than the DinoLite but a more moderately priced microscope than the Leica is suggested.

The reference library for the static microscopic images, the 3-D manipulatable models, and the associated toolmark information are available at the Forensic Anthropology Center at Texas State (FACTS). A goal of this research is that the collection of images may serve as an educational databank or for research purposes. Access and research requests will be processed by FACTS.

Proper handling and analysis of burned remains is necessary for accurately assessing bones for evidence of toolmarks and for preserving the integrity of the bone for future analysis and repatriation to loved ones. As forensic anthropologists increasingly

engage in trauma analysis, research that examines trauma in burned remains must continue to grow and to fill in the gaps in knowledge regarding the subject. With the complexities that come from different types of trauma and from thermal alterations separately, the combination of the two leaves substantial room for development in the realm of research. Increased literature on the subject may eventually introduce standardization in proper excavation, analytical, and preservation techniques. This, in turn, will offer more robust statements in a courtroom setting.

APPENDIX SECTION

APPENDIX A

Glossary of Terms

Calcined	Bone that has lost its organic material and reached its final state of thermal decomposition. Calcined bone is grey, white, and/or blue in color
Carbonized/charred	The stage of thermal alteration in which bone is burned and blackened in color
Clinker	the buildup up debris on and around the bone as a result of incompletely incinerated bone marrow and other soft tissue residues that form from oxygen deficient contexts
Cutmark	A toolmark or kerf mark in bone made from a sharp object
False start mark	A saw mark that does not completely separate two portions of bone and may be adjacent to a complete saw mark; previously termed "hesitation mark"
Flat-edge	A blade without a serrated margin; smooth blade surface
Fracture	A complete or partially broken bone due to trauma from force(s) that occurred to the bone
IACUC	Institutional Animal Care and Use Committee; protects the welfare of animals in research
IRB	Institutional Review Board; approves, modifies, or disapproves research using living individuals or populations for research to protect their privacy, welfare, and other rights
Kerf	A cutmark consisting of walls and a floor
Perimortem	An event that occurs to remains at or around the time of death
Postmortem	An event that occurs to remains after the time of death
Saw mark	A toolmark made by use of a saw
Serrated-edge	A blade that has a scalloped or serrated edge blade
Sharp-blunt trauma	Sharp force trauma that includes blunt force characteristics such as cortical crushing
Sharp force trauma	Trauma that occurs to an individual by use of a sharp object; includes cutmarks, punctures, saw marks, stabs, and more
Striae / striations	A linear mark or groove left in a kerf often from a serrated blade
Thermal alterations	Changes that occur to remains due to exposure to high heat
Tool class	Characteristics of a toolmark including its impression, shape, and dimensions that help investigators determine tool type
Toolmark	A characteristic feature left on or in bone by an external object
Tooth-hopping/jumping	The movement of a saw blade, often reciprocating, outside the main kerf that leave striae visible around the kerf

APPENDIX B

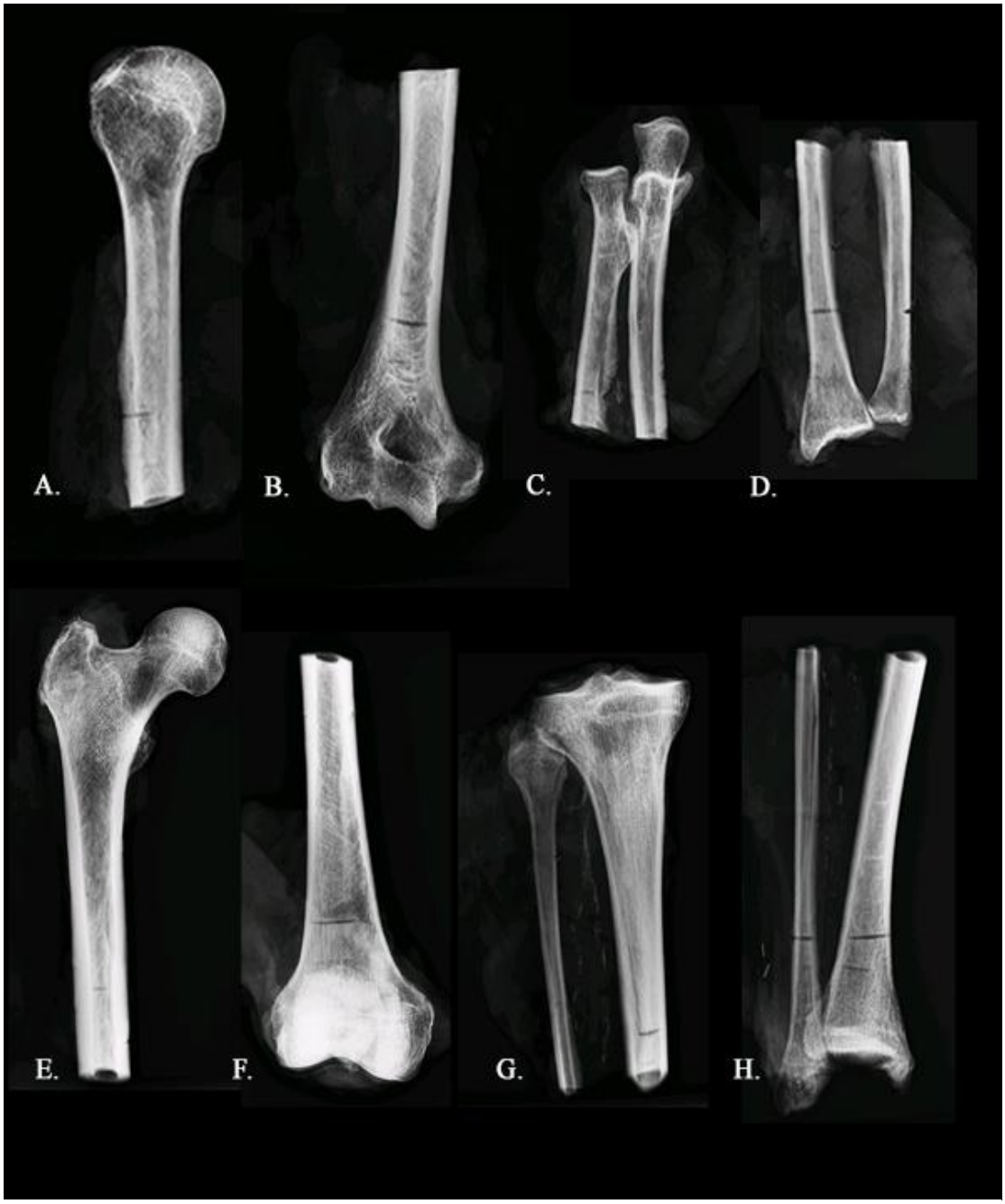

Figure 31. Post-trauma Long Bone Radiographs. *Radiographic images taken of the human sample of bone for this study following trauma. A.) Anterolateral view of proximal humerus B.) Anterior view of distal humerus C.) Anterior view of proximal radius and ulna D.) Anterior view of distal radius and ulna E.) Anterior view of proximal femur F.) Anterior view of distal femur G.) Anterior view of proximal fibula and tibia and H.) Anterior view of distal fibula and tibia. All elements are from the right side of the individual. The distal halves of each respective bone were burned.*

Figure 32. Post-trauma Rib Radiographs. *Radiographs of the two right rib groups following trauma used in this study. A.) Ventrolateral view of ribs 4, 5, 6, and 7 and B.) Ventrolateral view of ribs 8, 9, and 10. Notice the irregular curvature of the ribs – this was due to fracturing from the impact of the trauma carriage and from full separation of kerfs from the flat-edge blade.*

APPENDIX C

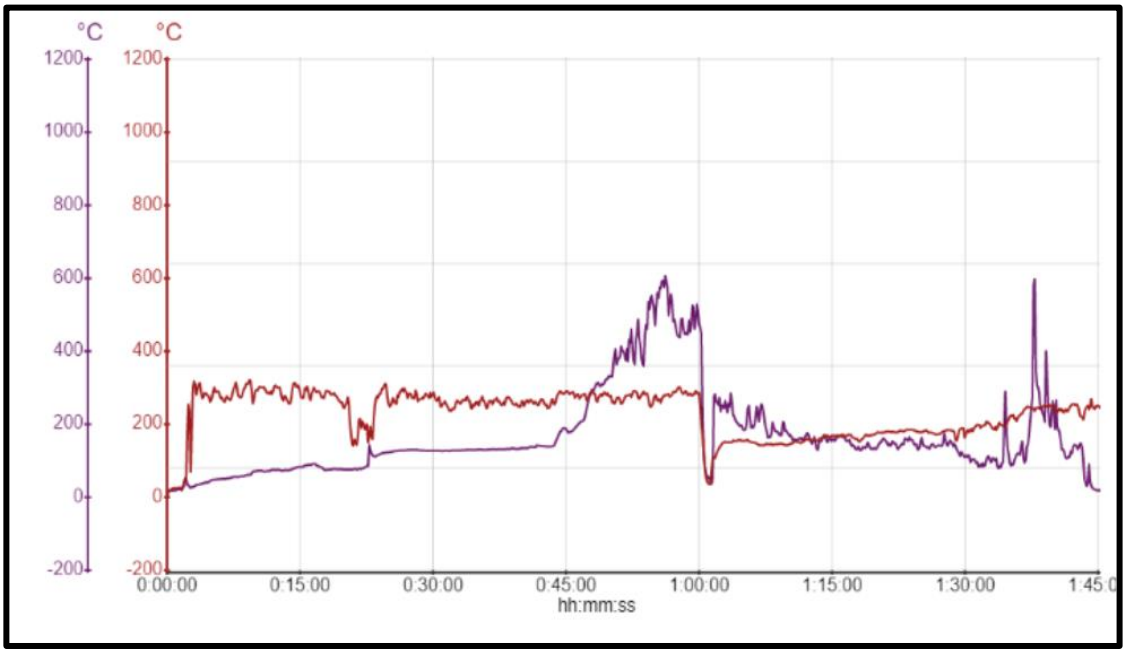

Figure 33. NeuLog® Pig Burn Temperature Graph. *This burn graph was generated by the NeuLog® data logger. This graph represents the temperature tracking of the pig femur and humerus burns with the red line tracking the charcoal and the purple line tracking the anterior surface of the samples. Notice the two flares of temperature that occurred. These were due to fatty regions catching fire.*

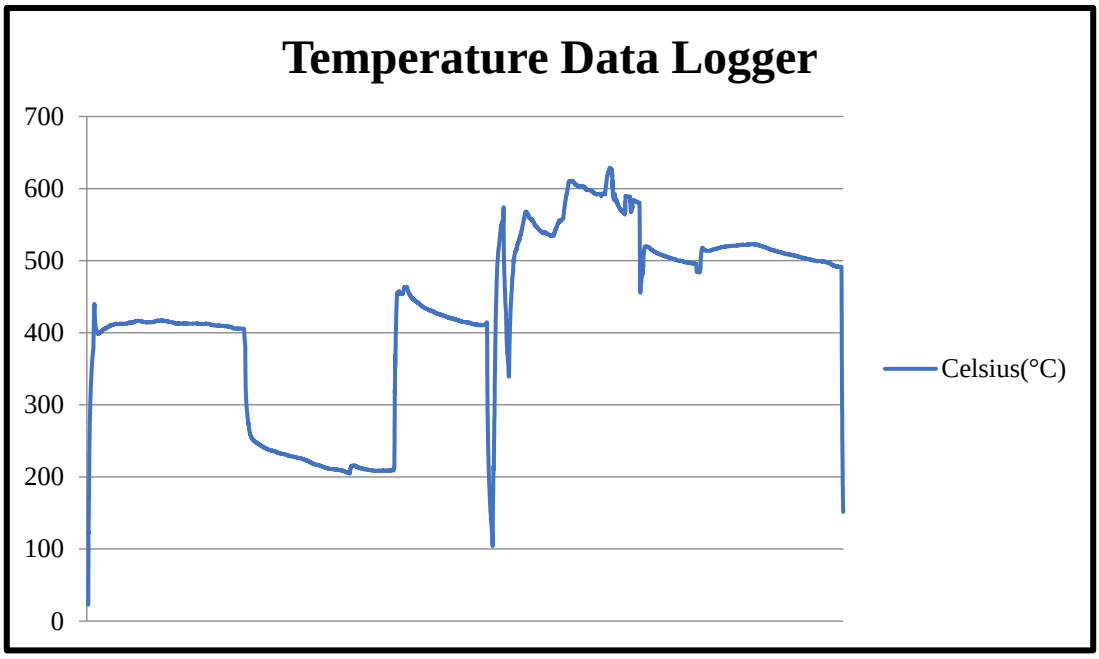

Figure 34. ThermoWorks® Pig Burn Temperature Graph. *ThermoWorks temperature of the charcoal under the samples. There are some inconsistencies in the burn patterns, and this may have been partially due to differences in air flow reaching the charcoal based on wind speed and direction. Additionally, the wetness of the samples sometimes dampened the charcoal before the fat ignited.*

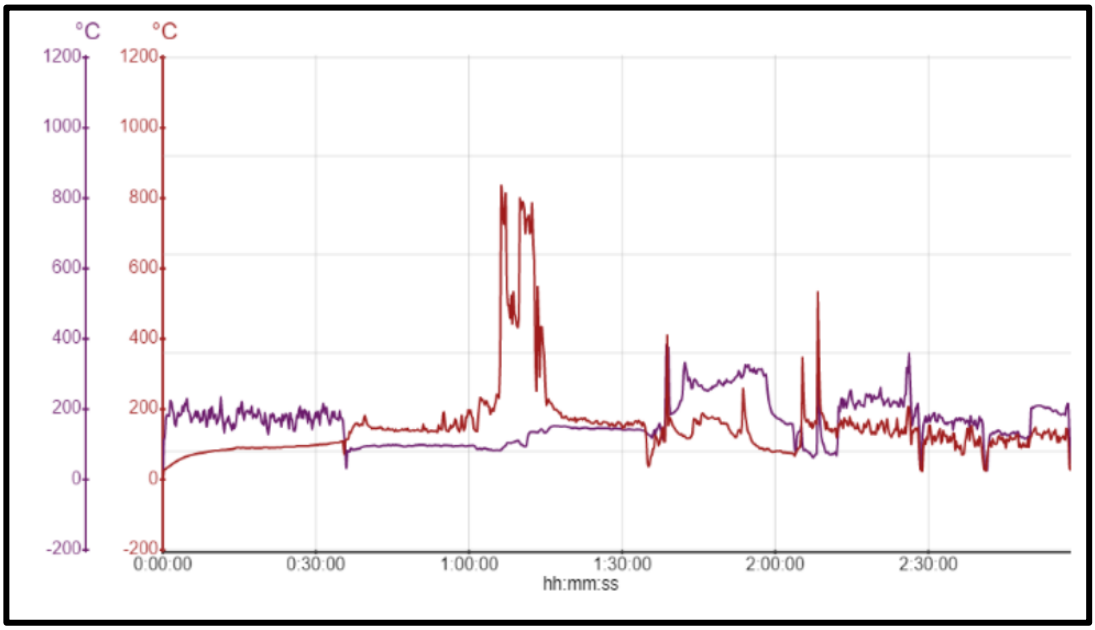

Figure 35. NeuLog® Pig Burn Temperature Graph. *This burn graph was generated by the NeuLog® data logger. This graph represents the temperature tracking of the pig tibia, fibula, radius, and ulna. The purple line tracked the anterior surfaces of the tibia and fibula, and the red line tracked the anterior surfaces of the radius and ulna.*

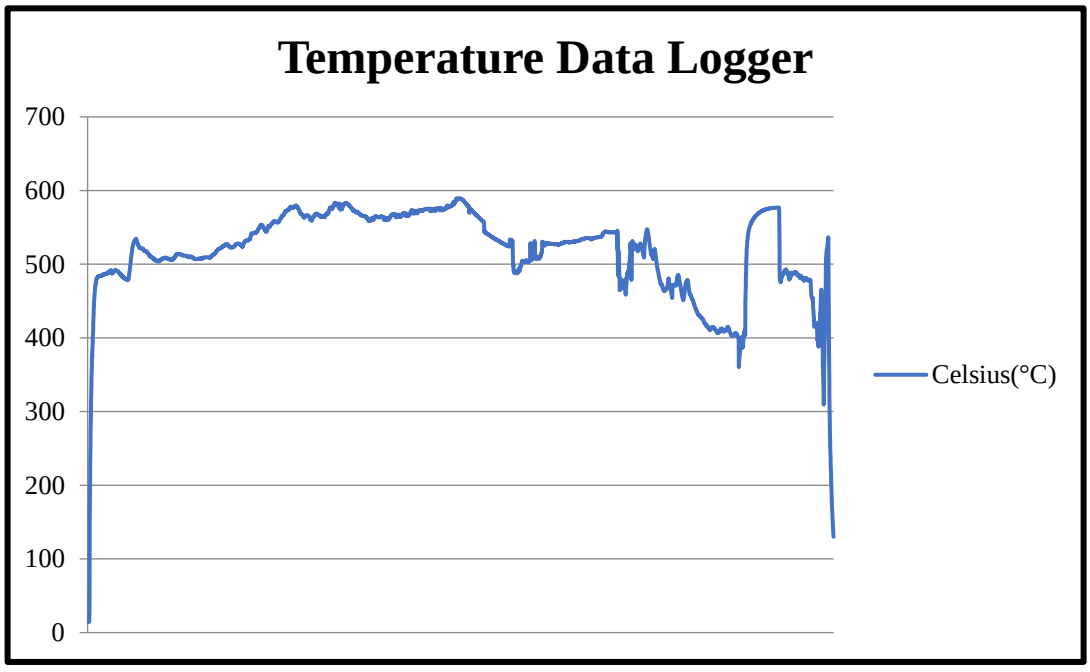

Figure 36. ThermoWorks® Pig Burn Temperature Graph. *ThermoWorks temperature of the charcoal under the samples. The temperatures here tracked much more evenly than the past study.*

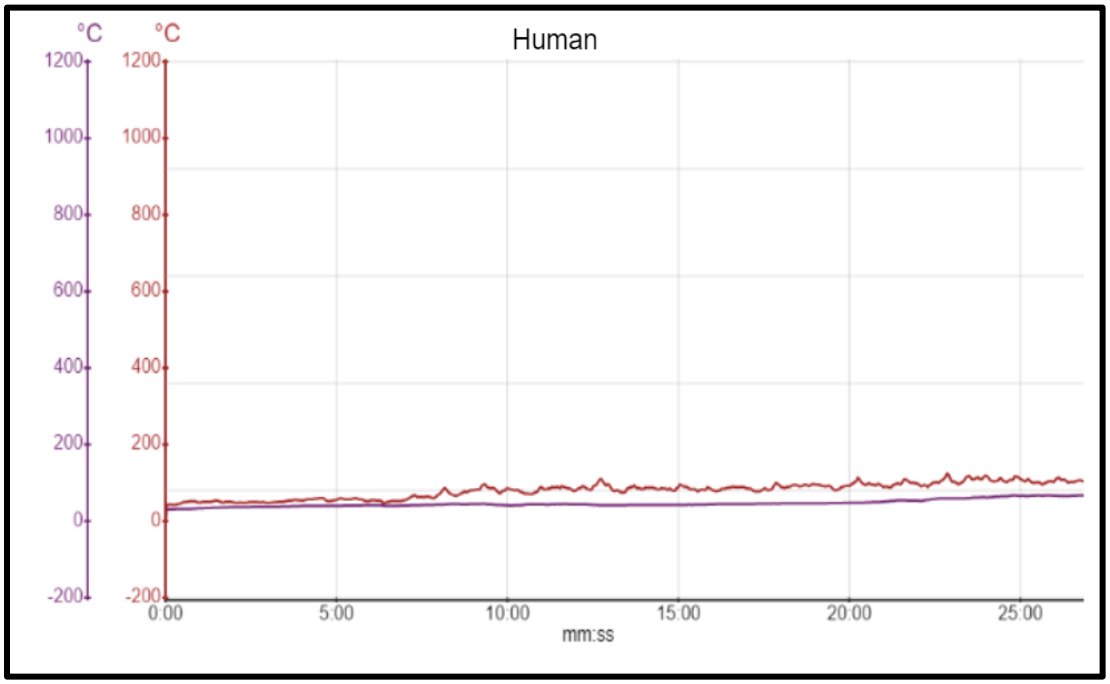

Figure 37. NeuLog® Human Burn Temperature Graph. *This graph was generated by the NeuLog® data loggers. Unfortunately, the data loggers were too damaged to accurately track temperature for the human element burns and were turned off after approximately 25 minutes. Temperature data information was then collected solely by the ThermoWorks ® data logger.*

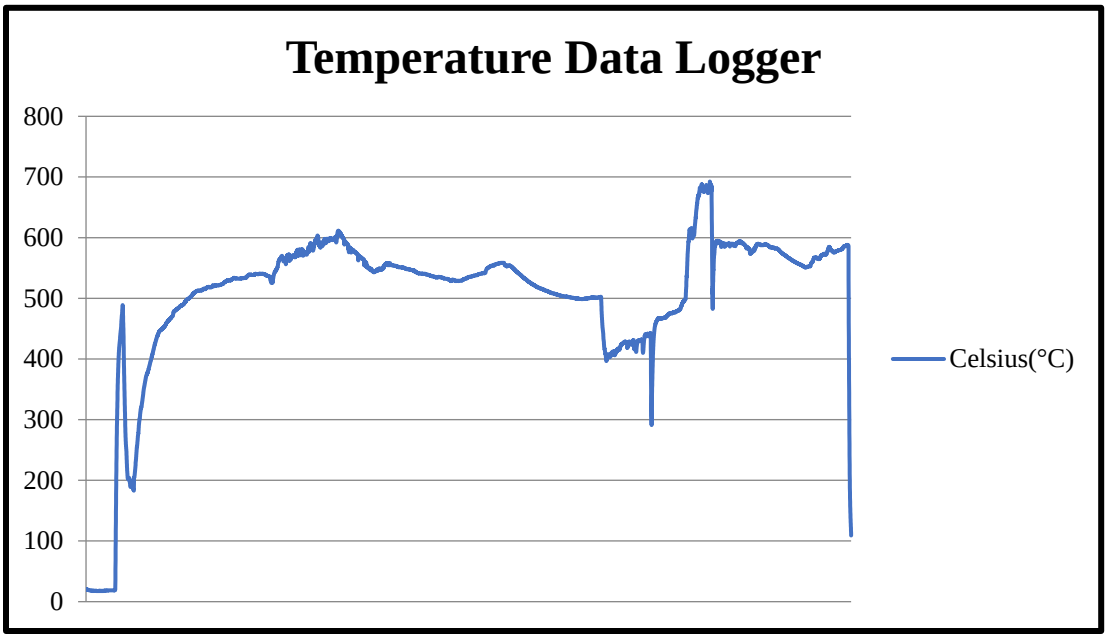

Figure 38. ThermoWorks® Human Burn Temperature Graph. *ThermoWorks temperature of the charcoal under the samples. The temperatures achieved are closely related with the temperatures achieved in the previous study.*

APPENDIX D

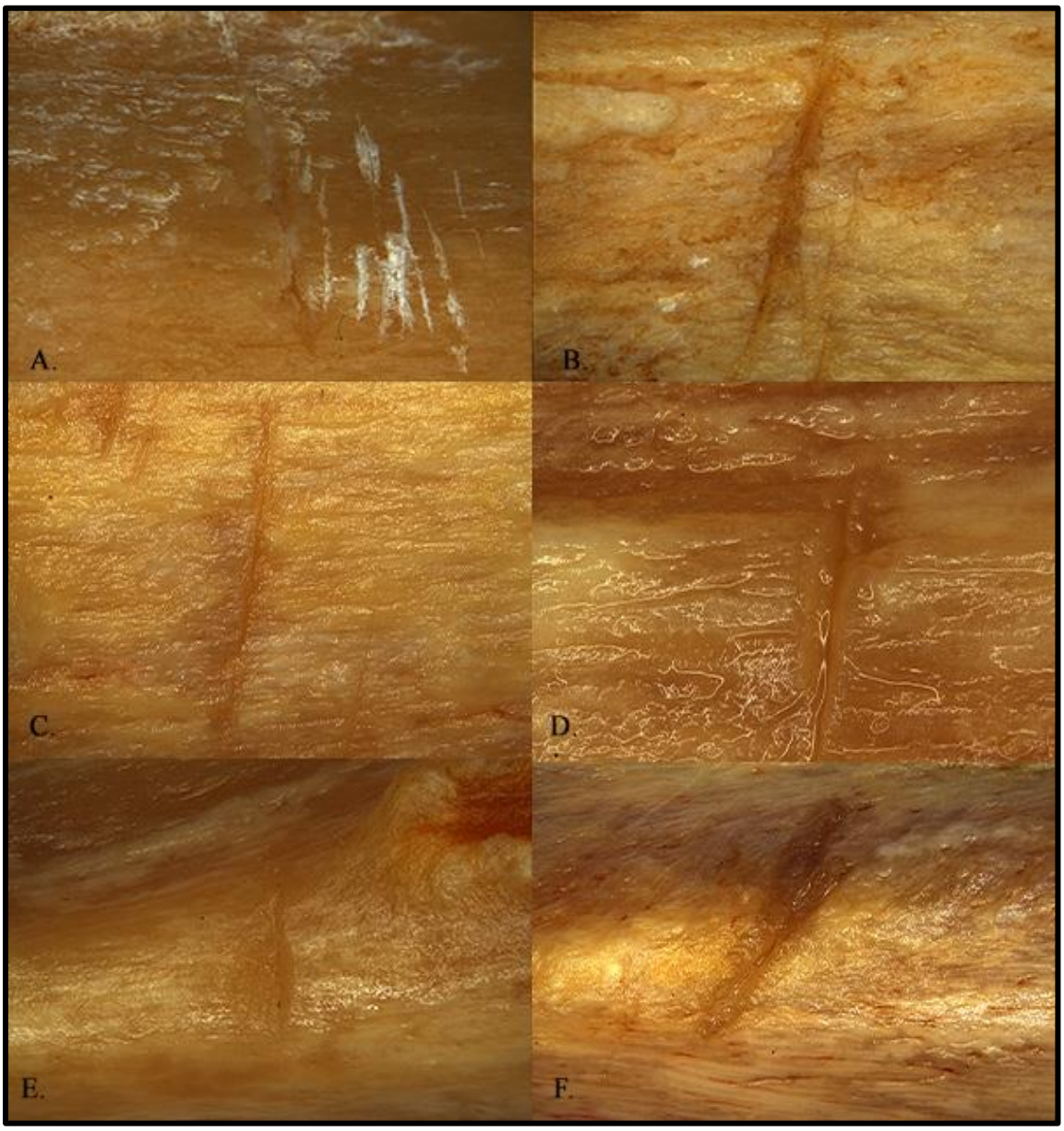

Figure 39. Control Flat-edge Cutmarks. *Leica stereomicroscopic images of flat-edge (FE) blade trauma in control human elements. A.) Femur FE with multiple rebounds; B.) Humerus FE; C.) Tibia FE; D.) Fibula FE with grease shine; E.) Ulna FE, wide due to the blade nicking a chunk of the interosseous crest; F.) Radius FE*

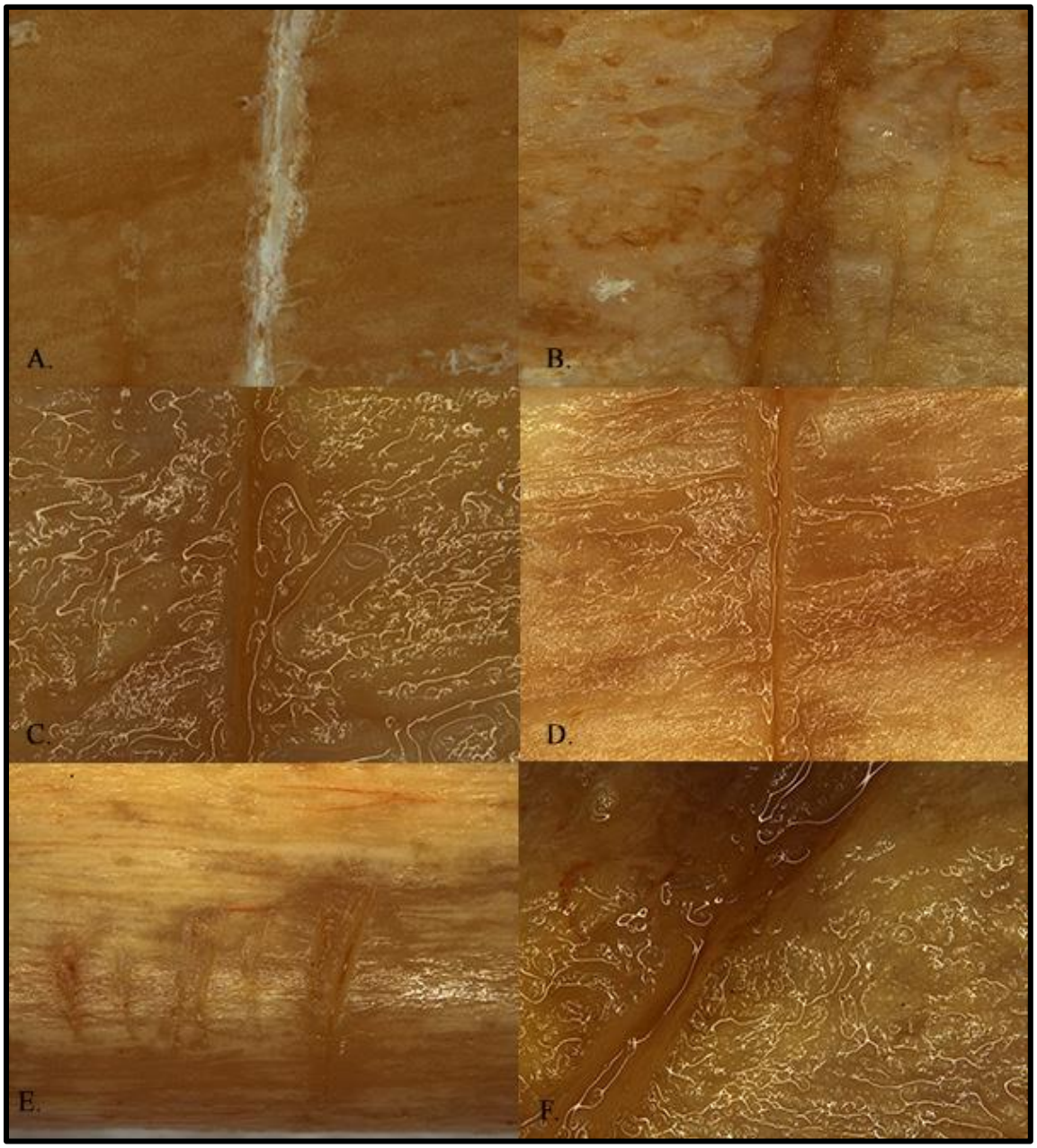

Figure 40. Control Serrated-edge Cutmarks. *Leica stereomicroscopic images of serrated-edge (SE) blade trauma in control human elements. A.) Femur SE; B.) Humerus SE with wide kerf; C.) Tibia SE with grease shine; D.) Fibula SE, notice the widening toward the upper portion of the image; E.) Ulna SE with multiple rebounds; F.) Radius SE with grease shine, notice widening of kerf*

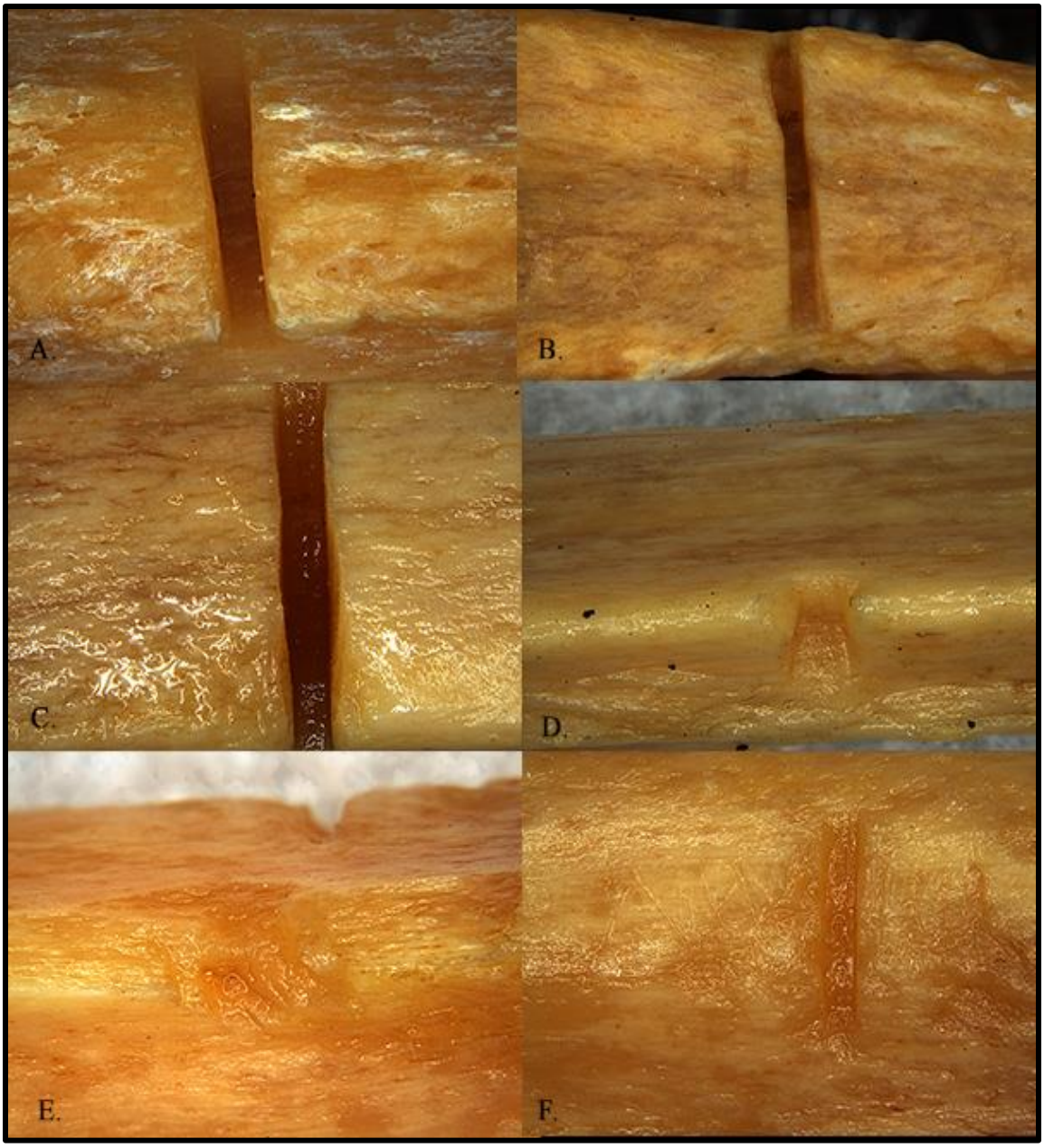

Figure 41. Control Reciprocating Saw Marks. *Leica stereomicroscopic images of reciprocating saw (RS) trauma in control human elements. A.) Femur RS with parallel sides; B.) Humerus RS with square bottom visible; C.) Tibia RS with slight widening of middle; D.) Fibula RS; E.) Ulna RS, very shallow, center of image; F.) Radius RS, parallel sides visible*

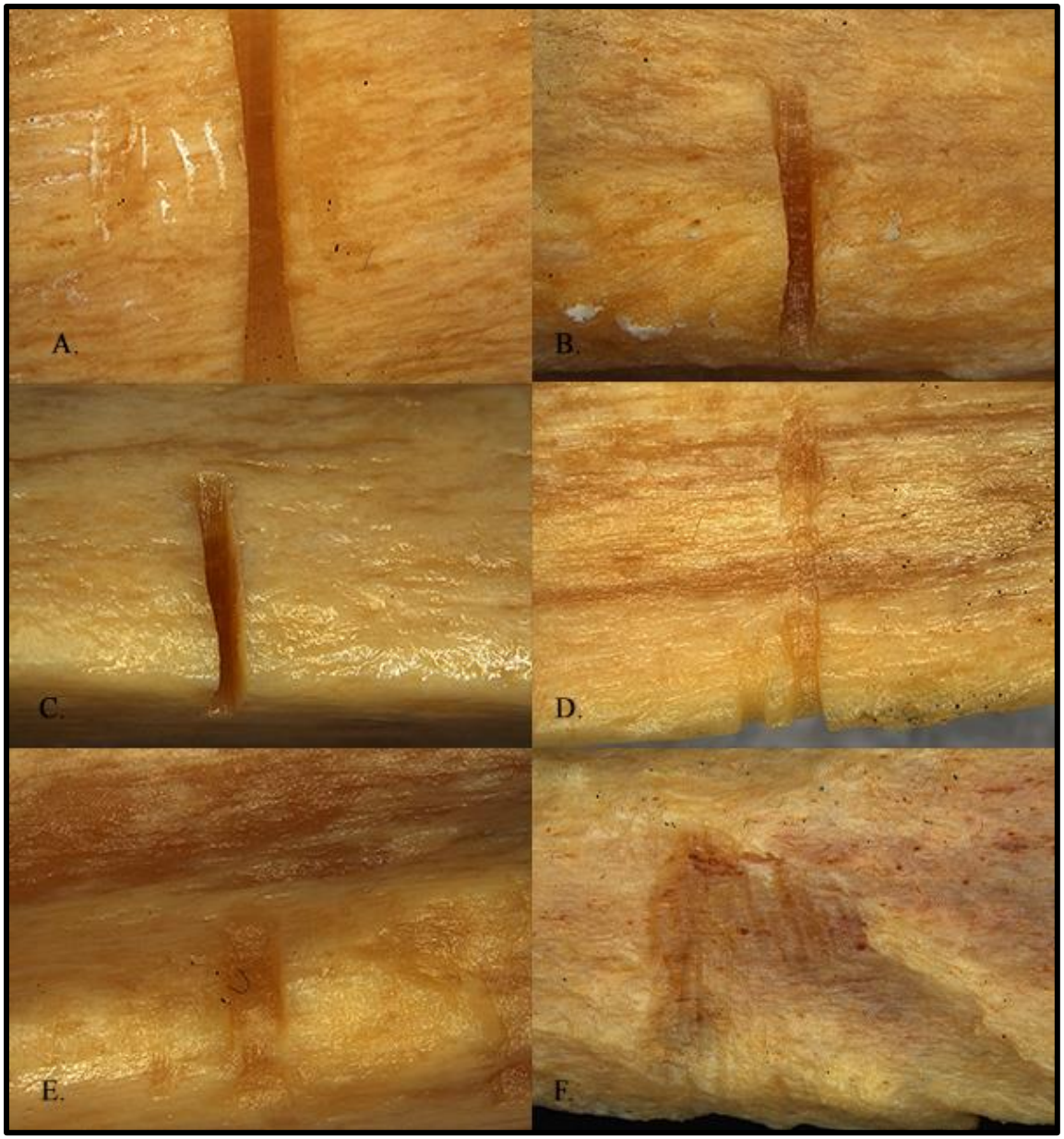

Figure 42. Control Handsaw Marks. *Leica stereomicroscopic images of handsaw (HS) trauma in control human elements. A.) Femur HS with bowed or necked sides; B.) Humerus HS with bowed sides; C.) Tibia HS through anterior crest; D.) Fibula HS, shallow, irregular with a false start on the right; E.) Ulna HS, very shallow, false start to the right; F.) Rib HS, irregular, very closely spaced striae visible indicating a high TPI*

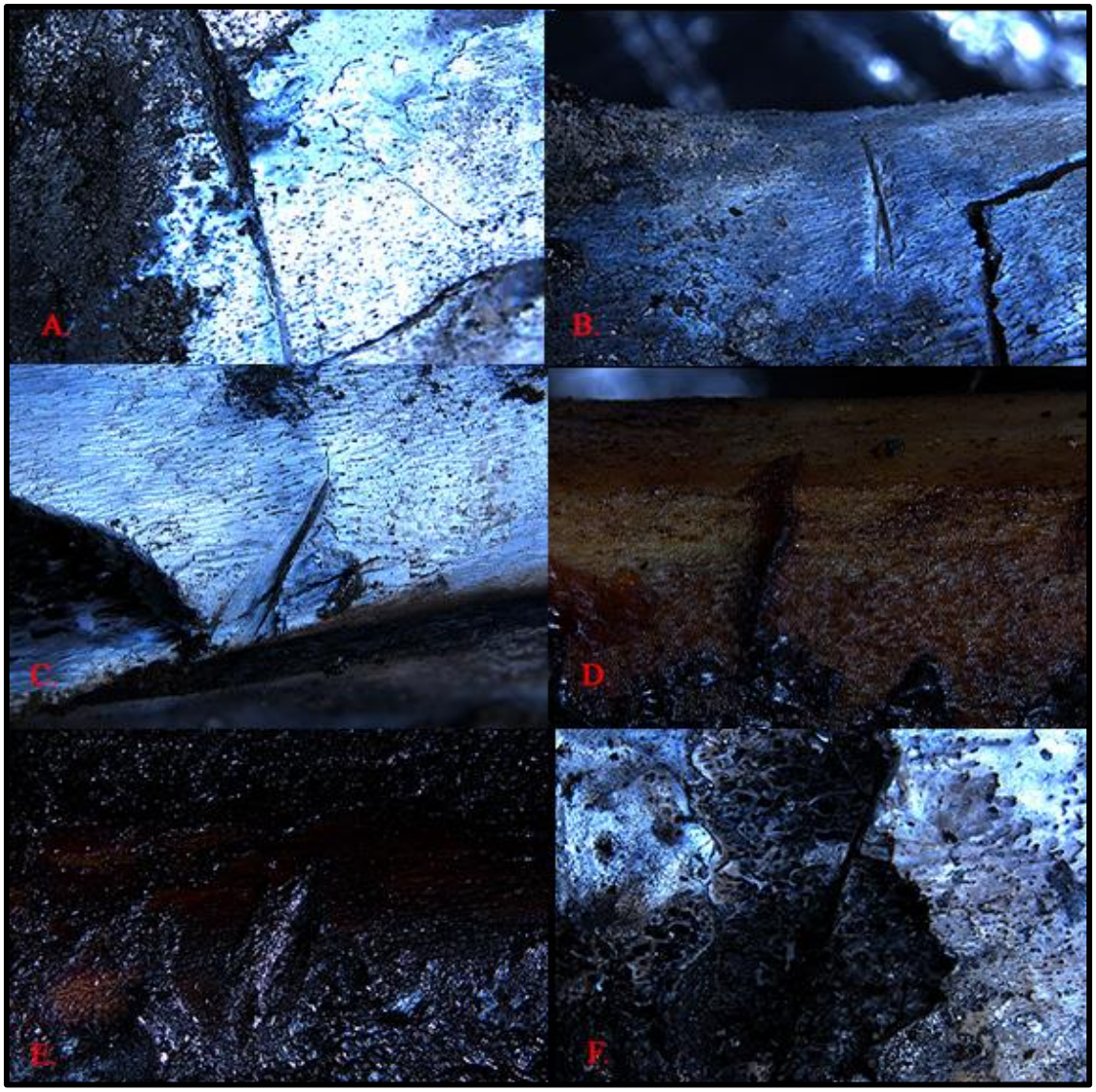

Figure 43. Burned Flat-edge Cutmarks. *Leica stereomicroscopic images of flat-edge (FE) blade trauma in burned pig elements. A.) Femur FE; B.) Humerus FE, lateral view; C.) Tibia FE with shearing; D.) Fibula FE, largely unburned; E.) Ulna FE, wide due to the blade nicking a chunk of bone; F.) Radius FE, running from the bottom middle up to the top right*

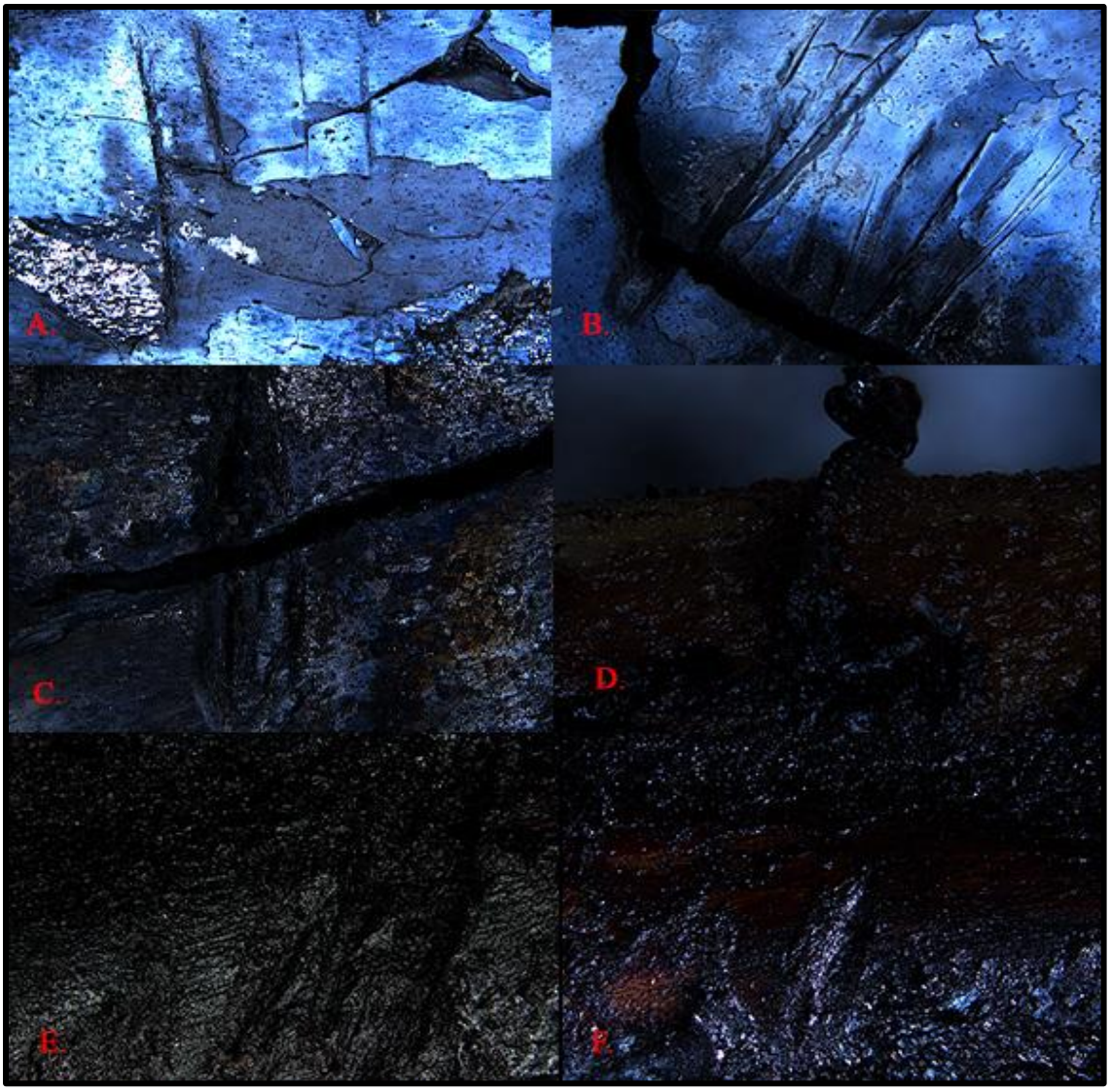

Figure 44. Burned Serrated-edge Cutmarks. *Leica stereomicroscopic images of serrated-edge (SE) blade trauma in burned pig elements. A.) Femur SE with multiple rebounds; B.) Humerus SE with multiple rebounds; C.) Tibia SE with widening; D.) Fibula SE, difficult to image, some shouldering present; E.) Ulna SE with multiple rebounds; F.) Radius SE with widening of kerf*

Figure 45. Burned Reciprocating Saw Marks. *Leica stereomicroscopic images of reciprocating saw (RS) trauma in burned pig elements. A.) Femur RS with parallel sides running left to right; B.) Humerus RS with parallel sides and some visible tooth jump; C.) Tibia RS with parallel sides; D.) Rib C RS; E.) Rib O RS with parallel sides; F.) Radius RS, full separation of kerf*

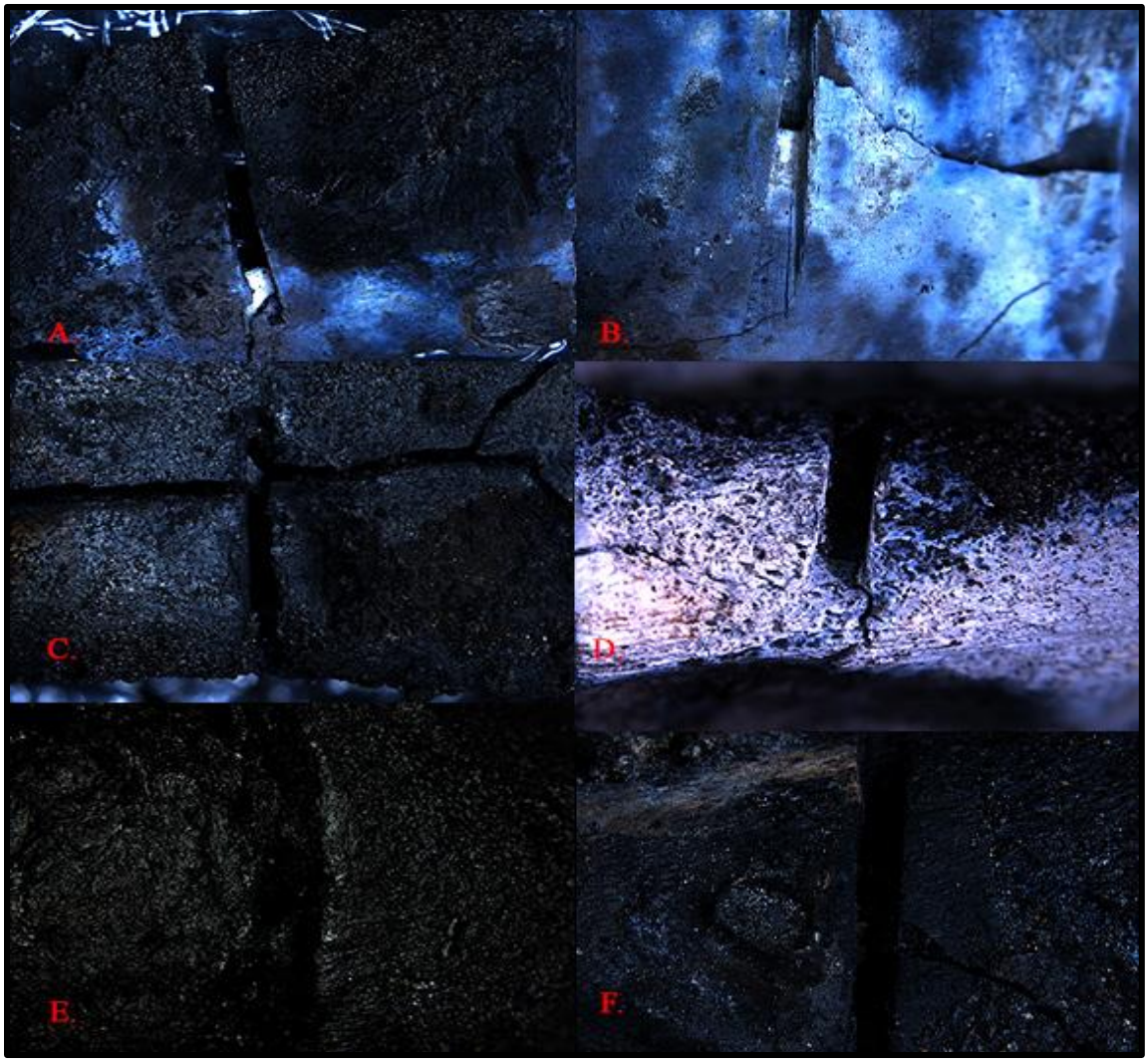

Figure 46. Burned Handsaw Marks. *Leica stereomicroscopic images of handsaw (HS) trauma in burned pig elements. A.) Femur HS with bowed or necked sides; B.) Humerus HS with flared end and obvious striae; C.) Tibia HS with thermal fracture; D.) Fibula HS, with very square bottom and slight bowing; E.) Ulna HS, center; F.) Radius HS, full separation of kerf*

APPENDIX E

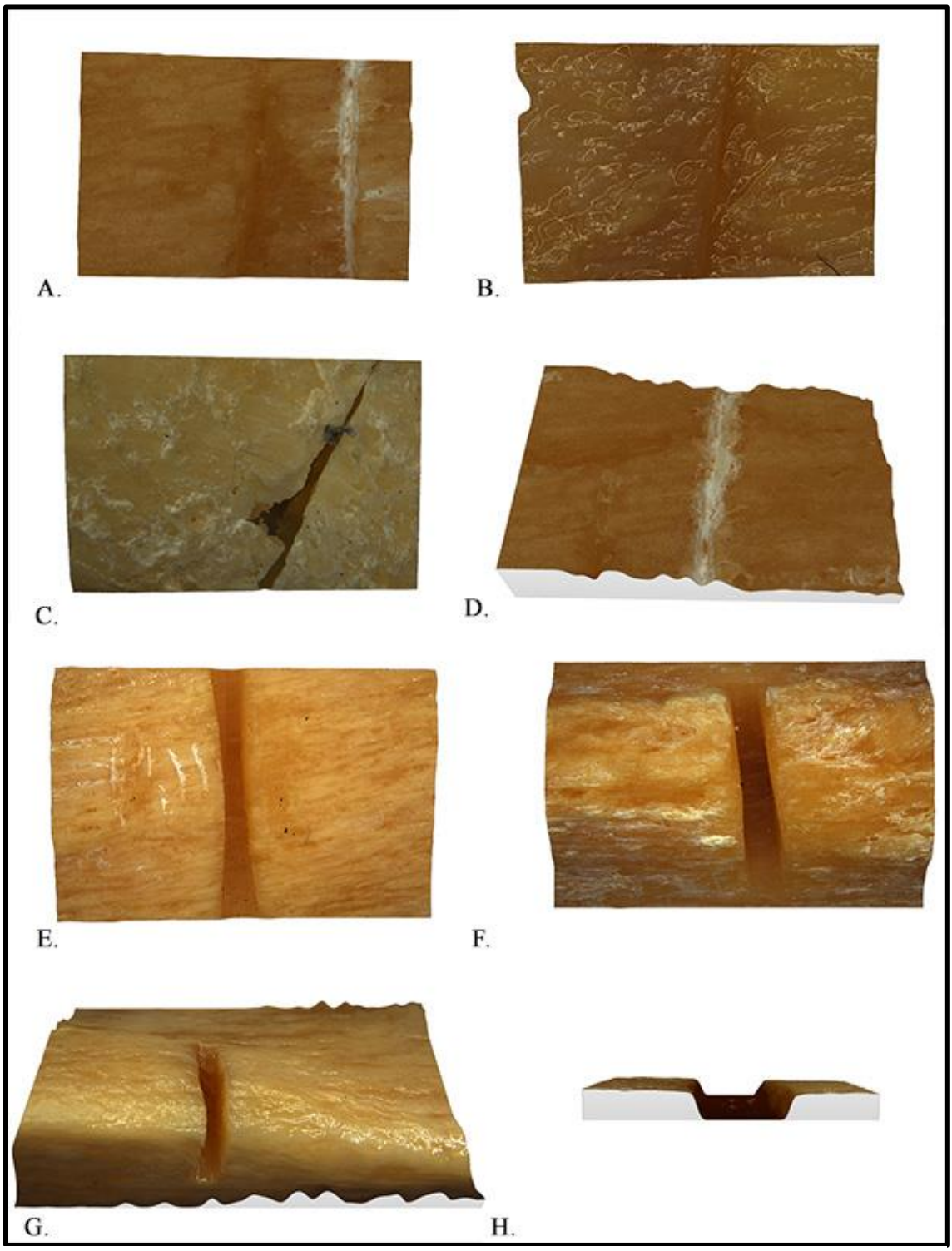

Figure 47. Leica 3-D Control Cutmark Models. *Human samples. A.) Flat-edge and serrated-edge kerfs on the femur B.) Flat-edge kerf on the tibia C.) Serrated-edge kerf on the fifth rib D.) Serrated-edge kerf on the femur E.) Handsaw kerf on the femur F.) Reciprocating saw kerf on the femur G.) Handsaw kerf on the tibia and H.) Profile view of a reciprocating saw kerf on the tibia showing the square kerf morphology.*

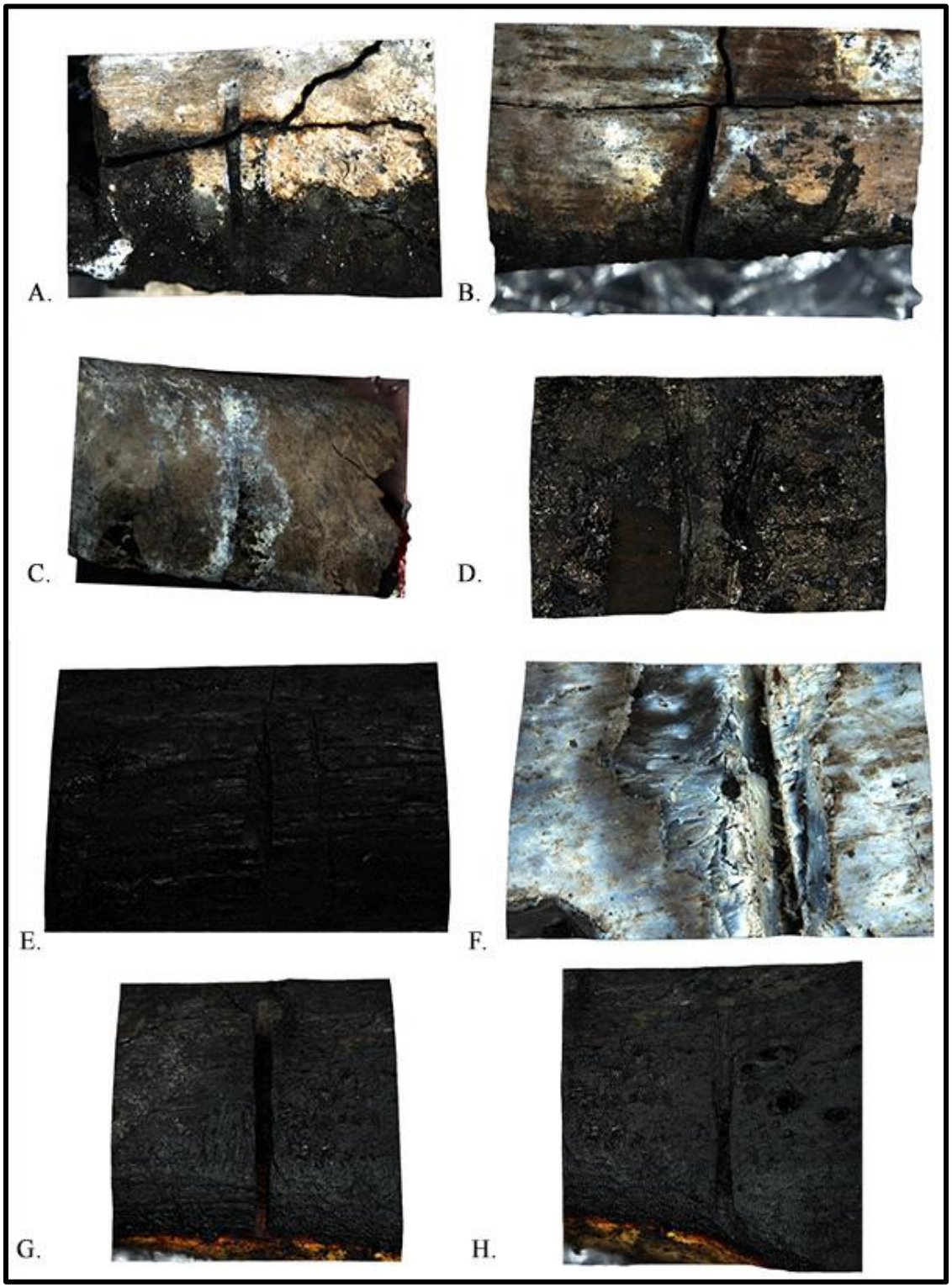

Figure 48. Leica 3-D Burned Cutmark Models. *Human sample. A.) Handsaw kerf on tibia B.) Flat-edge kerf on tibia C.) Reciprocating saw kerf on rib C, shallow D.) Handsaw kerf on radius E.) Flat-edge kerf on femur F.) Serrated-edge kerf on tibia G.) Reciprocating saw kerf on femur H.) Handsaw kerf on femur.*

APPENDIX F

Kruskal-Wallis results from each measurement run against control human, control pig, burned human, and burned pig elements. Green shading indicates significance.

FE Length	
Kruskal-Wallis H	**4.352**
df	3
Asym. Sig.	.226
FE Width Max	
Kruskal-Wallis H	**8.737**
df	3
Asym. Sig.	.033
FE Width Min	
Kruskal-Wallis H	**4.361**
df	3
Asym. Sig.	.225
FE Depth Max	
Kruskal-Wallis H	**2.379**
df	3
Asym. Sig.	.498
FE Depth Mean	
Kruskal-Wallis H	**3.42**
df	3
Asym. Sig.	.330
FE OA°	
Kruskal-Wallis H	**4.351**
df	3
Asym. Sig.	.226

SE Length	
Kruskal-Wallis H	**11.294**
df	3
Asym. Sig.	.010

SE Width Max	
Kruskal-Wallis H	**1.488**
df	3
Asym. Sig.	.685

SE Width Min	
Kruskal-Wallis H	**2.675**
df	3
Asym. Sig.	.444

SE Depth Max	
Kruskal-Wallis H	**4.196**
df	3
Asym. Sig.	.241

SE Depth Mean	
Kruskal-Wallis H	**3.341**
df	3
Asym. Sig.	.342

SE OA°	
Kruskal-Wallis H	**3.566**
df	3
Asym. Sig.	.312

RS Length	
Kruskal-Wallis H	**3.103**
df	3
Asym. Sig.	.376

RS Width Max	
Kruskal-Wallis H	**10.868**
df	3
Asym. Sig.	.012

RS Width Min	
Kruskal-Wallis H	**3.517**
df	3
Asym. Sig.	.319

RS Depth Max	
Kruskal-Wallis H	**1.834**
df	3
Asym. Sig.	.608

RS Depth Mean	
Kruskal-Wallis H	**1.582**
df	3
Asym. Sig.	.663

HS Length	
Kruskal-Wallis H	**4.624**
df	3
Asym. Sig.	.201

HS Width Max	
Kruskal-Wallis H	**1.564**
df	3
Asym. Sig.	.668

HS Width Min	
Kruskal-Wallis H	**4.498**
df	3
Asym. Sig.	.212

HS Depth Max	
Kruskal-Wallis H	**4.665**
df	3
Asym. Sig.	.198

HS Depth Mean	
Kruskal-Wallis H	**4.444**
df	3
Asym. Sig.	.217

Mann-Whitney test results for each measurement run against the following pairs. Green shading indicates significance, and yellow shading indicates trending (near) significance.

Control Human versus Burned Human	Control Pig versus Burned Pig
Control Human versus Control Pig	Burned Human versus Burned Pig

Control Human versus Burned Human

FE Length

Z	**-1.443**
Asymp. Sig. 2-tailed	0.149
Exact Sig. 1-tailed	0.167

SE Length

Z	**-2.911**
Asymp. Sig. 2-tailed	0.004
Exact Sig. 1-tailed	0.002

FE Width Max

Z	**-2.143**
Asymp. Sig. 2-tailed	0.032
Exact Sig. 1-tailed	0.035

SE Width Max

Z	**-0.913**
Asymp. Sig. 2-tailed	0.361
Exact Sig. 1-tailed	0.429

FE Width Min

Z	**-1.192**
Asymp. Sig. 2-tailed	0.233
Exact Sig. 1-tailed	0.247

SE Width Min

Z	**-0.915**
Asymp. Sig. 2-tailed	0.360
Exact Sig. 1-tailed	0.429

FE Depth Max

Z	**-1.286**
Asymp. Sig. 2-tailed	0.199
Exact Sig. 1-tailed	0.234

SE Depth Max

Z	**-0.183**
Asymp. Sig. 2-tailed	0.855
Exact Sig. 1-tailed	0.931

FE Depth Mean

Z	**-1.714**
Asymp. Sig. 2-tailed	0.086
Exact Sig. 1-tailed	0.101

SE Depth Mean

Z	**-0.183**
Asymp. Sig. 2-tailed	0.855
Exact Sig. 1-tailed	.931

FE OA°

Z	**-1.492**
Asymp. Sig. 2-tailed	0.136
Exact Sig. 1-tailed	0.171

SE OA°

Z	**-0.313**
Asymp. Sig. 2-tailed	0.754
Exact Sig. 1-tailed	0.841

RS Length

Z	**-1.540**
Asymp. Sig. 2-tailed	0.124
Exact Sig. 1-tailed	0.139

HS Length

Z	**-1.155**
Asymp. Sig. 2-tailed	0.248
Exact Sig. 1-tailed	.274

RS Width Max

Z	**-1.061**
Asymp. Sig. 2-tailed	0.288
Exact Sig. 1-tailed	0.315

HS Width Max

Z	**-0.976**
Asymp. Sig. 2-tailed	0.329
Exact Sig. 1-tailed	.364

RS Width Min

Z	**-0.108**
Asymp. Sig. 2-tailed	0.914
Exact Sig. 1-tailed	0.958

HS Width Min

Z	**-1.777**
Asymp. Sig. 2-tailed	0.075
Exact Sig. 1-tailed	.075

RS Depth Max

Z	**-1.244**
Asymp. Sig. 2-tailed	0.214
Exact Sig. 1-tailed	0.237

HS Depth Max

Z	**-1.239**
Asymp. Sig. 2-tailed	0.216
Exact Sig. 1-tailed	0.224

RS Depth Mean

Z	**-1.066**
Asymp. Sig. 2-tailed	0.286
Exact Sig. 1-tailed	0.315

HS Depth Mean

Z	**-1.532**
Asymp. Sig. 2-tailed	0.126
Exact Sig. 1-tailed	0.145

Control Pig and Burned Pig

FE Length

Z	**-1.585**
Asymp. Sig. 2-tailed	0.113
Exact Sig. 1-tailed	0.118

SE Length

Z	**-0.926**
Asymp. Sig. 2-tailed	0.355
Exact Sig. 1-tailed	0.374

FE Width Max

Z	**-0.667**
Asymp. Sig. 2-tailed	0.505
Exact Sig. 1-tailed	0.525

SE Width Max

Z	**-0.551**
Asymp. Sig. 2-tailed	0.582
Exact Sig. 1-tailed	0.608

FE Width Min

Z	**-1.326**
Asymp. Sig. 2-tailed	0.185
Exact Sig. 1-tailed	.193

SE Width Min

Z	**-0.493**
Asymp. Sig. 2-tailed	0.622
Exact Sig. 1-tailed	0.652

FE Depth Max

Z	**0.000**
Asymp. Sig. 2-tailed	1.000
Exact Sig. 1-tailed	1.000

SE Depth Max

Z	**-1.488**
Asymp. Sig. 2-tailed	0.137
Exact Sig. 1-tailed	0.148

FE Depth Mean

Z	**-0.119**
Asymp. Sig. 2-tailed	0.906
Exact Sig. 1-tailed	0.922

SE Depth Mean

Z	**-1.253**
Asymp. Sig. 2-tailed	0.210
Exact Sig. 1-tailed	0.228

FE OA°

Z	**-0.825**
Asymp. Sig. 2-tailed	0.409
Exact Sig. 1-tailed	0.456

SE OA°

Z	**-2.208**
Asymp. Sig. 2-tailed	0.027
Exact Sig. 1-tailed	0.028

RS Length

Z	**-0.768**
Asymp. Sig. 2-tailed	0.443
Exact Sig. 1-tailed	0.471

HS Length

Z	**-1.054**
Asymp. Sig. 2-tailed	0.292
Exact Sig. 1-tailed	0.312

RS Width Max

Z	**-2.705**
Asymp. Sig. 2-tailed	0.007
Exact Sig. 1-tailed	.006

HS Width Max

Z	**-0.956**
Asymp. Sig. 2-tailed	0.339
Exact Sig. 1-tailed	0.365

RS Width Min

Z	**-1.848**
Asymp. Sig. 2-tailed	0.065
Exact Sig. 1-tailed	0.069

HS Width Min

Z	**-0.540**
Asymp. Sig. 2-tailed	0.589
Exact Sig. 1-tailed	0.624

RS Depth Max

Z	**-0.463**
Asymp. Sig. 2-tailed	0.643
Exact Sig. 1-tailed	0.678

HS Depth Max

Z	**-1.640**
Asymp. Sig. 2-tailed	0.101
Exact Sig. 1-tailed	0.108

RS Depth Mean

Z	**-0.347**
Asymp. Sig. 2-tailed	0.728
Exact Sig. 1-tailed	0.734

HS Depth Mean

Z	**-1.521**
Asymp. Sig. 2-tailed	0.128
Exact Sig. 1-tailed	0.140

Control Human versus Control Pig

FE Length

Z	**-0.396**
Asymp. Sig. 2-tailed	0.692
Exact Sig. 1-tailed	0.718

SE Length

Z	**-2.331**
Asymp. Sig. 2-tailed	0.020
Exact Sig. 1-tailed	0.019

FE Width Max

Z	**-0.201**
Asymp. Sig. 2-tailed	0.841
Exact Sig. 1-tailed	0.871

SE Width Max

Z	**-0.690**
Asymp. Sig. 2-tailed	0.490
Exact Sig. 1-tailed	0.503

FE Width Min

Z	**-1.908**
Asymp. Sig. 2-tailed	0.056
Exact Sig. 1-tailed	0.059

SE Width Min

Z	**-0.057**
Asymp. Sig. 2-tailed	0.955
Exact Sig. 1-tailed	1.000

FE Depth Max

Z	**-0.545**
Asymp. Sig. 2-tailed	0.586
Exact Sig. 1-tailed	0.622

SE Depth Max

Z	**-0.789**
Asymp. Sig. 2-tailed	0.430
Exact Sig. 1-tailed	0.443

FE Depth Mean

Z	**-0.389**
Asymp. Sig. 2-tailed	0.697
Exact Sig. 1-tailed	0.733

SE Depth Mean

Z	**-0.632**
Asymp. Sig. 2-tailed	0.527
Exact Sig. 1-tailed	0.574

FE OA°

Z	**-1.768**
Asymp. Sig. 2-tailed	0.077
Exact Sig. 1-tailed	0.088

SE OA°

Z	**-0.732**
Asymp. Sig. 2-tailed	0.464
Exact Sig. 1-tailed	0.524

RS Length

Z	**-1.035**
Asymp. Sig. 2-tailed	0.301
Exact Sig. 1-tailed	0.324

HS Length

Z	**-2.225**
Asymp. Sig. 2-tailed	0.026
Exact Sig. 1-tailed	0.026

RS Width Max

Z	**-2.419**
Asymp. Sig. 2-tailed	0.016
Exact Sig. 1-tailed	0.015

HS Width Max

Z	**-0.059**
Asymp. Sig. 2-tailed	0.953
Exact Sig. 1-tailed	0.977

RS Width Min

Z	**-0.791**
Asymp. Sig. 2-tailed	0.429
Exact Sig. 1-tailed	0.456

HS Width Min

Z	**-0.540**
Asymp. Sig. 2-tailed	0.589
Exact Sig. 1-tailed	0.624

RS Depth Max

Z	**-1.055**
Asymp. Sig. 2-tailed	0.291
Exact Sig. 1-tailed	0.314

HS Depth Max

Z	**-1.714**
Asymp. Sig. 2-tailed	0.086
Exact Sig. 1-tailed	0.093

RS Depth Mean

Z	**-1.121**
Asymp. Sig. 2-tailed	0.262
Exact Sig. 1-tailed	0.283

HS Depth Mean

Z	**-1.701**
Asymp. Sig. 2-tailed	0.089
Exact Sig. 1-tailed	0.096

Burned Human versus Burned Pig

FE Length

Z	**-0.408**
Asymp. Sig. 2-tailed	0.683
Exact Sig. 1-tailed	.711

SE Length

Z	**-1.859**
Asymp. Sig. 2-tailed	0.063
Exact Sig. 1-tailed	.068

FE Width Max

Z	**-2.645**
Asymp. Sig. 2-tailed	0.008
Exact Sig. 1-tailed	.006

SE Width Max

Z	**0.000**
Asymp. Sig. 2-tailed	1.000
Exact Sig. 1-tailed	1.000

FE Width Min

Z	**-1.253**
Asymp. Sig. 2-tailed	0.210
Exact Sig. 1-tailed	.219

SE Width Min

Z	**-1.209**
Asymp. Sig. 2-tailed	0.227
Exact Sig. 1-tailed	.256

FE Depth Max

Z	**-1.203**
Asymp. Sig. 2-tailed	0.229
Exact Sig. 1-tailed	.249

SE Depth Max

Z	**-1.519**
Asymp. Sig. 2-tailed	0.129
Exact Sig. 1-tailed	.147

FE Depth Mean

Z	**-1.604**
Asymp. Sig. 2-tailed	0.109
Exact Sig. 1-tailed	.118

SE Depth Mean

Z	**-1.302**
Asymp. Sig. 2-tailed	0.193
Exact Sig. 1-tailed	.220

FE OA°

Z	**-0.640**
Asymp. Sig. 2-tailed	0.522
Exact Sig. 1-tailed	.610

SE OA°

Z	**-1.225**
Asymp. Sig. 2-tailed	0.221
Exact Sig. 1-tailed	.286

RS Length

Z	**-0.192**
Asymp. Sig. 2-tailed	0.847
Exact Sig. 1-tailed	.888

HS Length

Z	**-0.355**
Asymp. Sig. 2-tailed	0.722
Exact Sig. 1-tailed	.762

RS Width Max

Z	**-1.944**
Asymp. Sig. 2-tailed	0.052
Exact Sig. 1-tailed	.050

HS Width Max

Z	**-0.231**
Asymp. Sig. 2-tailed	0.817
Exact Sig. 1-tailed	.867

RS Width Min

Z	**-1.062**
Asymp. Sig. 2-tailed	0.288
Exact Sig. 1-tailed	.328

HS Width Min

Z	**-1.025**
Asymp. Sig. 2-tailed	0.306
Exact Sig. 1-tailed	.354

RS Depth Max

Z	**-0.735**
Asymp. Sig. 2-tailed	0.462
Exact Sig. 1-tailed	.505

HS Depth Max

Z	**-1.193**
Asymp. Sig. 2-tailed	0.233
Exact Sig. 1-tailed	.263

RS Depth Mean

Z	**-0.630**
Asymp. Sig. 2-tailed	0.529
Exact Sig. 1-tailed	.574

HS Depth Mean

Z	**-1.162**
Asymp. Sig. 2-tailed	0.245
Exact Sig. 1-tailed	.282

Test Statistics[a]

	FE length (mm)	FE width max (mm)	FE width min	FE depth max (mm)	FE depth mean (mm)	FE FA°	SE length	SE width max (mm)	SE width min	SE depth max (mm	SE depth mean (mm)	SE FA°	RS Length (mm)	RS width max (mm)	RS width min	RS depth max (mm)	RS depth mean (mm)	HS length (mm)	HS width max (mm)	HS width min	HS depth max (mm)	HS depth mean (mm)
Mann-Whitney U	21.000	6.000	8.500	12.000	9.000	5.000	4.000	10.000	10.000	14.000	14.000	11.000	20.000	32.000	29.000	26.000	28.000	27.000	25.000	10.500	16.500	14.000
Wilcoxon W	57.000	27.000	23.500	40.000	37.000	15.000	32.000	25.000	25.000	35.000	35.000	26.000	65.000	77.000	50.000	81.000	83.000	82.000	80.000	65.500	61.500	59.000
Z	-1.443	-2.143	-1.192	-1.286	-1.714	-1.492	-2.911	-0.913	-0.915	-0.183	-0.183	-0.313	-1.540	-1.061	-0.108	-1.244	-1.066	-1.155	-0.976	-1.777	-1.239	-1.532
Asymp. Sig. (2-tailed)	0.149	0.032	0.233	0.199	0.086	0.136	0.004	0.361	0.360	0.855	0.855	0.754	0.124	0.288	0.914	0.214	0.286	0.248	0.329	0.075	0.216	0.126
Exact Sig. [2*(1-tailed Sig.)]	.167[b]	.035[b]	.247[b]	.234[b]	.101[b]	.171[b]	.002[b]	.429[b]	.429[b]	.931[b]	.931[b]	.841[b]	.139[b]	.315[b]	.958[b]	.237[b]	.315[b]	.274[b]	.364[b]	.075[b]	.224[b]	.145[b]

a. Grouping Variable: hcontrolvburn

b. Not corrected for ties.

Test Statistics[a]

	FE length (mm)	FE width max (mm)	FE width min	FE depth max (mm)	FE depth mean (mm)	FE FA°	SE length	SE width max (mm)	SE width min	SE depth max (mm	SE depth mean (mm)	SE FA°	RS Length (mm)	RS width max (mm)	RS width min	RS depth max (mm)	RS depth mean (mm)	HS length (mm)	HS width max (mm)	HS width min	HS depth max (mm)	HS depth mean (mm)
Mann-Whitney U	92.000	96.000	80.500	120.000	117.000	20.000	66.000	62.000	53.000	41.000	41.000	3.000	47.000	18.000	28.000	42.000	43.500	52.000	42.000	41.000	42.000	31.000
Wilcoxon W	245.000	232.000	216.500	256.000	253.000	65.000	171.000	153.000	119.000	132.000	119.000	39.000	138.000	109.000	106.000	78.000	79.500	107.000	147.000	77.000	97.000	67.000
Z	-1.585	-0.667	-1.326	0.000	-0.119	-0.825	-0.926	-0.551	-0.493	-1.488	-1.253	-2.208	-0.768	-2.705	-1.848	-0.463	-0.347	-1.054	-0.956	-0.540	-1.640	-1.521
Asymp. Sig. (2-tailed)	0.113	0.505	0.185	1.000	0.906	0.409	0.355	0.582	0.622	0.137	0.210	0.027	0.443	0.007	0.065	0.643	0.728	0.292	0.339	0.589	0.101	0.128
Exact Sig. [2*(1-tailed Sig.)]	.118[b]	.525[b]	.193[b]	1.000[b]	.922[b]	.456[b]	.374[b]	.608[b]	.652[b]	.148[b]	.228[b]	.028[b]	.471[b]	.006[b]	.069[b]	.678[b]	.734[b]	.312[b]	.365[b]	.624[b]	.108[b]	.140[b]

a. Grouping Variable: pcontrolvburn

b. Not corrected for ties.

Test Statistics[a]

	FE length (mm)	FE width max (mm)	FE width min	FE depth max (mm)	FE depth mean (mm)	FE FA*	SE length	SE width max (mm)	SE width min	SE depth max (mm	SE depth mean (mm)	SE FA*	RS Length (mm)	RS width max (mm)	RS width min	RS depth max (mm)	RS depth mean (mm)	HS length (mm)	HS width max (mm)	HS width min	HS depth max (mm)	HS depth mean (mm)
Mann-Whitney U	65.000	53.000	22.500	38.000	40.000	12.000	26.000	25.500	27.000	24.500	24.000	15.000	43.000	26.000	48.000	44.000	43.000	32.000	69.000	34.000	36.000	35.000
Wilcoxon W	201.000	189.000	158.500	158.000	160.000	57.000	131.000	40.500	93.000	39.500	39.000	51.000	88.000	117.000	126.000	99.000	98.000	87.000	124.000	89.000	81.000	80.000
Z	-0.396	-0.201	-1.908	-0.545	-0.389	-1.768	-2.331	-0.690	-0.057	-0.789	-0.632	-0.732	-1.035	-2.419	-0.791	-1.055	-1.121	-2.225	-0.059	-1.714	-1.701	-1.569
Asymp. Sig. (2-tailed)	0.692	0.841	0.056	0.586	0.697	0.077	0.020	0.490	0.955	0.430	0.527	0.464	0.301	0.016	0.429	0.291	0.262	0.026	0.953	0.086	0.089	0.117
Exact Sig. [2*(1-tailed Sig.)]	.718[b]	.871[b]	.059[b]	.622[b]	.733[b]	.088[b]	.019[b]	.503[b]	1.000[b]	.443[b]	.574[b]	.524[b]	.324[b]	.015[b]	.456[b]	.314[b]	.283[b]	.026[b]	.977[b]	.093[b]	.096[b]	.126[b]

a. Grouping Variable: Speciescontrol

b. Not corrected for ties.

Test Statistics[a]

	FE length (mm)	FE width max (mm)	FE width min	FE depth max (mm)	FE depth mean (mm)	FE FA*	SE length	SE width max (mm)	SE width min	SE depth max (mm	SE depth mean (mm)	SE FA*	RS Length (mm)	RS width max (mm)	RS width min	RS depth max (mm)	RS depth mean (mm)	HS length (mm)	HS width max (mm)	HS width min	HS depth max (mm)	HS depth mean (mm)
Mann-Whitney U	61.000	10.000	21.500	38.000	32.000	9.000	20.000	33.000	21.000	16.000	18.000	5.000	34.000	18.500	18.000	25.000	26.000	36.000	26.000	13.000	19.000	15.000
Wilcoxon W	214.000	31.000	36.500	66.000	60.000	19.000	48.000	99.000	87.000	37.000	39.000	20.000	70.000	63.500	39.000	61.000	62.000	91.000	62.000	49.000	74.000	51.000
Z	-0.408	-2.645	-1.253	-1.203	-1.604	-0.640	-1.859	0.000	-1.209	-1.519	-1.302	-1.225	-0.192	-1.944	-1.062	-0.735	-0.630	-0.355	-0.231	-1.025	-1.193	-1.162
Asymp. Sig. (2-tailed)	0.683	0.008	0.210	0.229	0.109	0.522	0.063	1.000	0.227	0.129	0.193	0.221	0.847	0.052	0.288	0.462	0.529	0.722	0.817	0.306	0.233	0.245
Exact Sig. [2*(1-tailed Sig.)]	.711[b]	.006[b]	.219[b]	.249[b]	.118[b]	.610[b]	.068[b]	1.000[b]	.256[b]	.147[b]	.220[b]	.286[b]	.888[b]	.050[b]	.328[b]	.505[b]	.574[b]	.762[b]	.867[b]	.354[b]	.263[b]	.282[b]

a. Grouping Variable: Speciesburned

b. Not corrected for ties.

Flat-edge vs. Serrated-edge Blade
Mann-Whitney U Test

Ranks

	ToolType	N	Mean Rank	Sum of Ranks
Width max (mm)	FlatEdgeBlade	43	30.23	1300.00
	SerratedEdgeBlade	35	50.89	1781.00
	Total	78		
Width mean (mm)	FlatEdgeBlade	42	27.75	1165.50
	SerratedEdgeBlade	34	51.78	1760.50
	Total	76		
Width min	FlatEdgeBlade	41	27.55	1129.50
	SerratedEdgeBlade	33	49.86	1645.50
	Total	74		
Depth max (mm)	FlatEdgeBlade	44	32.05	1410.00
	SerratedEdgeBlade	34	49.15	1671.00
	Total	78		
Depth mean (mm)	FlatEdgeBlade	44	32.08	1411.50
	SerratedEdgeBlade	33	48.23	1591.50
	Total	77		

Test Statistics[a]

	Width max (mm)	Width mean (mm)	Width min	Depth max (mm)	Depth mean (mm)
Mann-Whitney U	354.000	262.500	268.500	420.000	421.500
Wilcoxon W	1300.000	1165.500	1129.500	1410.000	1411.500
Z	-4.005	-4.720	-4.444	-3.305	-3.134
Asymp. Sig. (2-tailed)	.000	.000	.000	.001	.002

a. Grouping Variable: ToolType

Reciprocating saw vs. Handsaw
Mann-Whitney U Test

Ranks

	ToolType	N	Mean Rank	Sum of Ranks
Width max (mm)	ReciprocatingSaw	41	53.88	2209.00
	Handsaw	39	26.44	1031.00
	Total	80		
Width mean (mm)	ReciprocatingSaw	40	53.19	2127.50
	Handsaw	39	26.47	1032.50
	Total	79		
Width min	ReciprocatingSaw	37	48.72	1802.50
	Handsaw	35	23.59	825.50
	Total	72		
Depth max (mm)	ReciprocatingSaw	38	47.30	1797.50
	Handsaw	39	30.91	1205.50
	Total	77		
Depth mean (mm)	ReciprocatingSaw	38	44.13	1677.00
	Handsaw	36	30.50	1098.00
	Total	74		

Test Statistics[a]

	Width max (mm)	Width mean (mm)	Width min	Depth max (mm)	Depth mean (mm)
Mann-Whitney U	251.000	252.500	195.500	425.500	432.000
Wilcoxon W	1031.000	1032.500	825.500	1205.500	1098.000
Z	-5.280	-5.173	-5.093	-3.215	-2.725
Asymp. Sig. (2-tailed)	.000	.000	.000	.001	.006

a. Grouping Variable: ToolType

Chi-Square Test of Independence and Cramer's V for Reciprocating Saw Striae

Crosstab

			Status		
			Burn	Control	Total
RS_Striae	Striae Absent	Count	4	2	6
		% within RS_Striae	66.7%	33.3%	100.0%
		% within Status	17.4%	8.3%	12.8%
		% of Total	8.5%	4.3%	12.8%
	Striae Present	Count	19	22	41
		% within RS_Striae	46.3%	53.7%	100.0%
		% within Status	82.6%	91.7%	87.2%
		% of Total	40.4%	46.8%	87.2%
Total		Count	23	24	47
		% within RS_Striae	48.9%	51.1%	100.0%
		% within Status	100.0%	100.0%	100.0%
		% of Total	48.9%	51.1%	100.0%

Chi-Square Tests

	Value	df	Asymptotic Significance (2-sided)	Exact Sig. (2-sided)	Exact Sig. (1-sided)
Pearson Chi-Square	.865[a]	1	0.352		
Continuity Correction[b]	0.243	1	0.622		
Likelihood Ratio	0.878	1	0.349		
Fisher's Exact Test				0.416	0.312
N of Valid Cases	47				

a. 2 cells (50.0%) have expected count less than 5. The minimum expected count is 2.94.

b. Computed only for a 2x2 table

Symmetric Measures

		Value	Approximate Significance
Nominal by Nominal	Phi	0.136	0.352
	Cramer's V	0.136	0.352
N of Valid Cases		47	

Chi-Square Test of Independence and Cramer's V for Handsaw Striae

Crosstab

			Status		
			Burn	Control	Total
HS_Striae	Striae Absent	Count	4	3	7
		% within HS_Striae	57.1%	42.9%	100.0%
		% within Status	21.1%	13.0%	16.7%
		% of Total	9.5%	7.1%	16.7%
	Striae Present	Count	15	20	35
		% within HS_Striae	42.9%	57.1%	100.0%
		% within Status	78.9%	87.0%	83.3%
		% of Total	35.7%	47.6%	83.3%
Total		Count	19	23	42
		% within HS_Striae	45.2%	54.8%	100.0%
		% within Status	100.0%	100.0%	100.0%
		% of Total	45.2%	54.8%	100.0%

Chi-Square Tests

	Value	df	Asymptotic Significance (2-sided)	Exact Sig. (2-sided)	Exact Sig. (1-sided)
Pearson Chi-Square	.481[a]	1	0.488		
Continuity Correction[b]	0.077	1	0.782		
Likelihood Ratio	0.479	1	0.489		
Fisher's Exact Test				0.682	0.388
N of Valid Cases	42				

a. 2 cells (50.0%) have expected count less than 5. The minimum expected count is 3.17.

b. Computed only for a 2x2 table

Symmetric Measures

		Value	Approximate Significance
Nominal by Nominal	Phi	0.107	0.488
	Cramer's V	0.107	0.488
N of Valid Cases		42	

Goodness of Fit Tests for Striae in the Reciprocating Saw and Handsaw Kerfs

RS_Striae			
	Observed N	Expected N	Residual
Striae Absent	6	23.5	-17.5
Striae Present	41	23.5	17.5
Total	47		

HS_Striae			
	Observed N	Expected N	Residual
Striae Absent	7	21.0	-14.0
Striae Present	35	21.0	14.0
Total	42		

Test Statistics		
	RS_Striae	HS_Striae
Chi-Square	26.064[a]	18.667[b]
df	1	1
Asymp. Sig.	0.000	0.000

a. 0 cells (0.0%) have expected frequencies less than 5. The minimum expected cell frequency is 23.5.

b. 0 cells (0.0%) have expected frequencies less than 5. The minimum expected cell frequency is 21.0.

Wilcoxon Signed-Rank Test results for Leica digital stereomicroscope kerf measurements versus DinoLite Edge digital microscope matching kerf measurements.

Ranks				
		N	Mean Rank	Sum of Ranks
DinoLite - Leica	Negative Ranks	153[a]	127.15	19453.50
	Positive Ranks	69[b]	76.80	5299.50
	Ties	5[c]		
	Total	227		
a. DinoLite < Leica				
b. DinoLite > Leica				
c. DinoLite = Leica				

Test Statistics[a]	
	DinoLite - Leica
Z	-7.387[b]
Asymp. Sig. (2-tailed)	0.000
a. Wilcoxon Signed Ranks Test	
b. Based on positive ranks.	

APPENDIX G

DATA COLLECTION FORM FOR INITIAL TRAUMA LOCATIONS

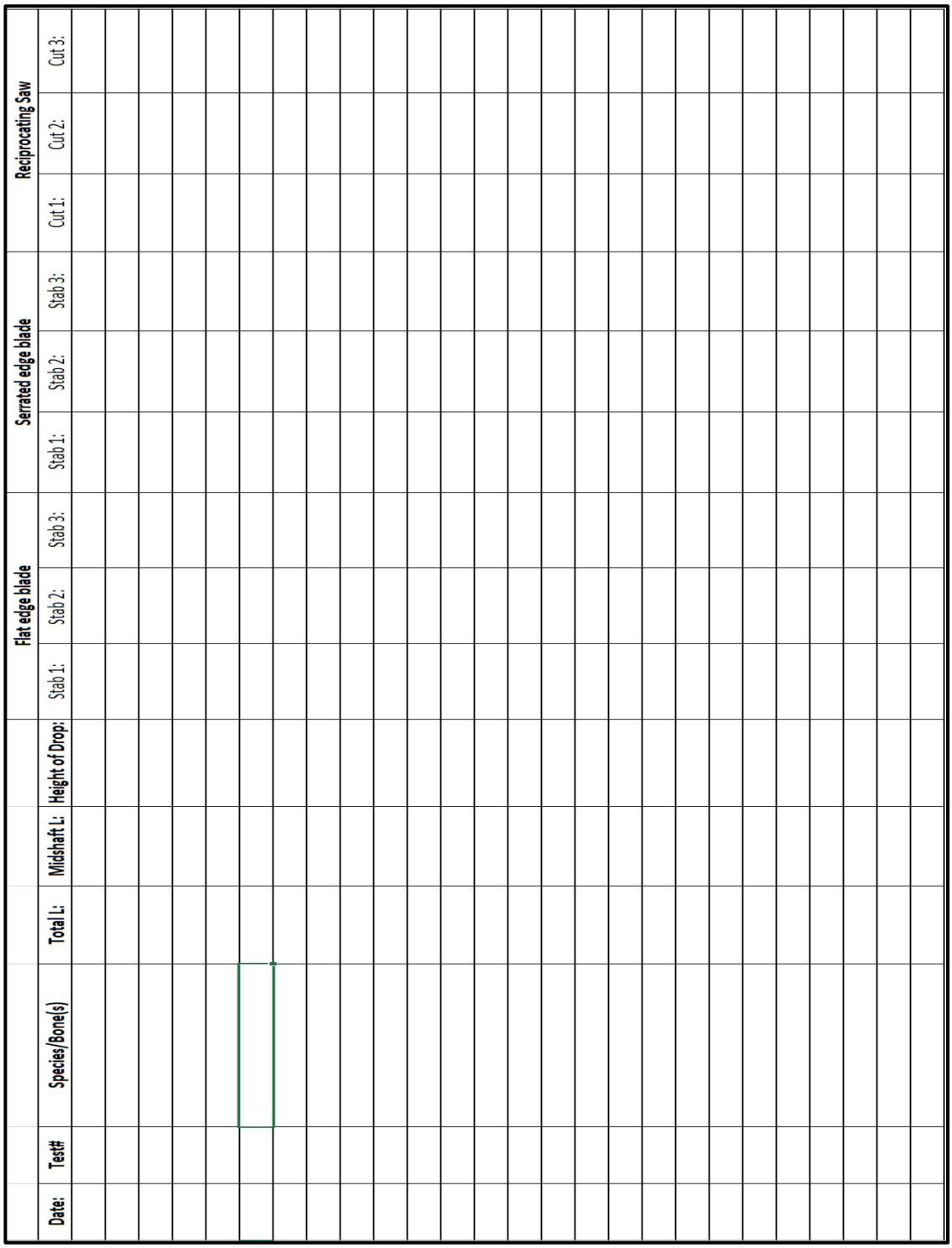

					Flat edge blade			Serrated edge blade			Reciprocating Saw		
Date:	Test#	Species/Bone(s)	Total L:	Midshaft L:	Height of Drop:	Stab 1:	Stab 2:	Stab 3:	Stab 1:	Stab 2:	Stab 3:	Cut 1:	Cut 2:	Cut 3:

DATA COLLECTION FORM FOR KERFS PRE AND POST BURN

Date	Sample #	Element	Duration of Burn	Avg. Temp	Max Temp	Calcine Bone Present	Blade Type	Kerf Length		Kerf Width (Max)		Kerf Depth	
								Pre-Burn	Post-Burn	Pre-Burn	Post-Burn	Pre-Burn	Post-Burn

REFERENCES

Aerssens, J., Boonen, S., Lowet, G., & Dequeker, J. (1998). Interspecies differences in bone composition, density, and quality: Potential implications for in vivo bone research *Endocrinology, 189*(2), 663-670.

Alunni-Perret, V., Borg, C., Laugier, J. P., Bertrand, M. F., Staccini, P., Bolla, M., . . . Muller-Bolla, M. (2010). Scanning Electron Microscopy Analysis of Experimental Bone Hacking Trauma of the Mandible. *The American Journal of Forensic Medicine and Pathology*(4), 326. doi:10.1097/PAF.0b013e3181e2ed0b

Associated Press. (2007, 3/25/2007). Police: Student was Killed, then Burned on Grill. *NBC News*.

Baier, W., Norman, D. G., Warnett, J. M., Payne, M., Harrison, N. P., Hunt, N. C. A., . . . Williams, M. A. (2017). Novel application of three-dimensional technologies in a case of dismemberment. *Forensic Science International, 270*, 139-145. doi:https://doi.org/10.1016/j.forsciint.2016.11.040

Bailey, J. A., Wang, Y., van de Goot, F. R. W., & Gerretsen, R. R. R. (2011). Statistical analysis of kerf mark measurements in bone. *Forensic Science, Medicine, And Pathology, 7*(1), 53-62. doi:10.1007/s12024-010-9185-6

Bandini, A., Chicot, D., Berry, P., Decoopman, X., Pertuz, A., & Ojeda, D. (2013). Indentation size effect of cortical bones submitted to different soft tissue removals. *Journal of the Mechanical Behavior of Biomedical Materials, 20*, 338-346. doi:https://doi.org/10.1016/j.jmbbm.2013.02.011

Buikstra, J., & Swegel, M. (1989). Bone modification due to burning: Experimental evidence In R. Bonnichsen & M. Sorg (Eds.), *Bone Modification* (pp. 247-258). Orono, Maine: Center for the Study of First Americans.

Carroll, E. L., & Smith, M. (2018). Burning questions: Investigations using field experimentation of different patterns of change to bone in accidental vs deliberate burning scenarios. *Journal of Archaeological Science: Reports, 20*, 952-963. doi:10.1016/j.jasrep.2018.02.001

Castillo, R. F., Ubelaker, D., Acosta, J. A. L., & de la Fuente, G. A. C. (2013). Effects of Temperature on Bone Tissue. Histological Study of the Changes in the Bone Matrix. *Forensic Science International, 226*, 33-37.

Chadwick, E. K. J., Nicol, A. C., Lane, J. V., & Gray, T. G. F. (1999). Biomechanics of Knife Stab Attacks. *Forensic Science International, 105*, 35-44.

Coelho, L., & Cardoso, H. F. V. (2013). Timing of blunt force injuries in long bones: The effects of the environment, PMI length and human surrogate model. *Forensic Science International, 233,* 230-237. doi:10.1016/j.forsciint.2013.09.022

Collini, F., Amadasi, A., Mazzucchi, A., Porta, D., Regazzola, V. L., Garofalo, P., . . . Cattaneo, C. (2015). The Erratic Behavior of Lesions in Burnt Bone. *Journal of Forensic Sciences, 60*(5), 1290-1294. doi:10.1111/1556-4029.12794

Croft, A. M., & Ferllini, R. (2007). Macroscopic Characteristics of Screwdriver Trauma. *Journal of Forensic Sciences, 52*(6), 1243-1251. doi:10.1111/j.1556-4029.2007.00552.x

Crowder, C., Rainwater, C., & Fridie, J. (2013). Microscopic analysis of sharp force trauma in bone and cartilage: A validation study *Journal of Forensic Sciences, 58,* 1119-1126.

de Gruchy, S. B. A., & Rogers, T. L. P. D. (2002). Identifying Chop Marks on Cremated Bone: A Preliminary Study. *Journal of Forensic Sciences, 47*(5), 1-3.

Derose, J. (2018). What You Always Wanted to Know About Digital Microscopy, but Never Got Around to Asking. *Quality, 57*(9), 30-33.

DiGangi, E. A., & Moore, M. K. (2012). Introduction to Research in Skeletal Biology. In E. A. DiGangi & M. K. Moore (Eds.), *Research Methods in Human Skeletal Biology*. San Diego, CA: Elsevier Science & Technology.

Dirkmaat, D., Olson, G., Klales, A., & Getz, S. (2012). The Role of Forensic Anthropology in the Recovery and Interpretation of the Fatal-Fire Victim. In D. Dirkmaat (Ed.), *A Companion to Forensic Anthropology*. Hoboken, United Kingdom: John Wiley & Sons, Incorporated.

Dittmar, J. M., Errickson, D., & Caffell, A. (2015). The comparison and application of silicone casting material for trauma analysis on well preserved archaeological skeletal remains. *Journal of Archaeological Science: Reports, 4*, 559-564. doi:10.1016/j.jasrep.2015.10.008

Feeser, L. R. (2019). *Rib fracture analysis of infant cardiopulmonary resuscitation methods using porcine surrogates*, (Thesis). Texas State University, San Marcos.

Fujisaki, K., Hasegawa, A., Yokoyama, H., & Sasagawa, K. (2017). Demineralization of cortical bone for improvement of Charpy impact fracture characteristics. *Journal of Biomechanical Science and Engineering, 12*(3), 16-24.

Gin, K., Tovar, J., Bartelink, E. J., Kendell, A., Milligan, C., Willey, P., . . . Selden, R. F. (2020). The 2018 California Wildfires: Integration of Rapid DNA to Dramatically Accelerate Victim Identification. *Journal of Forensic Sciences*. doi:10.1111/1556-4029.14284

Gonçalves, D., Cunha, E., & Thompson, T. J. U. (2015). Estimation of the pre-burning condition of human remains in forensic contexts. *International Journal of Legal Medicine, 129*, 1137-1143.

Gonçalves, D., Thompson, T. J. U., & Cunha, E. (2011). Implications of heat-induced changes in bone on the interpretation of funerary behaviour and practice. *Journal of Archaeological Science, 38*(6), 1308-1313. doi:https://doi.org/10.1016/j.jas.2011.01.006

Gourrier, A., Chadefaux, C., Lemaitre, E., Bellot-Gurlet, L., Reynolds, M., Burghammer, M., . . . Reiche, I. (2017). Nanoscale Modifications in the Early Heating States of Bone are Heterogeneous at the Microstructural Scale. *PloS ONE, 12*(4), 1-23.

Haglund, W., & Sorg, M. (1997). Introduction to forensic taphonomy. In W. Haglund & M. Sorg (Eds.), *Forensic taphonomy: The postmortem fate of human remains*. Boca Raton, FL: CRC Press.

Herrmann, N. P., & Bennett, J. L. (1999). The differentiation of traumatic and heat-related fractures in burned bone. *Journal of Forensic Sciences, 44*(3), 461-469.

Humphrey, Kumaratilake, J., & Henneberg, M. (2017). Characteristics of Bone Injuries Resulting from Knife Wounds Incised with Different Forces. *Journal of Forensic Sciences, 62*(6), 1445-1451. doi:10.1111/1556-4029.13467

Humphrey, J. H. B. A., & Hutchinson, D. L. P. D. (2001). Macroscopic Characteristics of Hacking Trauma. In (Vol. 46, pp. 228-233).

Jackson, D. W. (2005). *An Investigation into Identifying Sharp Force Trauma on Burned Bones.* (Thesis), Texas State University San Marcos, Texas.

Kasbleek, N., & Richter, J. (2006). Preservation of burned bones: An investigation of the effects of temperature and pH on hardness. *Studies in Conservation, 51*(2), 123-138.

Kooi, R. J. B. S., & Fairgrieve, S. I. P. D. (2013). SEM and Stereomicroscopic Analysis of Cut Marks in Fresh and Burned Bone. In (Vol. 58, pp. 452-458).

Liebschner, M. A. K. (2004). Biomechanical considerations of animal models used in tissue engineering of bone. *Biomaterials, 25*(9), 1697-1714.

Macoveciuc, I., Márquez-Grant, N., Horsfall, I., & Zioupos, P. (2017). Sharp and blunt force trauma concealment by thermal alteration in homicides: An in-vitro experiment for methodology and protocol development in forensic anthropological analysis of burnt bones. *Forensic Science International, 275*, 260-271. doi:10.1016/j.forsciint.2017.03.014

Marciniak, S.-M. (2009). A Preliminary Assessment of the Identification of Saw Marks on Burned Bone. *Journal of Forensic Sciences, 54*(4), 779. doi:10.1111/j.1556-4029.2009.01044.x

Marinho, L., & Cardoso, H. F. V. (2016). Comparing Known and Reconstructed Circumstances of Death Involving a Blunt Force Trauma Mechanism through a Retrospective Analysis of 21 Skeletonized Individuals. *Journal of Forensic Sciences, 61*(6), 1416-1430. doi:10.1111/1556-4029.13128

Mason, J. a. B. P. (Ed.) (2000). *The Pathology of Trauma* (Third ed.). New York: Oxford University Press.

Miller, S. A., & Jones, S. D. (1996). Kinematics of Four Methods of Stabbing: A Preliminary Study. *Forensic Science International, 82*, 190-193.

Murder Victims by Weapon, 2012-2016. (2016). Department of Justice.

Ní Annaidh, A., Cassidy, M., Curtis, M., Destrade, M., & Gilchrist, M. D. (2013). A combined experimental and numerical study of stab-penetration forces. *Forensic Science International, 233*(1-3), 7-13. doi:10.1016/j.forsciint.2013.08.011

Nogueira, L., Alunni, V., Bernardi, C., & Quatrehomme, G. (2018). Saw marks on bone in dismemberments: Preliminary results. *Revue de Medecine Legale*. doi:10.1016/j.medleg.2018.08.003

Nogueira, L., Quatrehomme, G., Rallon, C., Adalian, P., & Alunni, V. (2016). Saw marks in bones: A study of 170 experimental false start lesions. *Forensic Science International, 268*, 123-130.

Nolan, G., Hainsworth, S. V., & Rutty, G. N. J. I. J. o. L. M. (2018). Forces generated in stabbing attacks: an evaluation of the utility of the mild, moderate and severe scale. *132*(1), 229-236. doi:10.1007/s00414-017-1702-7

Norman, D. G., Watson, D. G., Burnett, B., Fenne, P. M., & Williams, M. A. (2018). The cutting edge — Micro-CT for quantitative toolmark analysis of sharp force trauma to bone. *Forensic Science International, 283*, 156-172. doi:https://doi.org/10.1016/j.forsciint.2017.12.039

O'Callaghan, P., Jones, M., James, D., Leadbeatter, S., Holt, C., & Nokes, L. (1999). Dynamics of stab wounds: Force required for penetration of various cadaveric human tissues *Forensic Science International, 104*, 173-178.

Pelletti, G., Cecchetto, G., Viero, A., Fais, P., Weber, M., Miotto, D., . . . Giraudo, C. (2017). Accuracy, precision and inter-rater reliability of micro-CT analysis of false starts on bones. A preliminary validation study. *Legal Medicine, 29*, 38-43. doi:https://doi.org/10.1016/j.legalmed.2017.10.003

Pelletti, G., Viel, G., Fais, P., Viero, A., Visentin, S., Miotto, D., . . . Giraudo, C. (2017). Micro-computed tomography of false starts produced on bone by different hand-saws. *Legal Medicine, 26*, 1-5. doi:https://doi.org/10.1016/j.legalmed.2017.01.009

Pope, E. J. M. A., & Smith, O. B. C. M. D. (2004). Identification of Traumatic Injury in Burned Cranial Bone: An Experimental Approach. *Journal of Forensic Sciences, 49*(3), 431-440.

Poppa, P., Porta, D., Gibelli, D., Mazzucchi, A., Brandone, A., Grandi, M., & Cattaneo, C. (2011). Detection of Blunt, Sharp Force and Gunshot Lesions on Burnt Remains: A Cautionary Note. *American Journal of Forensic Medicine and Pathology, 32*(3), 275-279.

Prat, N., Rongieras, F., de Freminville, H., Magna, P., Debord, E., Fusai, T., . . . Voiglio, E. (2012). Comparison of thoracic wall behavior in large animals and human cadavers submitted to an identical ballistic blunt thoracic trauma *Forensic Science International, 222*, 179-185.

Prieto, J. L. (2007). Stab wounds: the contribution of forensic anthropology: a case study. In M. B. Brickley & R. Ferllini (Eds.), *Forensic Anthropology: Case Studies from Europe.* (pp. 19-37). Springfield, IL: Charles C Thomas.

Schmidt, C.W. (2015). Burned Human Teeth. In C.W. Schmidt & S.A. Symes (Eds.), *The Analysis of Burned Human Remains.* (pp.61-81). Amsterdam: Elsevier/Academic Press.

Schmidt, C. W., & Symes, S. (2015). *The Analysis of Burned Human Remains* (2nd ed.). Amsterdam: Elsevier/Academic Press.

Shipman, P., Schoeninger, M., & Foster, G. (1984). Burnt bones and teeth: an experimental study of color, morphology, crystal structure and shrinkage. *Journal of Archaeological Science, 11*(4), 307-325. doi:10.1016/0305-4403(84)90013-X

Siegert, C. C. (2016). *The application of consolidation materials to burned bone : a comparative approach.* (Thesis), Texas State University, San Marcos, TX.

Symes, S. A., Chapman, E. N., Rainwater, C., Cabo, L., & Myster, S. (2010). *Knife and Saw Toolmark Analysis in Bone: A Manual Designed for the Examination of Criminal Mutilation and Dismemberment*.

Symes, S. A., Dirkmaat, D. C., Ousley, S., Chapman, E., & Cabo, L. (2012). *Recovery and Interpretation of Burned Human Remains*. Retrieved from

Tegtmeyer, C. E. (2012). *A comparative analysis of serrated and non-serrated sharp force trauma to bone.* (Thesis), Texas State University, San Marcos, TX.

Thompson, T. J. U. (2005). Heat-induced dimensional changes in bone and their consequences for forensic anthropology. *Journal of Forensic Sciences, 50*(5), 1008-1015.

Vassalo, A. R., Cunha, E., Batista de Carvalho, L. A. E., & Goncalves, D. (2016). Rather yield than break: assessing the influence of human bone collagen content on heat-induced warping through vibrational spectroscopy. *International Journal of Legal Medicine, 130*(6), 1647-1656. doi:10.1007/s00414-016-1400-x

Walsh-Haney, H. A. B. A. (1999). Sharp-Force Trauma Analysis and the Forensic Anthropologist: Techniques Advocated by William R. Maples Ph.D. *Journal of Forensic Sciences, 44*(4), 720-723.

Waltenberger, L., & Schutkowski, H. (2017). Effects of heat on cut mark characteristics. *Forensic Science International, 271*, 49-58. doi:10.1016/j.forsciint.2016.12.018

Wang, X., Mabrey, J. D., & Agrawal, C. M. (1998). An interspecies comparison of bone fracture properties. *Bio-Medical Materials & Engineering, 8*(1), 1.

Waterhouse, K. (2013). The effect of victim age on burnt bone fragmentation: Implications for remains recovery. *Forensic Science International, 231*(1-3), 409.e401-409.e407. doi:10.1016/j.forsciint.2013.04.032

Wells, C. (1960). A Study of Cremation. *Antiquity, 34*, 29-47.

Wieberg, D. A. M., & Wescott, D. J. (2008). Estimating the Timing of Long Bone Fractures: Correlation Between the Postmortem Interval, Bone Moisture Content, and Blunt Force Trauma Fracture Characteristics. *Journal of Forensic Sciences, 53*(5), 1028-1034. doi:10.1111/j.1556-4029.2008.00801.x

Zavala, E. (2018, 12/4/2018). Witness: Convicted San Antonio Killer Chopped up Girlfriend. *San Antonio Express News*.

Zeder, M., Lemoine, X., & Payne, S. (2015). A new system for computing long-bone fusion age profiles in Sus scrofa. *Journal of Archaeological Science, 55*, 135-150.

Zephro, L., & Galloway, A. (2014). The Biomechanics of Fracture Production. In V. Wedel & A. Galloway (Eds.), *Broken Bones: Anthropological Analysis of Blunt Force Trauma* (2nd ed.). Springfield, IL: Charles C Thomas.

Zephro, L., Galloway, A., & Wedel, V. (2014). Theoretical Considerations in Designing Experimental Trauma Studies and Implementing Their Results. In V. Wedel & A. Galloway (Eds.), *Broken Bones: Anthropological Analysis of Blunt Force Trauma* (2nd ed.). Springfield, IL: Charles C Thomas.